Master's thesis

NTNU
Norwegian University of Science and Technology
Faculty of Economics and Management
Dept. of Industrial Economics and Technology Management

Anders Bennæs, Martin Skogset, Tormod Svorkdal

Supply Chain Optimization for Carbon Capture and Storage

A German–Norwegian Case Study

Master's thesis in Industrial Economics and Technology Management
Supervisor: Kjetil Fagerholt
Co-supervisor: Frank Meisel, Lisa Herlicka, Wilfried Rickels
June 2022

NTNU
Norwegian University of Science and Technology

Anders Bennæs, Martin Skogset, Tormod Svorkdal

Supply Chain Optimization for Carbon Capture and Storage

A German–Norwegian Case Study

Master's thesis in Industrial Economics and Technology Management
Supervisor: Kjetil Fagerholt
Co-supervisor: Frank Meisel, Lisa Herlicka, Wilfried Rickels
June 2022

Norwegian University of Science and Technology
Faculty of Economics and Management
Dept. of Industrial Economics and Technology Management

NTNU

Kunnskap for en bedre verden

Preface

This master's thesis is part of our Master of Science at the Norwegian University of Science and Technology, Department of Industrial Economics and Technology Management. It is the result of the subject TIØ4905 - Managerial Economics and Operations Research, Master's Thesis. It was written in the spring semester of 2022 and builds on our project report written in the fall of 2021 (Bennæs et al. 2021).

We want to thank our supervisors, Kjetil Fagerholt, Frank Meisel, Lisa Herlicka, and Wilfried Rickels, for their advice and feedback. Their experience, enthusiasm, and willingness to help have been precious and motivating.

Trondheim, June 9, 2022

Anders Bennæs, Martin Skogset and Tormod Svorkdal

Abstract

The world is faced with the challenge of drastically reducing its emission of greenhouse gases to reach the two-degree goal of the Paris Agreement. Efforts toward switching to green and renewable energy sources are essential. However, other measures must also be considered to handle industries that will continue to rely on emission-intensive processes. Carbon Capture and Storage (CCS) is one of these measures. CCS is the process of capturing carbon dioxide (CO_2) before it is released into the atmosphere, in order to transport and store it in underground geological formations that can retain the CO_2 for millennia. While being a proven concept, the development of efficient and commercially viable CCS projects has been limited.

A prerequisite for effective CCS projects is a cost-efficient supply chain. While there are many global initiatives intending to capture CO_2 from different emission sources, there is a lack of projects considering the whole supply chain, where emission sources are connected to suitable storage locations. This thesis presents a mixed integer programming (MIP) model developed to provide valuable decision support for the CCS Supply Chain Design problem (CCS-SCDP). The CCS-SCDP concerns setting up the whole supply chain for capturing CO_2 at emission sources, transporting it across land and sea, and storing it in geological storage facilities at the lowest possible cost. When solving the CCS-SCDP, the model makes a set of decisions; which emission sources to capture the CO_2 from; whether to use pipelines or ships as the offshore transportation mode; construction of the onshore and offshore pipeline networks; placement and dimensioning of port infrastructure; and hiring and routing of ships. The model solutions provide decision support to policy-makers faced with the challenge of designing a CCS supply chain that is reliant on both onshore and offshore transportation.

We perform a computational study investigating the supply chain design implications of seven CCS development scenarios, where the CO_2 is captured at industrial CO_2 emission sources in Germany and stored in a suitable geological storage formation on the Norwegian continental shelf. Four of the scenarios represent a German CCS development where the capture rates increase from 5 to 100 megatonnes per annum (Mtpa) by gradually adding the largest CO_2 emitters to the supply chain. At 5 Mtpa, ships are used for offshore transportation, with a supply chain cost of 103.1 euro per tonne. At 20 Mtpa, ships are substituted by pipelines, and the supply chain cost is reduced to 87.3 euro per tonne. Due to economies of scale, this is further reduced to 76.5 euro per tonne when considering 100 Mtpa. In the final three scenarios, we analyze emissions from relevant German industrial sectors, namely steel, cement, and organic chemicals. For the latter, we achieved a supply chain cost of 49.3 euro per tonne. With the current CO_2 allowance price of about 80 euro per tonne within the European Union Emission Trading System (EU ETS), we have shown that CCS could be a cost-competitive alternative to emission already today.

Sammendrag

For å nå togradersmålet satt i Parisavtalen, står verdenssamfunnet ovenfor utfordringen med å drastisk redusere utslippene av drivhusgasser. Tiltak som bidrar til overgangen fra fossile til fornybare energikilder er essensielle for å nå dette målet. Samtidig må andre alternativer også vurderes for å ta høyde for industrier som vil fortsette å være avhengige av utslippsintensive prosesser i framtiden. Karbonfangst og -lagring (carbon capture and storage, CCS) er et slikt alternativ. CCS er en prosess som går ut på å fange karbondioksid (CO_2) før den slippes ut i atmosfæren, for så å frakte og lagre den i underjordiske geologiske formasjoner hvor den kan bevares i årtusener. Til tross for at CSS har vist seg å være et fungerende konsept, har utviklingen av effektive og økonomisk gjennomførbare CCS-prosjekter vært begrenset.

Kosnadeseffektive transport- og forsyningskjeder er en forutsetning for vellykkede CCS-prosjekter. Til tross for et økende initiativ til å fange CO_2 rundt om i verden er det en mangel på prosjekter som tar hele forsyningskjeder i betraktning, slik at utslippskilder kan knyttes til lagringslokasjoner. Denne avhandlingen presenterer en blandet heltallsmodell utviklet for å kunne gi verdifull beslutningsstøtte i problemet vedrørende å designe en CCS-forsyningskjede (the CCS Supply Chain Design Problem, CCS-SCDP). CCS-SCDP omhandler å konstruere en fullstendig forsyningsskjede, hvor CO_2 fanges hos utslippskilder, transporteres over land og hav, og til slutt lagres permanent i geologiske lagringsformasjoner – alt til en lavest mulig kostnad. Modellen løser CCS-SCDP gjennom et sett med beslutninger: hvilke utslippskilder man skal fange CO_2 fra; om man skal transportere CO_2 med skip eller rør over havet; hvordan man skal konstruere et rørnettverk på land og til havs; plassering og dimensjonering av havne-infrastruktur; hvilke typer skip som skal benyttes, og når og hvor de skal seile. Modellens løsninger er ment å gi beslutningsstøtte til de som skal utforme en forsyningskjede for CCS som avhenger av både land- og sjøtransport.

Vi analyserer syv scenarioer, hvor alle omhandler utslipp fra industrielle utslippskilder i Tyskland og lagring i egnede lagringslokasjoner under den norske kontinentalsokkelen. Fire av scenarioene representerer en gradvis opptrapping i omfanget av karbonfangst i Tyskland. Det minste scenarioet ser på fangst av 5 megatonn i året (megatonnes per annum, Mtpa), og det største ser på fangst av 100 Mtpa. Ved 5 Mtpa blir skip brukt til sjøtransport, noe som resulterer i en forsyningskjedekostand på 103.1 euro per tonn CO_2. Ved 20 Mtpa byttes skipene ut med rør, hvilket bidrar til at kostnadene reduseres til 87.3 euro per tonn. Som et resultat av stordriftsfordeler reduseres dette ytterligere til 76.5 euro per tonn når vi når 100 Mtpa. De tre siste scenarioene omhandler hver sin relevante, industrielle sektor, henholdsvis produksjon av sement, stål og organiske kjemikalier. For sistnevnte har vi oppnådd en kostnad på 49.3 euro per tonn. Tatt i betraktning dagens pris for CO_2-utslipp innenfor EUs kvotesystem på omtrent 80 euro per tonn, har vi vist at CCS kan være et kostnadsmessig konkurransedyktig alternativ til utslipp allerede i dag.

Contents

List of Figures

List of Tables

Abbreviations

CAPEX. Capital expenditures for a given time period.

CCS. Carbon capture and storage.

CCS-SCDP. CCS Supply Chain Design Problem.

CO_2. Carbon dioxide.

DAC. Direct air capture.

ETS. Emission Trading System.

EU ETS. Emission Trading System in the European Union.

LNG. Liquefied natural gas.

LPG. Liquefied petroleum gas.

MIP. Mixed integer program/programming.

Mtpa. Megatonnes per annum. Used to denote yearly amounts of CO_2.

OPEX. Operational expenditures for a given time period.

STL-buoy. Submerged turret loading buoy.

Chapter 1

Introduction

According to The International Energy Agency (IEA) and the Intergovernmental Panel on Climate Change (IPCC), it is extremely probable that the climate change we are facing today is connected to anthropogenic CO_2 emissions. Moreover, it is an established fact that CO_2 is a greenhouse gas and that greenhouse gases are one of the main drivers of global warming. Under the 2015 Paris Agreement, almost 200 countries pledged to limit global warming to 2°C higher temperatures than pre-industrial levels by 2100, with an additional aim to keep warming at or below 1.5°C. To limit global warming to 1.5°C, IPCC projects that we must reduce yearly emissions of greenhouse gases by 84% by 2050 (IPCC 2022). Carbon Capture and Storage (CCS) might be an essential technology for reaching the decarbonization goals, as it can be applied to many emission contributing industries.

Carbon Capture and storage is the process of CO_2 capturing CO_2 before it enters the atmosphere, to further transport it to and store it in a permanent underground storage site. If done right, the CO_2 can be retained at the storage site for millennia and thus contribute to the permanent mitigation of climate gases. According to IEA, CCS should be an important measure to reach the goals of the Paris Agreement. Through their scenario of reaching net zero emissions by 2050, we should reach 7.6 Gt of CO_2 captured each year by 2050 (IEA 2021). Therefore, CCS has been much discussed for the energy sector in particular, as it accounts for the majority of CO_2 emissions (Ritchie and Roser 2020). However, several analyses point to the application of CCS technology in the industrial sector as more urgent (Holz et al. 2021). Some of the actors in the industrial sectors can be substantially decarbonized through an increased supply of green and renewable energy sources, but not all of them. For the emission-intensive but necessary sectors like steel, cement, fertilizer, and chemicals production, CCS is part of a limited set of emission abatement options. However, while these industrial sectors have more limited options and should be prioritized, CCS should not be excluded as an option for the energy sector. Considering that fossil fuels such as oil, coal, and natural gas account for about 80 percent of the world's energy supply (Environmental and Energy Study Institute 2022), CCS should also be seen as an important technology for reducing the energy sector's emissions while moving towards the green shift.

There are only two operating CCS projects in Europe today, namely in the offshore natural gas fields Sleipner, which has been operating since the 1990s, and Snøhvit,

since the mid-2000s, both located in Norway. The situation seemed to develop differently in the early 2000s when CCS was widely supported as a CO_2 mitigation option. Being at the forefront of CCS development, Europe had more than 30 announced demonstration projects in the power and industry sectors. However, all of them have been canceled during the last ten years. This is likely due to the public and private focus on short-term recovery after the global financial crisis. As the world economy has stabilized, a new wave of CCS projects has arrived in recent years. On a global scale, there are 135 commercially intended CCS projects today (Kearns et al. 2021). Of these, only 27 are operational, and most are in phases of advanced or early development. Several projects have been initialized in Europe as well. However, there is still a need for applied and fundamental research within CCS, as the process is neither fully understood, nor are the costs in a commercial range (Holz et al. 2021).

The need for developing novel technologies and the risks tied to the project-specific investments make CCS costly. It is doubtful that large-scale CCS will be a viable business case until CCS costs (euro per tonne CO_2 captured, transported, and stored) decrease to below the carbon emission allowance prices within Emission Trading Systems (ETS) or below the carbon tax prices that some countries use. Therefore, further research and development are crucial to reach commercially viable costs for CCS. The capturing process is the most costly part of the CCS supply chain, ranging between 40 and 70 percent of the total system cost. Several private companies and industrial research departments have started developing technologies to increase the efficiency of carbon capture processes and lower the associated costs (Bohlsen 2021). Despite being the most costly part of the supply chain, capture only represents the first step in the CCS process.

To be able to utilize CCS at a large scale, the availability of infrastructure to transport CO_2 safely and reliably is essential. Based on experience from similar products, such as liquefied natural gas and liquefied petroleum gas (LNG and LPG), ships and pipelines are considered the main options for large-scale CO_2 transportation for CCS. Ship-based transportation and pipeline transportation have different technological and economic challenges connected to them (Metz et al. 2005). Pipelines were early seen as the most economical way of transporting large volumes of CO_2 onshore but are faced with higher costs when applied offshore. Additionally, many countries, including Norway, Sweden, Denmark, and the Netherlands, only grant permissions for offshore CCS storage projects. Acknowledging that there exists a public opposition to onshore underground storage of CO_2, the need for techno-economic assessments of offshore transportation technologies has increased (Holz et al. 2021).

Germany has consistently produced the most CO_2 emissions in Europe since the turn of the century. In 2020 their emissions summed up to 605 million metric tonnes of CO_2, which is more than the two runner-ups, Italy and Poland, combined. The German government considers CCS as one of the instruments for achieving net-negative CO_2 and net zero greenhouse gas emissions by 2050, thus contributing to reaching the goals of the Paris Agreement. As Norway possesses potential offshore storage locations for CO_2, German CCS initiatives want to establish a strategic partnership for the transfer and deposition of CO_2 from Germany to Norway (Wintershall Dea 2022). Norway has already started the development and construction of the world's first open-source CO_2 transport and storage infrastructure, the Northern Lights project. With the Northern Lights project, the collaborating parts Equinor, Shell, TotalEnergies, and The Norwegian government aims to offer CO_2 transportation and storage

as a service to companies and governments eager to reduce their emissions through carbon capture. In its initial phase, Northern lights will provide a CO_2 transportation and storage capacity of 1.5 megatonnes per annum (Mtpa) by mid-2024 and expand in phase two to 5 Mtpa as demand grows across Europe. The long-distance offshore transportation in the initial phases is planned to be done by ships, but pipelines are likely to be a viable option as demand and capacity increase. With a growing interest in CCS as a decarbonization strategy in Germany and a promising transportation and storage initiative in Norway, the task that remains is to decide how to connect these two in the most efficient way to achieve a viable full-scale CCS supply chain.

Therefore, the main objective of this master thesis is to develop a strategic optimization model that provides valuable insights into the design of a viable CCS supply chain between Germany and Norway. Since Germany and Norway are divided by the North Sea, offshore transportation is central to the model. The problem investigated is referred to as the CCS Supply Chain Design Problem (CCS-SCDP). Designing a CCS supply chain is a complex task, as its components and operations are numerous and various. As a result, most of the existing relevant literature on CCS supply chains concentrates on specific supply chain components, whether it is capture technology, the configuration of transportation modes, or storage operations. Full-scale supply chain optimization is also present in the literature. Still, the work either focuses on small supply chains with only one transportation technology, e.g., ship transportation (Bjerketvedt et al. 2022), or large-scale continental chains with limited practical utility (d'Amore et al. 2021). The goal of our model of the CCS-SCDP is to bridge this gap. We aim to include all relevant transportation modes and supply chain components needed to capture CO_2 from a set of emission sources, transport it across land and sea, and store it in a suitable geological storage location. This is achieved by formulating a new mixed integer programming (MIP) model for CCS that captures relevant supply chain design questions regarding onshore and offshore pipeline connections, fleet size and mix, fleet deployment, and fleet scheduling. The model also considers decisions regarding the capacity of infrastructure and equipment within the supply chain. Through an analysis of CO_2 volume scenarios with various German emissions sources, the model provides solutions with the cost-optimal supply chain configurations for the respective volumes and emission source locations. The information from the solutions can be used as guidance for policy-makers, either private or governmental, responsible for CCS deployment strategies in Germany and Norway.

Nine chapters are outlined for this thesis. Chapter 2 introduces the CCS supply chain and provides background information about the supply chain components included in our model. It also gives an overview of international trends within CCS development and some of the most relevant ongoing CCS projects for the context of this thesis. Then, in Chapter 3, we do a comprehensive review of relevant literature for the CCS-SCDP, while Chapter 4 presents the problem description. Next, in Chapter 5, the mathematical model formulation with the applied modeling approach, assumptions, and model enhancement methods are presented. Chapter 6 details the model input and explains the motivation and calculations behind the sets and parameters. In Chapter 7, we perform a computational study consisting of a technical and an economic part. First, we test several proposed model enhancement methods to find the optimal run configuration for the model. Then, we present and discuss the results from different German CO_2 capture scenarios and perform a number of sensitivity analyses. Lastly, Chapter 8 makes some concluding remarks, and Chapter 9 proposes a set of directions for future research within the domain of this thesis.

Chapter 2

Background: The CCS Supply Chain

The CCS supply chain mainly consists of three elements: the capture of CO_2, transportation, and storage. However, these supply chain elements can take different forms in terms of technology. For example, there are several capture technologies, and which one to choose depends on the CO_2-generating industrial process at the emission source. Transportation can be done through offshore and onshore pipelines, with ships or by rail or truck, and storage can occur both onshore and offshore. While successful ongoing and long-lasting CCS projects are present today, all elements of the CCS supply chain are still subject to research and development. Figure 2.1 gives an overview of different CCS supply chains for offshore storage with different capture technologies and onshore and offshore transportation modes. The elements marked in green represent the technologies investigated in this thesis.

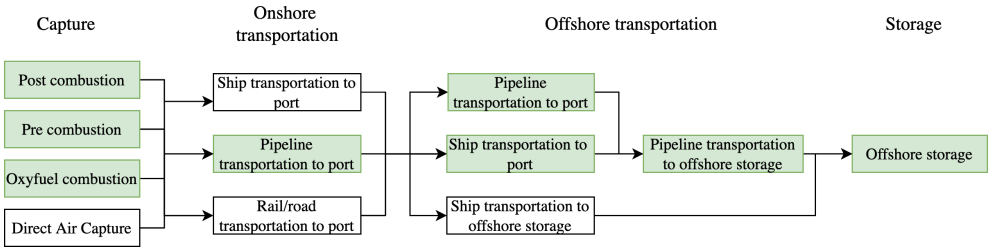

Figure 2.1: An overview of possible CCS supply chains with offshore storage and different onshore and offshore transportation modes.

Sections 2.1, 2.2, and 2.3 give an introduction to the most important technologies in the CCS supply chain elements capture, transportation, and storage, respectively. In Section 2.4 we discuss the global development of CCS projects and present some ongoing CCS projects which are relevant to the scope of this thesis. Lastly, Section 2.5 explains the concept of carbon pricing policies, which aim to limit emissions.

2.1 Capture

The first part of the CCS supply chain, which also represents the highest cost, is the capturing of CO_2 (Skagestad et al. 2014). There exist several capture technologies and contexts where capture can take place. The four main methods used to capture CO_2 are post-combustion, pre-combustion, oxyfuel combustion, and direct air capture (DAC). The combustion-based technologies can be applied to large-scale emissions processes, like coal and gas-fired power generation, natural gas processing, cement, iron, and steel production. Direct air capture is used for extracting CO_2 directly from the atmosphere.

Post-combustion

The post-combustion process of capturing CO_2 separates the CO_2 from combustion exhaust gases. After the combustion of fuel, the exhaust gases are sent to a tank where most of the CO_2 binds chemically to amines and form a CO_2-rich amine blend. The CO_2 can then be separated from the amine blend through heating, which results in a high purity CO_2-stream, which is sent for further transportation and storage. The method has been used successfully in small incineration plants for years. It is a technology that is widely used for capturing CO_2 used in the food and beverage industry (Global CCS Institute 2016). One of the advantages of post-combustion capture is that it can be fitted relatively easily on already existing emission sources. It works on any large stationary source, including industrial emissions.

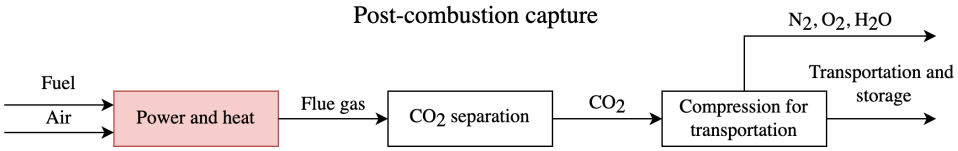

Figure 2.2: Flow chart for a post-combustion capture process.

Pre-combustion

Pre-combustion processes separate the CO_2 before the combustion takes place. The process converts fuel into a gaseous mixture of hydrogen and CO_2 known as a syngas, where the hydrogen is separated and can be burnt without producing CO_2. This method utilizes pressure to capture the CO_2, which in turn requires a smaller and cheaper capture installment. The method is especially relevant in the context of plants producing electrical energy and hydrogen (Hofstad 2022). However, this technology is generally only practical for new plants, as retrofitting already existing emission sources would require heavy plant modification.

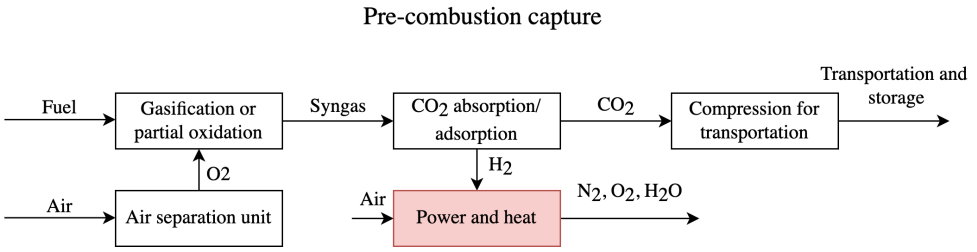

Figure 2.3: Flow chart over a pre-combustion capture process.

Oxyfuel combustion

Oxyfuel combustion processes use oxygen instead of air for the combustion of fuel. The exhaust produced in the process consists mainly of water vapor and CO_2 which can be easily separated to produce a high purity CO_2 stream. The capture rates from oxyfuel are very high, making it possible to capture close to 100% of the CO_2. However, impurities in the fuel may require additional purification of the CO_2 stream, making low-quality fuels less suited for this capture process. Oxyfuel can be retrofitted to some types of existing power plants, but not all. Oxyfuel combustion is usually applied in the glass industry, metallurgical industry, and thermal energy engineering (Wang 2018).

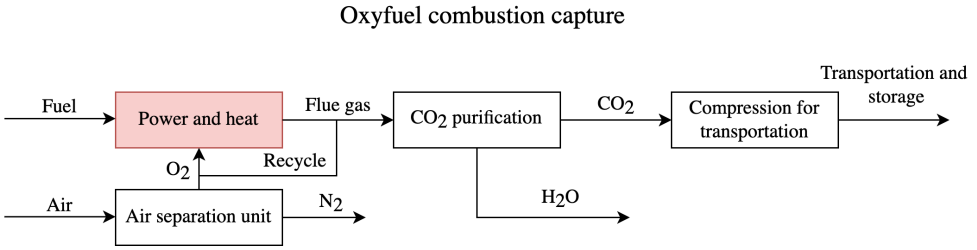

Figure 2.4: Flow chart for an oxyfuel-combustion capture process.

Direct Air Capture (DAC)

Today, there are two technology approaches for capturing CO_2 directly from the air: liquid and solid DAC. Liquid DAC passes air through chemical solutions such as hydroxide solutions, which removes the CO_2. Solid DAC uses solid sorbent filters that can bind chemically with CO_2. When the filters are heated and placed under a vacuum, they release the concentrated CO_2, which is then captured for storage or use (Budinis 2021). There are currently 19 DAC plants operating worldwide, capturing only 0.1 Mtpa. Most of them sell their CO_2 to other industries, such as the carbonated drink industry. The first large-scale DAC plant is under construction in the US and aims to capture 1 Mtpa for storage.

2.2 Transportation

CO_2 is used as a raw material in industries such as enhanced oil recovery (EOR) and the food and beverage industry (Metz et al. 2005), resulting in a demand for large-scale transportation methods. Today, CO_2 is transported in pipelines when used for EOR or by ship, truck, or rail for the smaller volumes in the food and beverage industry. While being a mature market, there is still a need for research and development within transportation for CCS purposes due to the significant volumes of CO_2 associated with CCS (Gassnova 2019).

In the CCS context, where volumes range megatonnes of CO_2, only transportation of CO_2 by ship or in pipeline systems is considered feasible (Metz et al. 2005). Many studies have compared the two transportation methods (Skagestad et al. 2014, Apeland et al. 2011 and Roussanaly et al. 2014). Which transportation method to choose for a particular CCS project is heavily dependent on aspects such as distance from the source to the injection well, expected annual amount of transported CO_2, the time horizon for the project, and the price of the technology. When comparing pipelines and ship-based transportation, pipelines are considered the most viable option for short distances and high volumes. In contrast, shipping may be more economical for longer distances and smaller volumes (Roussanaly et al. 2014). The transportation options and their associated supply chain elements are described below.

2.2.1 Transportation by pipelines

In this thesis, two types of CO_2 pipeline transportation are addressed: onshore and offshore pipelines. Pipeline transportation of CO_2 is done by compressing the CO_2 to a supercritical fluid and moving it through pipelines at high pressure. Pipeline transportation of CO_2 is a mature concept. There exist over 50 CO_2 pipelines with a combined length of 6600 km in North America alone. The North American pipelines transport 60 Mtpa, primarily for enhanced oil recovery purposes (Debarre et al. 2021). In 2018, 17 operational industrial-scale CCS projects used pipeline transportation, with an accumulated capacity for capturing, transporting, and storing 31.2 Mtpa (Onyebuchi et al. 2018). From an economic perspective, pipelines are subject to high capital expenditures (CAPEX) compared to ships (Skagestad et al. 2014). This means that for a large-scale deployment of pipelines as a transportation option for CCS, the commercial interest and demand for CCS solutions must be high. Pipelines also bring more risk to the investment decision, as it is a less flexible option than ship transportation. While ships can be redesigned and used for purposes other than CCS, such as LPG shipping, offshore pipelines will not necessarily have that property due to strict technical regulations. Thus, pipelines will have limited residual value (Apeland et al. 2011). However, pipelines can handle large volumes of CO_2 over short distances in a cost-effective way, as low operational expenditures (OPEX) ensure economies of scale.

Pipeline CO_2 transportation conditions

The design and composition of the pipeline transportation system are dependent on several factors. The main factors are the temperature and pressure of the CO_2 to be transported, the gas mixture, the required capacity, topographic conditions, and the length of the pipeline. There are four feasible pipeline transportation conditions

for CO_2; gaseous, liquid, dense, and supercritical state transportation, which can be seen as a midway between gaseous and liquid. The temperature and pressure combinations corresponding to these conditions can be seen in Figure 2.5. While all are feasible, supercritical state transportation has become the standard practice. Supercritical state transportation has advantages over gaseous transportation due to lower volume, higher density, and lower pressure losses (Peletiri et al. 2018). These advantages also apply to liquid transportation, reducing volume and pressure losses compared to the supercritical state. However, the liquefaction process is costly, and to ensure single phase flow through the pipeline, it requires extra insulation of the pipelines in warmer climates.

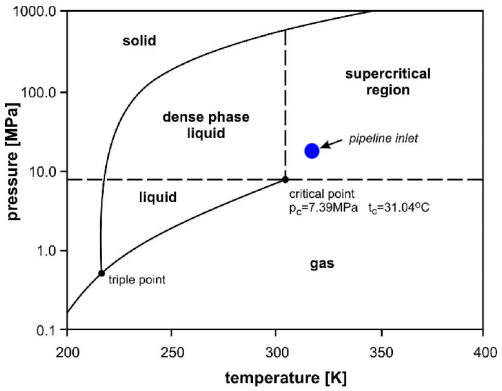

Figure 2.5: A phase diagram for CO_2 (Witkowski et al. 2014).

Pipeline design: material and dimensions

The material used in pipelines is carbon steel, which is seen as the most economical option (Noothout et al. 2013). However, carbon steel is vulnerable to corrosion when the CO_2 stream includes water, and thus requires dehydration of CO_2 streams with water content above the allowable limit, which is 50 ppmv (parts per million volume) for European offshore pipelines. Therefore, external corrosion prevention is done through cathodic protection, sometimes combined with a protective coating.

The pipeline's inner diameter must be compatible to handle a given flow rate of CO_2 at a specified temperature and pressure. There is a direct connection between the pipeline's maximum capacity and the inner diameter. The optimal pipeline diameter is the smallest diameter that is large enough for a given volume transported without resulting in excessive velocities. The optimal pipeline diameter avoids excessive pressure losses and reduces the number of boosting stations needed to handle a given volume of CO_2.

Pipelines must have sufficient wall thickness to withstand the flowing and surrounding pressures. The maximum operating pressure dictates the pipe wall thickness, and pipes with higher thickness can withstand higher pressure without failing.

Compressors and booster stations

Compressors are needed to convert the gas from atmospheric pressure to the supercritical state. The compressor stations can be divided into two subgroups: the originating compressor at the start of the pipeline and booster stations placed along the pipeline. The latter compensates for pressure drops due to friction and elevation losses and is installed to keep the pressure of the CO_2 flow above the critical point of 73.8 bar. In general, the longer the pipeline, the more compressor power is needed to transport the CO_2 to its destination at the required delivery pressure. Several booster stations can be placed along an onshore pipeline to handle the pressure drop. Many studies regarding CO_2 pipeline design indicate that a booster station is needed roughly every 200km of pipeline (Knoope et al. 2013). The size, power, and number of compressors also depend on the pipeline diameter, wall thickness, and topography.

Offshore pipelines cannot rely on intermediate booster stations for practical and technical reasons and thus require higher inlet pressure from the originating compression (Ogden and Johnson 2010) to handle the pressure drop. The higher inlet pressure requires thicker pipeline walls than otherwise equivalent onshore pipelines, making offshore pipelines more expensive.

Metering stations and valves

Metering stations are placed periodically along the pipelines to allow monitoring and management of the CO_2 in the pipes. They measure the flow of CO_2 along the pipelines without impending the CO_2 movement and allow tracking of the flow through the pipeline. Valves control functions around compressor and metering stations and at the injection sites. By placing valves along the pipeline, one can isolate sections of the pipeline in case of leakage or maintenance. Therefore, one crucial consideration in pipeline design is the distance between valves. Valves are often installed more frequently near critical locations such as urban areas to ease maintenance and repairs in case of leakage or rupture.

Control stations

Sophisticated control systems are required to monitor the status of the CO_2 pipelines at any time. Centralized control stations collect and manage data received from monitoring and compressor stations along the pipe. Supervisory control and data acquisition systems continuously measure the flow rate through the pipeline and track the operational status, pressure, and temperature. These systems allow for swift responses to equipment malfunctions, leaks, or unusual activity along the pipeline. They also allow for remote operations of, e.g., compressor stations to immediately adjust flow rates in case of any unforeseen events.

2.2.2 Transportation by ship

Today's commercial transportation of CO_2 by ship is done with CO_2 in a liquid state at pressure levels between 15 and 20 bar, temperatures between -20 °C and -30 °C and with ship capacities of approximately 1000 tonnes (Amlie et al. 2018). Transporting CO_2 in a liquid state rather than as gas allows for transportation of more CO_2 for a given ship size due to the higher density of the liquid. When determining the ship designs for CO_2 transportation in the context of CCS, one must decide on

tank sizes, pressure, and temperature conditions for the tanks. These decisions are affected by the characteristics of the location, the structure of the CO_2 sources, and the purity of the CO_2. Ship transportation of liquid CO_2 is considered for various CO_2 conditions, including high-, medium-, and low-pressure with corresponding temperatures. An overview of the transportation conditions for liquid CO_2 with corresponding pressures, temperatures, and densities is presented in Table 2.1.

Table 2.1: Liquid CO_2 transportation conditions with corresponding ranges for pressure, temperature and density (Amlie et al. 2018).

Pressure range	**Temperature (°C)**	**Pressure (Bar)**	**Density of liquid (kg/m^3)**
High	30	72	607
	10	45	861
Medium	-19.5	20	1029
	-30	14	1076
Low	-41	9.8	1119
	-55	5.5	1173

Choosing ships as the desired means of transportation leads to several ship-specific network design specifications, as can be seen in Figure 2.6. In addition to the ships themselves, the specifications include liquefaction and reconditioning facilities, buffer storage, and loading/unloading equipment when shipping between onshore ports. The alternative to shipping between onshore ports is shipping from an onshore port to an offshore site. The offshore site can either be a platform or a submerged turret loading buoy (STL-buoy) that facilitates direct injection from the transporting ship. The platform can either be a floating rig or another ship located at the water surface above the geological storage point, facilitating unloading, buffer storage, reconditioning, and the injection to geological storage. In the direct injection scenario, the ship itself is equipped to pressurize and heat the CO_2 to reach the condition required for permanent storage and to pump the CO_2 to the geological storage through the STL-buoy. However, the "shipping to an offshore site"-networks require more research and development to be feasible and are of higher technical complexity than the port-to-port networks (Gasnova and Gassco 2016). Therefore, we present the different parts of the ship-specific port-to-port supply chain to give a better understanding of the ship-based CO_2 transportation option that is considered in this thesis.

Liquefaction

For the shipping of CO_2 to be cost-effective, the CO_2 should be in liquid form instead of gaseous. At atmospheric pressures, CO_2 can only be either gaseous or solid. It is not economically viable to transport CO_2 by ships in neither gaseous nor solid form. For the gaseous form, this is due to the low density of the CO_2. For the solid form, it is because of the significant effort required to load and unload the CO_2. Therefore, CO_2 transportation is performed with CO_2 in a liquid form, at pressures above atmospheric pressures as presented in Table 2.1. The liquefaction process consists of a combination of stages of cooling and compression of the CO_2 to reach the desired temperature and pressure. The process has two design options, namely *closed* and *open* systems. They differ in the way the system cools the CO_2. The closed systems use an external refrigeration system, while the open system cools the CO_2 solely by

compression and expansion. For both systems, removal of water and other contaminants is necessary to prevent hydration, freezing, corrosion, and dry ice formation (Amlie et al. 2018).

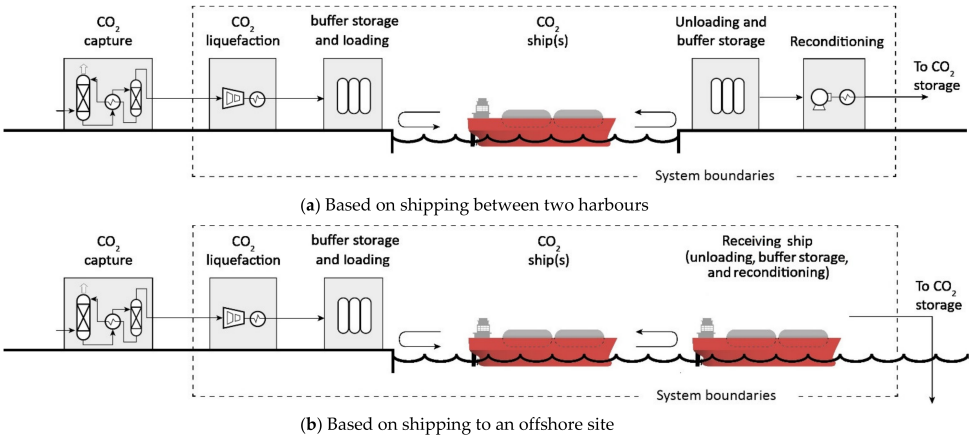

(**a**) Based on shipping between two harbours

(**b**) Based on shipping to an offshore site

Figure 2.6: The two types of ship-based CO_2 transportation networks, with the system boundaries for ship transportation (Roussanaly et al. 2021).

The main input factor in the liquefaction process is the electricity needed for compression and refrigeration. The energy requirement is dependent on the CO_2 condition when entering the liquefaction unit. The CO_2 can be either pressurized if transported to liquefaction through pipelines or at atmospheric pressure if it is liquefied directly after the capture process. The energy requirement also depends on the desired condition of the CO_2 after the liquefaction process. The preferred pressure level and temperature depend on the buffer storage and ship tank designs. Since the first stage of the liquefaction process usually is compression, the energy requirement is much smaller if the CO_2 is pre-pressurized rather than at atmospheric pressure when it arrives at the liquefaction facility. The pre-pressurized scenario would be the case if, for instance, the CO_2 is transported to liquefaction from emitters through pipelines, which usually means a pressure of between 73.8–100 bar (Amlie et al. 2018).

Buffer storage

The fact that ship transportation is a discrete batch operation and that capturing is a continuous process necessitates buffer storage (also known as intermediate storage) for temporal CO_2-storing before loading it onto the ships. The flow of CO_2 to the loading ports from the emitters is continuous, and buffer storage is needed to handle the flow when no ships are in the port. Similarly, buffer storages are needed when the ships unload the CO_2. The terms "intermediate storage" and "buffer storage" are used interchangeably in the literature, and we choose to use the term "buffer storage" for the storage operations at the ports before and immediately after the ship transportation. The specifications and designs of the buffer storage tanks are usually assumed to be similar or identical to the tanks on board the ships that are used for transportation (Amlie et al. 2018).

Several studies have discussed the size of the tanks in the buffer storage, which is

often set to a multiple of the corresponding ship tank sizes. With a larger buffer storage tank than the ship tank, one ensures some operational margin and can handle deviations from the planned ship traffic. However, if the buffer storage gets too large, it compromises the cost efficiency. Based on experience in LNG shipping and to balance the operational flexibility and cost-efficiency, Yoo et al. (2013) suggest a buffer storage size of 120% compared to the ship's tank size. The buffer tank's design, materials, and wall thickness differ based on the condition (pressure and temperature) of the stored CO_2. High and medium-pressure tanks require more steel but are the least energy-demanding, and low-pressure tanks need more energy and have high insulation requirements (Gasnova and Gassco 2016). The CO_2 will be present in both liquid and gaseous form in the tank. The bottom of the tank will contain liquid CO_2 at the given temperature and pressure, and above it, there is gaseous CO_2 at the same temperature and pressure. The gaseous share of the tank is intentional and is present to prevent a hydraulic lock, which can result in catastrophic equipment failure (Amlie et al. 2018). As the tank is filled with liquid CO_2, the pressure of the gaseous CO_2 increases, and some of the CO_2 is released. This is known as boil-off gas. Conversely, to prevent a rapid pressure drop when emptying the tank, CO_2 vapor is added during the emptying process to avoid solidification of the tank content.

Loading and unloading

The loading of the CO_2 ships happens from the shore at a loading terminal or a port. The equipment needed for loading is a ship loading pump with a head designed to transfer the liquid CO_2 from the buffer storage onto the ship. Another critical item is the loading arm, which does the actual loading. A loading arm is the preferred solution as opposed to a hose system due to lower failure rates (Vermeulen 2011). For loading of CO_2, three loading arms are needed: two liquid CO_2 lines for loading the ship and one vapor return line. The vapor return line handles the boil-off gas to prevent pressure build-up. This boil-off gas is either returned to the buffer storage tank to prevent solidification under loading or to the liquefaction facility (Amlie et al. 2018). The loading costs only account for a small portion of the total transportation costs, but the impact of the loading time can be significant. To avoid a substantial increase in loading time, the number of loading arms should increase with bigger ships. This allows us to assume that the loading time is independent of ship capacity, which is an assumption made in several studies (Amlie et al. 2018). The unloading process, meaning transferring CO_2 from the ships to onshore buffer storage before injection, requires the same infrastructure components as loading.

Ships

In the feasibility study for the Norwegian full-scale project, three different ship designs denoted low-, medium-, and high-pressure were examined for a planned annual throughput of the CCS system of 1.5 Mtpa CO_2 (Gasnova and Gassco 2016). The designs are differentiated based on pressure levels in the ship tanks, which in turn affects the required temperature of the transported CO_2 and the realizable cargo capacity. However, the different ship options in the feasibility study were designed to handle approximately the same cargo capacity. Ship capacities are either measured in tonnes or m^3. A cubic meter typically holds between 600 and 1200 kg of CO_2, depending on the density of the liquid CO_2 as described in table 2.1.

While today's commercial CO_2 ships have medium-pressure tanks, low-pressure design is seen as the most economical option due to higher theoretical loading capacities. Roussanaly et al. (2021) conclude that low-pressure ships are preferable over medium-pressure through a thorough techno-economic analysis of the two options. This conclusion is also supported by the results of Bennæs et al. (2021) which indicate that a low-pressure system is cheaper than a medium-pressure system. Amlie et al. (2018) points out that due to commercial and technological concerns, it is not considered practical with ship capacities above 10,000 m^3 for medium-pressure ships. Therefore, we only look at the low-pressure alternative for ship transportation of CO_2.

Low-pressure CO_2-ships are part of ongoing research and can, with a combination of a 7 bar pressure level and a temperature of about -50°C, enable a shipping capacity of 50 000 m^3 or more (Roussanaly et al. 2021). The ship design is based on semi-refrigerated LPG ships with big cylindrical tanks or modifications of those. The low-pressure ships will transport CO_2 with the highest density of the three ship design options, as can be seen in table 2.1. Therefore, they can be smaller than the other pressure-type ships with a similar capacity. A proposed design of low-pressure CO_2 ships is given in Figure 2.7.

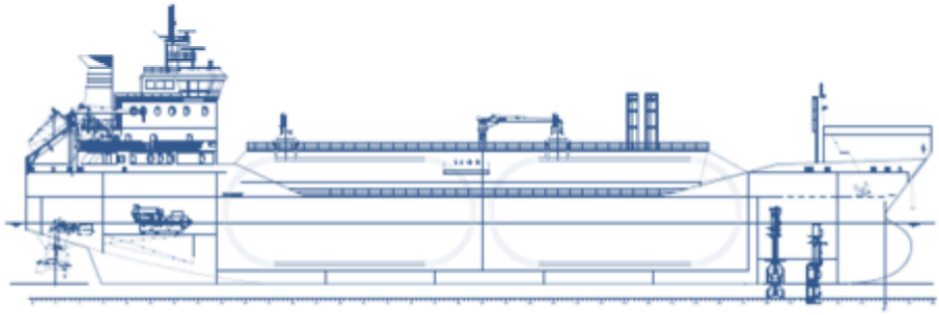

Figure 2.7: A design sketch of a low-pressure CO_2-ship with a cargo capacity of 6000–7770 m^3 (Gasnova and Gassco 2016).

During transportation, some of the CO_2 will be let out as boil-off gas to control the pressure levels in the tanks (IEA 2004). Based on the same source, the amount lost due to boil-off during ship transportation seems to hover around 0.1-0.2% of the ship's tank capacity. Technology to handle this issue is currently a research field, and Yoo (2017) presents a study on CO_2 boil-off gas re-liquefaction on CO_2 ships. Still, as this technology matures, boil-off gas from the ship tanks during transportation will continue to be an issue that needs to be considered.

Reconditioning

The CO_2 is transported from the buffer storage to the geological storage site through pipelines, which requires a pressure of about 73.8 – 100 bar. This means that the CO_2 must be transformed from the conditions of ship transportation and buffer storage to those of pipeline transportation. The process of reaching this condition is called reconditioning (Roussanaly et al. 2021). Before the injection of CO_2 into geological storage, the temperature and pressure of the CO_2 must be suitable for the geological

storage reservoir. The suitable condition depends on the characteristics of the storage reservoir, but pressures of 50–400 bar and temperatures between +15°C to +20°C are discussed in the literature (Amlie et al. 2018).

2.3 Storage

A critical feature in CCS is the actual storage of CO_2. The whole concept is based on storing the CO_2 in such a way that it will not be emitted and thus mitigate global warming. The storage is done in deep geological formations suitable for trapping the CO_2, either onshore or offshore. Examples of such formations are depleted oil and gas fields, coal formations, and saline aquifers, which is a deep underground rock formations composed of permeable materials and highly saline fluids. It is considered likely that when injecting CO_2 into carefully selected sites, 99% or more of the CO_2 will be retained for 1000 years or more (Metz et al. 2005). The actual storage operation is derived from knowledge from the oil and gas industry, including well drilling, injection technology, computer simulations of storage reservoir dynamics, and monitoring. The oil and gas industry has been the main driver of early and current applications of CO_2 storage. Injection of CO_2 into oil fields to boost oil recovery, known as enhanced oil recovery, has proven to be a successful strategy for oil production. The method has been used on oil fields in Texas since the early 1970s, and it is a widespread methodology in the world today. Equinor has been successfully capturing and storing 1 Mtpa CO_2 in the Sleipner field since 1996 and 0.7 Mtpa since 2008 from the separation process of CO_2 and natural gases on the Snøhvit field.

The storage part of the supply chain differs from the rest, as establishing a storage site requires a series of phases and activities to be realized. The storage also has a naturally restricted lifetime based on its capacity, making it a limited resource. ZEP (2011) describes the lifecycle associated with CO_2 storage in terms of phases to give an overview of the complete process.

The first phase, named potential storage, includes an initial screening of multiple sites, the characterization of selected sites, and the permitting process. This is a costly process, as drilling and examining exploration wells to review the characteristics of potential storage sites are needed before choosing one site. The sites must also go through injection tests to appraise the injectivity and capacity of the field on a large scale. Finally, a storage permit application must be completed before the phase ends with a final investment decision.

The operational storage phase includes preparing a field development plan, constructing and installing necessary infrastructure, and commissioning and injection operations. When the field development plan is finished, the construction and installation of infrastructure can begin. The construction refers to injection well drilling, which is similar to offshore oil wells. According to Equinor (2019), the infrastructure includes two main components in addition to the actual well. The first is a land-connected umbilical system that provides power, signal, and fluids to control, monitor, and operate subsea wells. The second is a subsea facility that connects the feeding transportation pipelines, well, and umbilical. This facility should also have additional connection opportunities to extend or reuse the infrastructure when extending/moving to different injection sites. An example of such a facility can be seen in Figure 2.8.

When the storage site is operational and injection takes place, control, monitoring,

measurements, and verification are critical operations. These are done through an onshore control center connected to the well through the umbilicals. The operations and maintenance of the well and infrastructure are assumed to be similar to that of oil and gas operations.

The third phase, closure, occurs when the injection point's storage capacity is reached. Then, the injection well and offshore structure are decommissioned, and the well is plugged and abandoned. However, the monitoring of the wells continues to make sure that regulatory requirements regarding containment of the CO_2 are met.

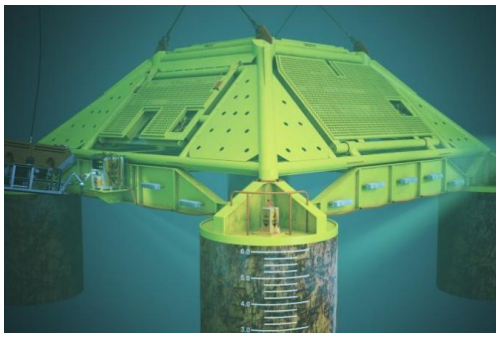

Figure 2.8: Northern lights subsea storage facility: a pilot satelite structure with suction anchors and trawl protection (Equinor 2019).

2.4 Global CCS development and relevant ongoing projects

According to Kearns et al. (2021), there are 135 commercial CCS projects today on a global basis. 27 of these projects are operational, four are under construction, 102 are in early or advanced development, and two are suspended. The total operational capacity of capture and storage sums up to 36.6 Mtpa. In contrast, the capacity, including the projects under construction and development, adds up to a future total of 147.2 Mtpa. Most of the currently operational projects capture the CO_2 from natural gas processing, such as the Norwegian Snøhvit and Sleipner projects described in Section 1. The projects under construction and development will contribute to a more diverse selection of emission sources. They plan to capture from industries like coal-fired and natural gas-fired power generation, chemical and petrochemical production, and the production of hydrogen, fertilizer, ethanol, cement, iron, and steel.

Historically, CCS projects have been vertically integrated, where each capture plant has its own downstream transportation system. This favors large-scale capture projects which can benefit from economies of scale. However, the trend now is an emergence of collaborative open source CCS networks where CO_2 capture projects share the transportation and storage infrastructure, including pipelines, ship transportation, port facilities, and storage wells. CO_2 hubs are centralized ports that can collect CO_2 from several capture sites for further transportation. By establishing such hubs, the costs for the involved capture sites can be reduced. Thus, these networks contribute to making small scale CO_2 capture projects (0.2 Mtpa or smaller) viable. There

are 32 such CCS networks worldwide, either in operation or early or advanced development. Most of the networks use, or plan to use, pipelines or a combination of pipelines and ships for transportation. Examples of such networks are the Northern Lights project (1.5-5 Mtpa), the dutch Aramis CCS network (3-12 Mtpa), the french Dartagnan project (4-6 Mtpa), the American Summit Carbon Solutions project (12 Mtpa) and the german BlueHyNow project (30-40 Mtpa).

Figure 2.9 gives an overview of the Aramis project. The figure shows how the port of Rotterdam could work as a hub that collects CO_2 from surrounding emission sources through ship transportation on rivers, canals, and the sea. The hub can then send the CO_2 through an offshore pipeline to a storage reservoir consisting of depleted oil and gas fields in the north sea.

Figure 2.9: The transportation network in the dutch Aramis project with emission sources, collecting CO_2 hub in Rotterdam and pipeline transportation to storage in a depleted oil and gas field in the North Sea (Aramis 2022)

The Summit Carbon Solutions project plans to partner up with more than 30 ethanol plants across a five-state region in the US. They intend to capture CO_2 from ethanol plants in Iowa, Minnesota, North Dakota, South Dakota, and Nebraska, compress it, and transport it through an extensive onshore pipeline network to geological storage locations in North Dakota (Summit Carbon Solutions 2022). The onshore pipeline network, which is of a similar extension as some of the networks studied in this thesis, can be seen in Figure 2.10.

Another interesting project for this thesis is the German BlueHyNow project, governed by Wintershall Dea. They plan to produce eco-friendly hydrogen from natural gas in Wilhelmshaven and to capture, transport, and store the CO_2 emissions from the hydrogen production process in the North Sea. After establishing this combined hydrogen and CCS initiative, the goal is to make Wilhelmshaven a centralized hub for collecting and exporting CO_2 emissions of 30-40 Mtpa by 2040 from many energy-intensive industries from all over Germany (Wintershall Dea 2022). The port of Wilhelmshaven has an advantageous location and design for being a CCS hub. It is a deepwater port with the possibility of docking large tankers, and it is near the North Sea and its potential storage locations.

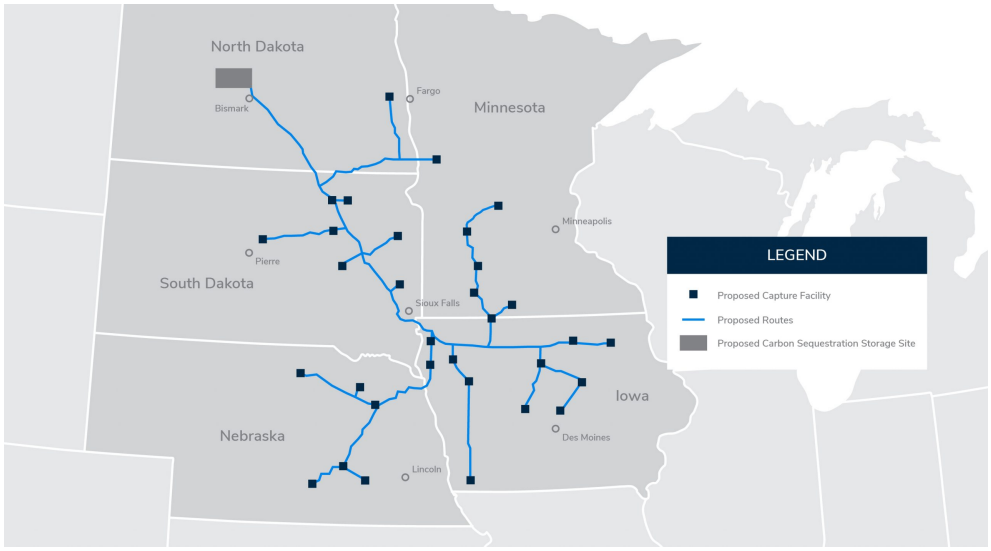

Figure 2.10: Illustration of the planned pipeline network in the Summit Carbon Solutions project (Summit Carbon Solutions 2022).

Northern Lights is a sub-project of the Norwegian full-scale CCS project known as Longship and makes up the transportation and storage part of the Longship supply chain. Longship is a Norwegian CCS project that includes capturing CO_2 from industrial sources in the Oslofjord region and shipping liquid CO_2 to an onshore terminal placed in Kollsnes on the Norwegian west coast. From there, the liquefied CO_2 is transported in offshore pipelines to a storage site on the seabed in the North Sea for permanent storage. The Longship project includes both Northern Lights and the capture processes at two Norwegian industrial emission sources, namely Norcem cement factory, and Fortum Oslo Varme waste-to-energy factory. In addition, Northern Lights aims at offering transportation and storage of CO_2 as a service for other European emission sources. Recently, a letter of intent between Northern Lights and Cory, a British recycling and waste-to-energy company, has been signed (Northern Lights 2022). The agreement is about collaborating on a CCS project where Cory, by 2030, wants to capture 1.5 Mtpa CO_2 from their waste to energy plant located in London, UK, and transport and store it on the Norwegian shelf with the help of Northern Lights.

The concept of the Northern Lights project is an open and flexible infrastructure to transport CO_2 by ship from capture sites to a terminal in western Norway for intermediate storage and then further transport the CO_2 through pipelines for permanent storage in an exploration field named EL001 in the Johansen saline aquifer formation on the Norwegian shelf. According to Equinor (2019), the initial long-distance transportation infrastructure consists of one ship for each of the two capture sites, each with a capacity of 7 500 m^3 and medium tank pressure. It includes onshore reconditioning facilities and buffer storage with capacities based on the ship capacities. Furthermore, the system has an export pump and heater for conditioning the CO_2 for transportation along the 100 km offshore pipeline. In addition, there are umbilical systems for controlling and monitoring pipelines and subsea facilities for connecting the pipeline, umbilical, and injection well, as shown in Section 2.3. The first phase of

the project, which will be completed by mid-2024, will have a capacity of up to 1.5 Mtpa. With an already planned CO_2 supply from Norcem and Fortum Oslo Varme of up to 0.8 Mtpa, there is an excess capacity of 0.7 Mtpa in this initial phase. The plan is to offer this excess capacity to ongoing and planned CO_2 capturing projects in Europe, like the Cory project. Dependent on the market demand, Northern Lights' ambition is to expand the capacity to 5 Mtpa in its second phase. Figure 2.11 shows the building blocks of the initial phase of Northern Lights.

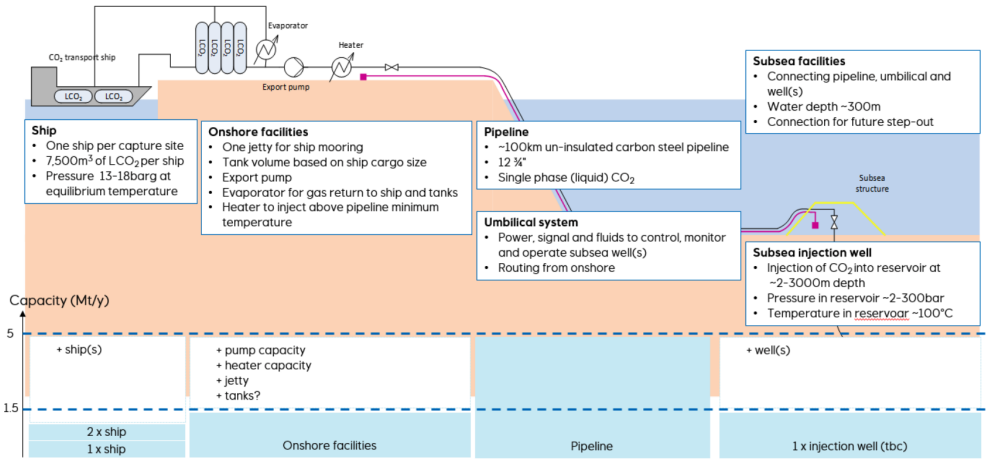

Figure 2.11: Northern Lights concept building blocks with capacities in the first phase shown with blue shading (Equinor 2019).

The development of CCS projects has historically been risky, a statement supported by the fact that the planned capacity for the worldwide development of CCS projects decreased year by year from 2011 to 2017 (Kearns et al. 2021). However, with the recent COP26 meeting and the Paris Agreement, the need for comprehensive solutions mitigating CO_2 emissions is even more evident today than before. In Sandberg et al. (2019), the future development of the Northern Lights project in the European CCS context is assessed. Different captured volume scenarios are established based on an expected increase in demand for CCS in the future. The first two scenarios are the 1.5 and 5 Mtpa scenarios, which are already under development and construction. Another potential scenario is the 20 Mtpa scenario, which can be triggered by a general increase in demand for Northern Lights' services in Europe, scale-ups of existing value chains already connected to Northern Lights, or a shift from medium-pressure to low-pressure ships enabling higher transportation volumes. The final scenario presented by Sandberg et al. (2019) is the 100 Mtpa scenario, in which Northern Lights would be a part of an extensive European network for CCS, where ship and pipeline transportation complement each other. Trigger points for this scenario are a further upscaling of CO_2 capture at already connected CO_2 sources and well-established CCS clusters around the North Sea and the Baltic Sea. The 20 Mtpa and 100 Mtpa scenarios are mainly dependent on successful research and development, uncertain demand forecasts, and an imposed cost of emitting carbon that makes CCS economically viable. Either way, the scenarios describe a possible future development in the European CCS industry.

2.5 Carbon pricing policies

As discussed above, many investments are required to implement a CCS supply chain, making CCS costly for industrial actors. On the other hand, just emitting CO_2 implies several high social costs. A standard political tool to reduce CO_2 emissions is to charge the emitters with a monetary cost per tonne of emitted CO_2, which is commonly referred to as a *carbon price*. This makes the emitters pay for their emissions, which in turn reduces their incentives to emit. Currently, 65 pricing initiatives are implemented globally, and in 2021, these covered 21.5% of the global emissions (The World Bank 2022). There are several ways of pricing carbon, and two common ways are taxation and Emission Trading Systems (ETS). Emission trading systems are also referred to as cap-and-trade systems, where there is a maximal allowed total emission within the system (a cap), and the parties within the system need to trade emission allowances. A tax system makes the price predictable, while ETS makes the emissions predictable. The ETS prices are determined by the supply and demand for emission allowances.

The cost of emitting one tonne of CO_2 is dynamic. For ETS systems, they are dynamic by nature, while tax rates could be adjusted over time. Figure 2.12 shows the development of the carbon price in the ETS system for the European Union (EU ETS). As the figure shows, the trend is increasing carbon prices over time. Moreover, the increase is relatively rapid, growing from around 35 euro per tonne to 80 euro per tonne in the recent 16 months. The European Commission has reduced the number of emission allowances in recent years. They will continue to reduce the number of allowances at a rate of 2.2% each year between 2021 and 2030. As the supply of emission allowances steadily decreases, the price may increase further in the coming years. Another example of increasing carbon prices is that the Norwegian Government aims to increase the carbon price from the 2021 level of around 69 euro per tonne to around 200 euro per tonne in 2030 (The Norwegian Government 2020).

The discussion of current and future carbon prices will be helpful when we present the economic implications of building a full-scale CCS supply chain in Chapter 7. If the cost of CCS is lower than the current or future carbon prices, it indicates that CCS could be a beneficial option to consider for companies and governments.

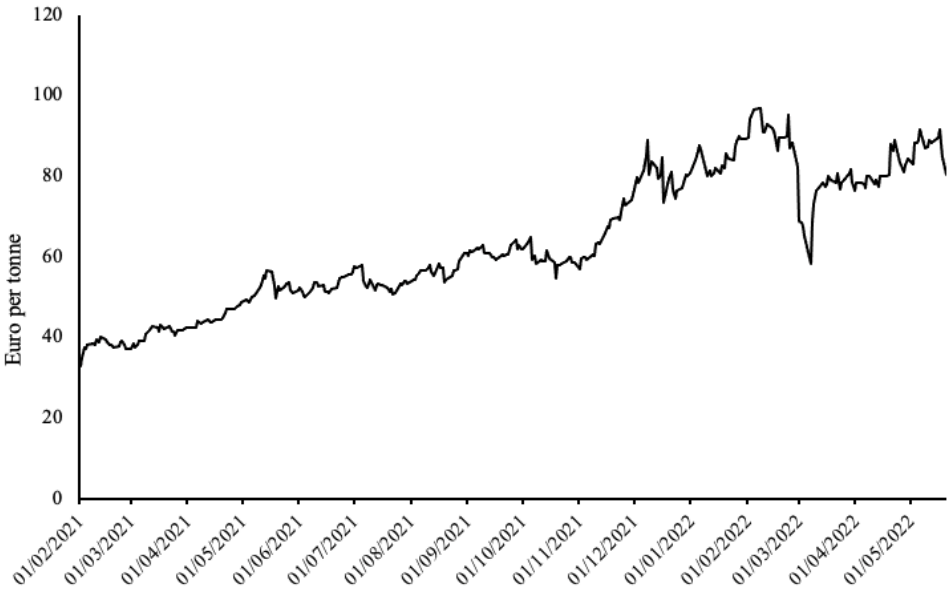

Figure 2.12: Price of emitting one tonne of CO_2 within the ETS in the European Union from early 2021 (Ember 2022).

Chapter 3

Literature Review

The problem of this thesis is to design an optimal supply chain for CCS, referred to as the CCS Supply Chain Design Problem (CCS-SCDP). A supply chain may be defined as an integrated network of facilities and transportation options for supplying, manufacturing, storing, and distributing materials and products (Garcia and You 2015). Supply chain design is an extensive research area. Models that aim at deciding the best possible supply chain design through various metrics have been applied to many industries, including the CCS industry. However, much of the research on CCS has focused on more granular optimization approaches such as capacity planning, operations, and process design, which focuses more on specific elements such as technologies and equipment rather than a full-scale supply chain. As we aim to develop a model that touches on all these aspects, we have collected and reviewed relevant literature that solves problems in different parts of the supply chain and the supply chain as a whole. As our thesis investigates supply chains with maritime components, Section 3.1 reviews literature related to CCS offshore transportation. Section 3.2 gives an overview of relevant studies on CCS onshore pipeline transportation, and Section 3.3 gives insight into literature that takes a broader CCS supply chain perspective. Finally, in Section 3.4, we summarize our contribution to the existing literature.

3.1 CCS offshore transportation

In the early and impactful CCS report from Metz et al. (2005), both pipeline and ship transportation were considered feasible for offshore CO_2 transportation. Aspelund et al. (2006) present a novel study on technical solutions for ship-based transport of CO_2 for enhanced oil recovery and do a cost and energy utilization analysis including dedicated ships, liquefaction, buffer storage, and offshore unloading using a commercial simulation tool. The study identifies CO_2 ship transportation conditions of 6.5 bar and -52 °C, referred to as low-pressure, as optimal. Since then, much of the work regarding ship transportation of CO_2 has been focusing on techno-economic cost estimation, feasibility studies, and comparison of ship and pipeline transportation, often with the ship transportation conditions presented in Aspelund et al. (2006) as an assumption.

The recent in-depth cost estimation study by Roussanaly et al. (2021) investigates the impact of the choice of low-pressure or medium-pressure (15 bar) ship transportation. They perform a general analysis for volumes of up to 20 Mtpa and transportation distances up to 2000 km. The analysis includes vital elements in the ship-based CO_2 transportation chain, where thorough cost estimates are calculated for liquefaction, intermediate storage, sailing, and reconditioning. As in Aspelund et al. (2006), the results point towards low-pressure as the optimal condition, with a cost reduction of 15% compared to medium-pressure. However, Roussanaly et al. (2021) point out that medium-pressure could be chosen in near-term implementations of CO_2 ship transportation due to its technological maturity compared to low-pressure. Nevertheless, since medium-pressure ships are limited to capacities of 10 kt, and our model of the CCS-SCDP aims to handle dozens of megatonnes of future CO_2-emissions, low-pressure ships are considered the most relevant for our model.

Roussanaly et al. (2014) use a CCS supply chain simulation tool to benchmark offshore pipeline transportation and low-pressure ship transportation to an offshore storage site in a base case analysis for a range of distances and yearly volumes. The ship capacities investigated are 25 to 50 kt. The results show that the switching distance, from where ships become cheaper than pipeline transportation, is 225 km for 2 Mtpa and 625 km for 20 Mtpa. The ship transportation technology used in Roussanaly et al. (2014), shipping to an offshore storage site, means that the ships are equipped with reconditioning and pumping capacities to facilitate the injection of CO_2 into the geological storage at sea. This is a less mature transportation technology than CO_2 ship transportation between two ports, which is used in our model of the CCS-SCDP. Roussanaly et al. (2013) achieve similar results using the same simulation tool to compare low-pressure ship transportation and *onshore* pipelines between ports. While both papers derive system costs and compare them for pipeline and ship transportation, they do not include the opportunity to combine the two transportation modes, which our model of the CCS-SCDP does.

Kjärstad et al. (2016) investigate offshore CO_2 transportation modes and their associated costs for CO_2 sources in the Nordic region through a module-based cost estimation methodology. Thus, costs of the relevant supply chain components of both ship and offshore pipeline transportation are calculated as a function of either volume, distance, or both. As in Roussanaly et al. (2014), low-pressure ships of up to 50 kt are considered. The study includes several Nordic emission sources and found that ship transportation was the cheapest option. Relatively modest CO_2 volumes, long distances, and the cost of underutilized pipelines are key drivers of these results.

While cost assessments have been the most common approach in research regarding offshore CO_2 transportation since the report from Metz et al. (2005), there has been a development in more recent times where optimization models have become part of the studies. Nam et al. (2013) formulate a strategic MIP to decide on the design of a ship-based offshore CCS transportation system in Korea. They divide the optimization problem into two subproblems; a CO_2 liquefaction plant location problem and an offshore CO_2 transportation problem. The former minimizes costs by determining the location and number of liquefaction facilities to which emission sources connect by pipelines. As opposed to our model, Nam et al. (2013) disregard docks and loading equipment and only consider liquefaction facilities with buffer storages of a predefined capacity. The goal of the transportation subproblem is to determine the optimal ship fleet size and mix (number and ship types), deployment (ship-to-route assignment),

and route service frequency (number of round trips) to transport annual volumes of CO_2 from the liquefaction plants to the offshore storage sites. The transportation subproblem is formulated more strategically than our formulation of the CCS-SCDP. For instance, it does not take into account the operational feasibility in terms of loading times and simultaneous docking of ships.

3.2 CCS onshore pipeline transportation

Researchers have also worked on methodologies to estimate the costs of CO_2 pipelines. Knoope et al. (2013) does a comprehensive review of cost models for CO_2 pipelines and booster stations. They found two main types of capital cost models: models where the costs are based on pipeline diameter and models where the costs are based on the amount of CO_2 flow through the pipeline. Knoope et al. (2013) found that the resulting capital costs of pipelines for a given mass flow and length varied by a factor of 10 when comparing different cost models. Furthermore, the cost range increased even further when adding operations and maintenance costs. The same conclusion applied to the cost of booster stations.

Chandel et al. (2010) present a techno-economic model that computes the cost of transporting captured CO_2 through pipelines of different diameters and distances. The study shows that pipeline transportation costs can be significantly reduced by using a large diameter trunk line that aggregates the CO_2 from the emission sources. They also investigate the difference between a single-diameter and a multiple-diameter (telescoping) trunk line. The multiple diameter trunk line increases its diameter and capacity as emission sources are connected to it, which is similar to how the onshore pipeline network is modeled in the CCS-SCDP. They find that the capital cost of the multiple diameter trunk line is much lower. Generally, there are significant economies of scale connected to trunk lines as opposed to each emission source connecting to the destination.

While Chandel et al. (2010) investigate the effects of oversized pipelines and telescoping trunk lines, another question is what to do if the supply of CO_2 increases with time. This is the scope of Wang et al. (2014), where they develop a two-stage methodology for the optimal design of onshore pipelines with a projected increase in CO_2 flow rate. They compare the cost of CO_2 transportation using an oversized pipeline design against the cost of using duplicate pipelines under different volume increase scenarios and lengths. They conclude that oversized pipelines are more attractive for shorter pipeline distances and less attractive for greater flow rates.

The optimization of CO_2 pipeline transportation is also about designing the most cost-optimal network of pipelines. As opposed to ships, which are flexible in what loading and unloading ports they visit, pipelines cannot easily be redirected or moved. Combined with the high capital cost associated with pipelines, the placement of the pipelines is of high strategic importance when determining the design of a CCS supply chain. Middleton and Bielicki (2009) develop a model to design a scalable transportation network for CCS, with onshore pipelines as the only transportation mode. By formulating a MIP, they decide the optimal geospatial arrangement and cost of a CCS pipeline system. The model is demonstrated on a network of 37 emission sources and 14 storage locations in southern California, with volumes of up to 50 Mtpa. Morbee et al. (2012) present a model that determines an optimal EU-wide pipeline

CO_2 transport network. The goal is to describe a likely extent and cost of a CO_2 transport network on a European scale. Through some methodological improvements compared to Middleton and Bielicki (2009), they achieve a computationally tractable pan-European model with close to 100 CO_2 clusters and storage locations combined. The novelty of the work lies in the high number of nodes in the network compared to previous work and the allowance of a gradual build-up of network extent and capacity over time.

3.3 CCS supply chain design

Since offshore transportation is a key element of the CCS-SCDP, we focus on supply chain design problems that include offshore transportation in this section. d'Amore et al. (2021) take a system-wide CCS supply chain design approach, and present a MIP model to determine the optimal design of a European CCS supply chain. The model comprises capturing CO_2 at European emission sources, ship transportation, offshore and onshore pipeline transportation, and storage. The solution of the model provides the optimal selection, sizing, and location of capture alternatives across different sectors, and the optimal transportation modes, with particular attention to choosing pipelines or ships to connect CO_2 sources to onshore and offshore geological storage sites. The broad scope of the model leads to a series of assumptions to reduce solving time. A notable assumption made in the model is that only medium-pressure ships with 10 kt capacity are available. This limits the usability of ship transportation, as it leads to a substantial increase in the number of ships needed to transport a given volume of CO_2, and hence also the cost, compared to using larger low-pressure ships (Roussanaly et al. 2021). Through a series of case-based scenarios reflecting variations in country-wise and European CO_2 reduction targets and restrictions regarding the allowance of onshore storage, d'Amore et al. (2021) conclude that European CCS collaboration can be economically desirable. Furthermore, they conclude that by only allowing offshore storage at offshore locations in the North Sea, the total supply chain cost per tonne increases by more than 20 euro from 60.5 to 81.4.

A recent study from Bjerketvedt et al. (2022) develops a multi-period strategic investment model to analyze the deployment of a CO_2 ship transportation infrastructure from nine Norwegian and Swedish industrial emission sources. Over a set of four two-year time periods, the model makes decisions on buffer storage investments, liquefaction, and reconditioning capacities, and decides the number of round trips needed on a set of predefined routes to transport a given yearly volume of CO_2. The model also allows for connecting more emission sources to the network in each time period. Thus, it can extend the supply chain and upgrade capacities as CCS demand increases. For emission sources close to each other, the model allows for establishing pipeline connections between them to form a hub with a shared port. In a case analysis, they apply the model to a network of nine emission sources located in the southern parts of Norway and Sweden and with storage capacity and infrastructure from the Northern Lights project in Kollsnes. By gradually extending the supply chain with 1–4 emission sources over a period of six years, and with volumes increasing from 0.8 Mtpa to 3.3 Mtpa, they achieve transportation costs of 32.8 euro per tonne. The study captures the vital feature of making investments dependent on the CCS development and how the transportation system should be adapted to future increased demand for CCS. However, the model only considers supply chain components related to ship transportation, and capture and storage are not included.

A recent study from Bjerketvedt et al. (2020) takes a more operational approach than the previously described models and investigates the impact of operational fluctuations and uncertainties on the design and expected cost of ship-based CO_2 transportation. The model is a two-stage stochastic capacity investment model for a ship-based CCS supply chain with one ship servicing one emission source and one storage site. Bjerketvedt et al. (2020) make investment decisions on the capacities of liquefaction, buffer storage, and reconditioning in the loading and unloading port. The optimal investment decisions are driven by the expected cost of operating the supply chain in stochastic scenarios. The model has a cost-minimizing objective function and decision variables regarding investments in capacities at the loading and unloading ports, inventory levels, and choice of speed strategies for the ships. Bjerketvedt et al. (2020) conclude that a buffer storage capacity of 118% of the ship capacity may be optimal to balance the uncertainties related to weather conditions. It also shows through a sensitivity analysis that seasonal variations in emissions lead to a preference for larger ships compared to when there are stable capture rates.

There are many similarities between the CCS and liquefied natural gas (LNG) supply chains. Natural gas is liquefied in order to be transported by ships from production plants to consumer markets in the LNG supply chain. This process includes many of the same elements as the ship-based CCS supply chain, such as liquefaction, reconditioning, buffer storage, and routing of ships. Bittante and Saxen (2020) develop a multi-period MIP model for designing a small-scale supply chain for LNG. Both tactical and strategic aspects in the supply chain design are addressed. The model formulation aims at minimizing the cost through decisions regarding time-discrete routing of a heterogeneous fleet of ships, truck connections from ports to inland customers, sizing of buffer storage, and location of satellite terminals. The supply chain is similar to that of CCS. However, instead of handling a supply of CO_2 from several emission sources as in the CCS supply chain, the LNG supply chain handles a supply from one supplier and distributes it to several customers. Furthermore, Bittante and Saxen (2020) do not include pipelines as a transportation mode, as offshore transportation is handled by ships, and onshore transportation is handled by trucks.

3.4 Our contribution to the literature

With this thesis, and with our model of the CCS-SCDP, we aim to broaden the scope of operations research within CCS and provide valuable decision support for the problem of designing operationally feasible maritime CCS supply chains with realistic cost estimates. To achieve this, we have developed a MIP model that encapsulates the entire CCS supply chain, including both onshore and offshore transportation and allowing for both ships and pipelines as offshore transportation modes.

While our model of the CCS-SCDP is meant to provide decision support for strategic decisions, we also aspire to give indications towards the operational feasibility of the resulting supply chains. Modeling ship transportation within CCS is often highly strategic, focusing on fleet size and mix and fleet deployment. Examples of such are Bjerketvedt et al. (2022), d'Amore et al. (2021) and Nam et al. (2013), where the number and capacities of the ships and the necessary round trips to handle a certain yearly volume of CO_2 are the major decisions regarding the fleet. If the volumes are small, which they are in the reviewed literature, this approach serves its purpose well. For small volumes, the required ship traffic is limited, and the probability of

a ship intervening in other ships' sailing and operations schedules in the ports is small. However, with larger volumes, ships might have to operate simultaneously in some ports. A modeling approach that does not consider this could lead to unrealistic infrastructure requirements and operational infeasibility.

In our model of the CCS-SCDP, we use time discretization to plan the ship operations in more detail. We keep track of and can decide the movement of the ships through variables regarding waiting, sailing, and port operations in each time period. Thus, we can get operationally feasible solutions. Simultaneous operations are allowed but require investments in a sufficient number of docks. This results in more realistic costs for the system, allowing for more detailed strategic insights. Furthermore, time discretizing enables us to keep track of the buffer storage inventory in the ports. This is further used to decide the buffer storage capacity, which adds strategic value to the model. Time-discrete ship routing is not a novel concept, and out of the reviewed literature, it is used by both Bittante and Saxen (2020) and Bjerketvedt et al. (2020). However, similar exploitation of time-discrete ship routing as a strategic supply chain dimensioning tool is not found in any reviewed work.

Another main contribution is the integration of ship transportation and pipeline transportation in the same MIP. As described in Section 3.1, both Kjärstad et al. (2016) and Roussanaly et al. (2014) include ship and pipeline transportation in their analyses. However, in the case studies of these reports, the systems are simulated separately and compared afterward based on the simulation results. Pipelines are also part of the solutions in the MIP models of Bjerketvedt et al. (2022) and Nam et al. (2013), but only as an option to connect emission sources that are close to each other. By integrating both transportation modes in the same MIP, our model can decide what transportation mode is the best fit for a given case, whether it is ships, pipelines, or a combination of the two. A similar integration is also done by d'Amore et al. (2021), but in a less detailed fashion than our model. The model of d'Amore et al. (2021) designs a Europe-wide CCS supply chain and simplifies both ship and pipeline transportation costs by encapsulating all cost elements in a calculation only dependent on volume and distance. They also marginalize the benefits of ship transportation by limiting ship capacities to 10 kt. The simpler transportation modeling approach merely indicates the costs and extent of a Europe-wide, cross-border supply chain. The goal of our model of the CCS-SCDP is to give decision support and deeper insight into the design, cost, dimensioning, and operational aspects of more specific CCS projects. This requires more detailed modeling of the supply chain components and solutions that can provide strategic, economic, technical, and operational insights.

Typical for many of the papers reviewed in this chapter, and for CCS operations research in general, is that they focus only on parts or particular configurations of the supply chain, such as Bjerketvedt et al. (2022), Chandel et al. (2010), Roussanaly et al. (2021) and Wang et al. (2014). Much of the research is also focused on techno-economic cost assessments of pipeline and ship transportation and comparisons of the system costs. In our model of the CCS-SCDP, we apply insight from these cost assessments and use state-of-the-art methodologies to estimate the cost of a complete supply chain. This strengthens the validity of our model solutions.

While the transportation network design makes up the core decisions of our model of the CCS-SCDP, it also provides decisions on the capture and storage part of the supply chain. Existing literature tends to either develop less detailed and less realistic

full-scale supply chain models (d'Amore et al. 2021), or they model and analyze the transportation part of the supply chain in a detailed fashion (Bjerketvedt et al. 2022). By taking emission sources' and storage sites' geographical locations and associated capture and storage costs as input, our model can find the cheapest combination of capture sites, transportation, and storage sites. Also, by including all vital parts of the supply chain, the resulting cost per tonne of the supply chain is directly comparable to the EU ETS price and other international CO_2 taxation policies. This eases the evaluation of the model's results for CCS policy-makers. Thus, the implementation of capture and storage costs strengthens both the novelty and usability of our model of the CCS-SCDP as a decision support tool for CCS supply chain design.

Chapter 4

The CCS Supply Chain Design Problem

This chapter formally defines the CCS Supply Chain Design Problem (CCS-SCDP). The CCS-SCDP is the problem of designing a maritime supply chain that can transport a supply of captured CO_2 from a given set of inland emission sources to another set of permanent storage locations. The supply chain includes capture technologies at emission sources, onshore and offshore pipelines, port infrastructure, ships, and storage infrastructure. Therefore, the CCS-SCDP can be seen as a strategic planning problem where the goal is to minimize the total investment and operational costs related to CO_2 capture, CO_2 transportation between different geographic regions, and storage of CO_2. Furthermore, the problem needs to be solved for a finite and representative planning horizon.

Figure 4.1 presents the CCS supply chain, where offshore pipeline transportation is an alternative to ship transportation. The supply chain starts by capturing the CO_2 at inland *emission sources*, which can be different types of production facilities. Each emission source has a given rate of CO_2 emissions per time period and a cost of capturing CO_2 based on the type of the facility. The rate at which CO_2 is captured can be assumed to be in a steady-state, thus equal across time periods. When the CO_2 is captured at the emission sources, it is transported through *onshore pipelines*, either to another emission source or to a shoreside CO_2 collecting hub, referred to as a *loading port*. The pipelines can have different diameters and capacities. The loading ports are the starting gate for offshore transportation, and all CO_2 from emission sources must eventually reach a loading port.

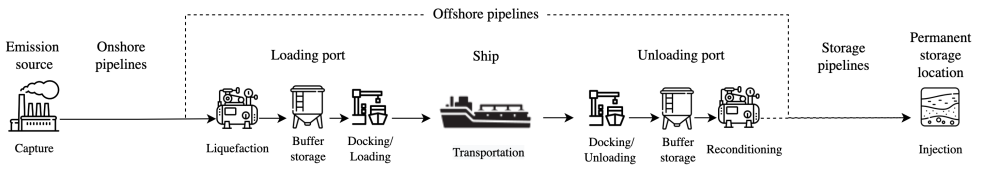

Figure 4.1: CCS supply chain CO_2 flow chart

After reaching a loading port, the CO_2 can be transported by either ships or *offshore pipelines*. If transported by ships, the CO_2 is liquefied and temporarily stored in buffer storage before being loaded onto ships in the loading ports. When loading is done, the ships sail to a CO_2 receiving and redistributing terminal, referred to as an *unloading port*, where they unload. Each loading port must have a liquefaction unit, intermediate buffer storage, loading equipment, and one or more ship docks to facilitate ship transportation. The latter is a place within a port where one ship can be moored and loaded or unloaded. Unloading ports must have similar equipment and capacities as the loading ports in terms of buffer storage and loading equipment, except that the loading equipment is replaced with unloading equipment. Furthermore, instead of liquefaction, the unloading ports have a reconditioning unit to regasify the liquefied CO_2 before it is transported through pipelines and further injected into a geological, permanent *storage location*. The ships are divided into *ship types*, where each type has a given load capacity. Ships that are used are doing one of the following activities at a given point in time. They are either sailing between a loading port or an unloading port, waiting outside a port, or operating in a port. Operating refers to loading or unloading CO_2, depending on the type of port.

The alternative to ship transportation between loading ports and unloading ports is offshore pipelines. Finally, the CO_2 must be directed to permanent storage through another set of pipelines, referred to as *storage pipelines*. A storage pipeline can either be onshore or offshore, dependent on the location of the permanent storage. All pipelines are similar, with different available capacities based on their diameters. If the amount of CO_2 in a loading port at a given time period exceeds the capacity of the buffer storage, it has to be emitted into the atmosphere due to overspill.

The CCS-SCDP deals with strategic, tactical, and operational decisions. On the strategic level, the primary decision is to choose pipelines or ships for offshore transportation. For ship transportation, one must decide the number of ships of each type and the number and capacity of supporting facilities needed in the selected ports. The latter comprises buffer storage, liquefaction and reconditioning facilities, loading and unloading equipment, and the number of ship docks. For all pipeline transportation, one must decide the number of pipelines of each diameter at every link between locations in the supply chain. The pipeline diameter decides the flow capacity of the pipeline. Implicitly, when placing pipelines, one needs to decide from which emission sources to transport CO_2. The decisions mentioned above constitute the fleet size and mix and fundamental network design decisions, which lay the foundation for lower-level decisions. The tactical decisions include the deployment of ships between ports, the number of times a ship should be used, the quantity to transport between the locations, and the quantity to capture. Finally, the operational and most short-term decisions are when and where a ship should sail to load and unload, and when to operate and wait. Additionally, the inventory levels in the buffer storages and the amount emitted due to overspill are decided.

The goal of the problem is to minimize the total costs of the maritime CCS supply chain over a planning horizon. The cost may be divided into six parts representing the overall cost for different supply chain elements. The first part is the capture cost, which is the sum of costs associated with the capture of CO_2 in emission sources. The capture cost is dependent on the captured amount and the type of emission source. The capture cost also includes the cost associated with pressurizing the CO_2 flow prior to pipeline transportation. The second element, the pipeline cost, applies to all types

of pipelines. It is divided into investment and operational costs. The pipeline investment cost comprises the cost of building a pipeline of a specific diameter between two locations. The pipeline operational cost consists of a fixed and a variable part. The fixed operational cost is determined as a percentage of the investment cost, which is dependent on location, length, and diameter. The variable operational cost is due to the energy needed to operate compressors and booster stations along these pipelines to handle the pressure drop between the two locations. Pipeline investment costs may be scaled by a terrain factor, adjusting for increased costs dependent on the terrain in which the pipelines are located. The third cost element is the shipping cost, which is further divided into investment and operational costs. The ship investment cost comprises the cost of hiring the ships throughout the planning horizon, dependent on the ship type. The operational costs are the cost of sailing, including port fees and waiting. The sailing cost depends on the distance sailed and the fuel consumption, where the ship type decides the latter. Waiting cost is a share of the sailing cost due to lower energy requirements for idle ships. The fourth cost element is port costs related to ship transportation. They comprise buffer storages, liquefaction, reconditioning, docks, loading, and unloading. Buffer storage costs depend on the required storage capacity. Liquefaction and recondition costs include both investment and operational costs, which depend on the flow capacities and actual flow, respectively. The dock cost translates to the cost of constructing the docks needed in a specific port. Lastly, the costs of loading and unloading facilities in the docks depend on the amount of CO_2 loaded and unloaded at a port. These costs also include investment and operational costs. The fifth cost element is the emission cost, which is the cost per tonne emitted from overspill. The last element is the storage cost, which is the cost per tonne stored at a permanent storage location. It reflects the investment and operational cost connected to establishing and operating a geological storage site of a given capacity.

Furthermore, the ship activities, sailing, waiting, and port operations, must be handled such that both the amount of CO_2 transported by ships, and the ship movements, are conserved consistently. The difference in the amount of CO_2 arriving at loading ports from onshore pipelines and the amount departing through offshore pipelines, ships, or overspills in a given time period needs to be equal to the net change in stored CO_2 in the buffer storages. The reversed logic applies to unloading ports, except that there is no overspill option and that the CO_2 is departing in storage pipelines. One should note that not all of the CO_2 transported by ships from loading ports arrive at unloading ports; the ships evaporate a certain share of the full shipload during sailing, referred to as boil-off gas. There must be sufficient docking capacity to moor and serve ships; all simultaneously operating ships in a port need one dock.

Chapter 5

Mathematical Model

This chapter presents the mathematical model used to solve the CCS-SCDP. The purpose of the model is to design the cheapest possible transportation network while fulfilling the demand for transport of captured CO_2 from a set of emission sources and further storing that CO_2 in permanent storage locations. Section 5.1 presents the modeling approach and assumptions. The notation used in the model is presented in Section 5.2, while Section 5.3 presents the mathematical model formulation.

5.1 Modeling approach and assumptions

The model is based on an *arc flow* formulation. Here, an arc is a direct CO_2 transportation link between two locations, where the locations serve a purpose in the CCS supply chain. As a result of the arc flow formulation, the model presents the optimal network as a set of arcs used. As described in Chapter 4, the model handles both pipeline and ship transportation. Hence, the model has two types of arcs, representing the two available transportation options. Pipeline arcs are defined both at sea and on land, while ship arcs are only an option at sea.

Since the model solves a strategic problem, the flow of CO_2 is modeled in a steady-state fashion. In this context, a steady-state means we assume that the amount of CO_2 that enters the system through emission sources at a certain point in time equals the amount that is injected into geological storage at the same point in time. Furthermore, we assume that the flow out from emission sources is constant, which implies that the flow out of the system and into the geological storage sites is constant.

Ship transportation is modeled as being time-discrete. With ship transportation, there are systematic changes in the CO_2 conditions through liquefaction and reconditioning, and accumulation of liquid CO_2 in buffer storages and ship tanks. Thus, the goal is to reach a stable solution in terms of the routing of the ships. This will ensure a steady-state system as defined above, where the flow in pipelines from unloading ports to storage locations is constant. The time discretization drastically increases the problem size and thus the solving time. For the model to be solvable within a reasonable time, the planning horizon cannot be too large. We assume that with a stable routing of the ships, a solution that represents a limited planning horizon can be scaled up and

represent longer, and thus more strategic, planning horizons as well. In practice, the solutions may be repeated for an arbitrary length of time.

Pipeline transportation

With our modeling approach to the CCS-SCDP, pipelines serve three different functions in the supply chain. Firstly, it is the only mode of transportation between emission sources and loading ports. Secondly, it is an alternative to ship transportation between loading and unloading ports. Finally, it is the only mode of transportation from unloading ports to geological storage. Pipelines can have different dimensions and resulting flow capacity. A pipeline connection between two nodes allows for an integer number of pipelines of each dimension to be established between the two nodes. This way, the pipeline connection can handle a flow higher than the capacity of a single pipeline.

The onshore pipeline network is modeled to allow emission sources to connect and form clusters that can share a higher capacity pipeline connecting them to another emission source or a loading port. This is similar to the telescoping trunkline approach of Chandel et al. (2010) and visualized in Figure 5.1. They found considerable cost savings when increasing the diameter of the trunkline in a telescoping fashion as emission sources are added along its path instead of establishing an oversized single dimension trunkline to which emission sources can connect.

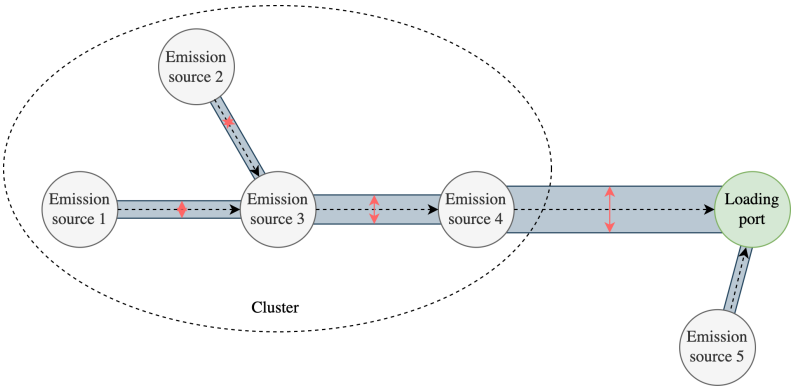

Figure 5.1: Emission sources can connect to each other to share pipeline capacity. Such connections are referred to as clusters. Capacity is a function of the inner diameter of the pipeline, which is visualized by red arrows. The figure is inspired by Chandel et al. (2010).

The flow from the onshore network that arrives in the loading port can be split; one part of the flow can be directed into an offshore pipeline to the unloading port, while the remaining flow can be directed into a liquefaction unit to be conditioned for ship transportation. This way, either one or both transportation modes can be used, depending on what is optimal for a given case. The flows from the two transportation modes are then merged in unloading ports before they are collectively transported in pipelines to final storage locations.

Time-discrete ship transportation

We model the ship transportation in a time-discrete manner. This means that time is divided into time intervals of equal length, referred to as *time periods*. Consequently, each time-dependent event is associated with one or more time periods. We have modeled all the ship activities to be time-dependent, including sailing, waiting, loading, and unloading. This may seem very detailed, bearing in mind that the model is strategic, and it is different from the approach of Bjerketvedt et al. (2022) and d'Amore et al. (2021). Instead of routing a set of ships in a time-discrete manner, they decide the number of ships and round trips needed to transport a certain yearly volume of CO_2. However, when volumes get big, a time-discrete model allows informed decisions regarding the dimensioning of the ports' docking and buffer storage capacities. For instance, if two ships load in a loading port simultaneously, the port needs one dock for each ship. Moreover, the buffer storage capacities are ensured to be large enough; for loading ports, the buffer storage needs to handle the steady-state flow from emission sources between ship visits; for unloading ports, it needs to handle the steady-state flow out to storage locations between ship visits. These are essential supply chain elements, and their dimensioning will impact the overall cost of the system. Furthermore, the time discretization of the ship voyages and the resulting dimensioning decisions ensure operational feasibility and, thus, a more realistic solution. Hence, the solution gives a more accurate system cost and informs about reasonable requirements concerning the construction and investment of all essential supply chain elements. A similar approach in terms of time-discrete ship transportation in a strategic system design context is made by Bittante and Saxen (2020). They implement a time-discrete model from which they can derive the optimal sizing of buffer storages in a network of LNG terminals.

Since time, in reality, is not discrete, it is essential to have small enough time periods to represent reality satisfactorily. As all ship activities span several hours to days, this is manageable in our model. Another benefit of the discrete time is connected to weather fluctuations, for instance, due to seasonality. In our model, we have modeled the sailing times to be dependent on the time periods in which the sailing occurs. In this way, we allow changes to the sailing speed based on the weather. We have also modeled the power consumption based on sailing at service speed under normal weather conditions. Thus, if there is challenging weather, we keep the power consumption constant and increase the sailing time through weather-adapted sailing speeds.

If a ship is supposed to sail from port i to port j, it must load or unload in port i before the voyage starts. Whether it is loading or unloading depends on the type of port. Hence, the variable that represents if a voyage takes place contains information regarding the start and end of the voyage and the port at which the ship loads or unloads. Loading and unloading are collectively referred to as port operations. Thus, a ship that loads or unloads, operates. For each ship, loading and unloading are assumed to take the same amount of time. If a ship arrives in a port and there are no available docks, the ship is allowed to wait outside the port until a time period with docks available. The waiting can only occur before the ship starts operating in the port. Thus, a ship needs to start sailing right after it has operated. Figure 5.2 illustrates this behavior. We assume that waiting outside a port after operations and before further sailing is equivalent to starting sailing immediately and rather wait outside the port it reaches next. By enforcing ships to only wait before the operation, we improve model solvability as we remove practically identical solutions.

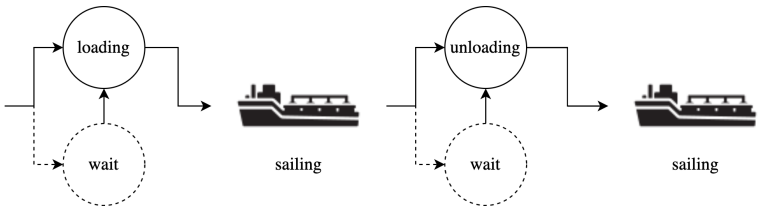

Figure 5.2: A ship activity sequence between a loading and an unloading port. Waiting is optional, which is visualized by the dotted lines. The solid lines represent required transitions.

Figure 5.3 illustrates how the model handles several ships arriving in the same port with limited docking capacity. Here, three ships arrive simultaneously in node j, which only has one dock. The first ship immediately starts operating, while the two others have to wait until the dock is idle.

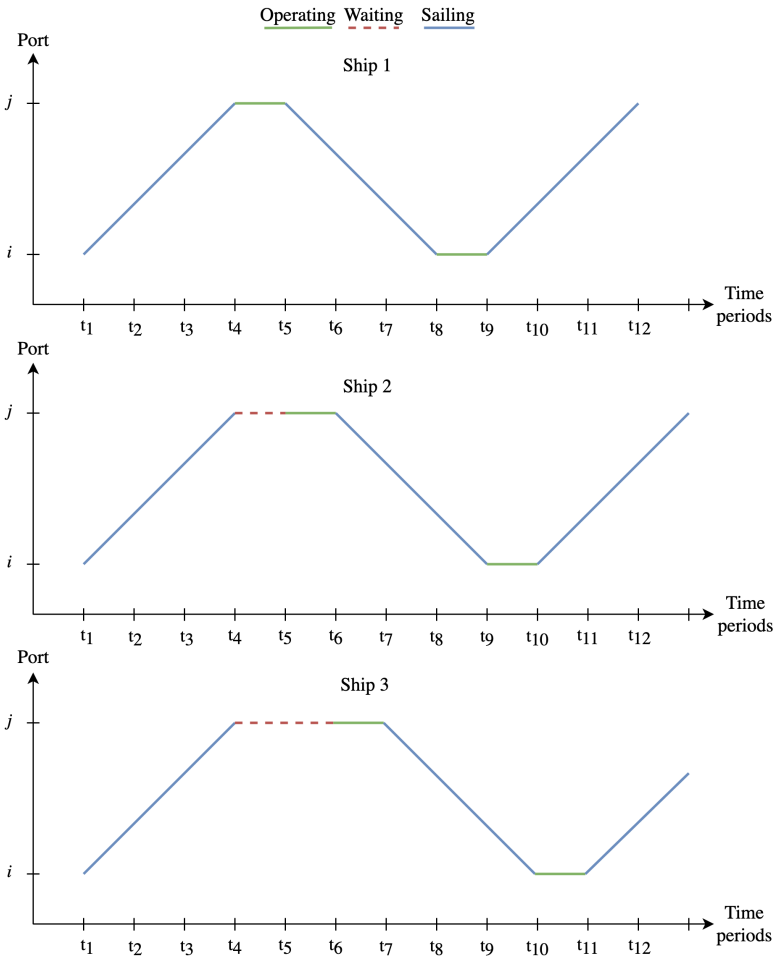

Figure 5.3: Waiting, operations and sailing in a system with three ships and one dock in port j.

If a ship is used, it must be hired. Moreover, if the ship is hired, it must be hired for the whole length of the *planning horizon*, which is the time interval the problem is solved for. A hired ship can only service one combination of a loading port and an unloading port. The assumption restricts ships from shifting routes throughout the planning horizon and that ships can sail between two loading ports or two unloading ports. The purpose of the model is to solve sizeable CO_2 flow scenarios, and thus the accumulated transport requirement along an arc is much larger than the capacity of any ship. Each ship will need to sail several round trips on an arc to fulfill the transport requirement, and hence the assumption is in practice not very restrictive.

Buffer storage

The buffer storages are where the steady-state pipeline flow and discrete ship transportation intersect. We assume a steady-state flow into the buffer storage from the emission sources in the loading ports. Similarly, we assume a steady-state flow out from the buffer storage in the unloading ports to the geological storage site. These assumptions make sure the model solution includes big enough buffer capacities to obtain a steady flow during and between ship visits.

Set of time periods

The combination of time-independent steady-state flow in pipelines and time-discrete ship transportation entails a need for a set of initial time periods. This is to avoid excessive flow into the loading ports before the empty ships arrive and to avoid any flow out from the unloading ports before they have received any shiploads of CO_2. We assume that the ships start sailing from an unloading port towards a loading port at the start of the first time period. Thus, if the flow of CO_2 from the emission sources starts at the first time period, there will be an initial accumulation of CO_2 in the buffer storage at the loading ports until the ships arrive. This will lead to the model requiring a higher buffer capacity than necessary under stable operating conditions. A similar phenomenon would appear in the unloading ports, which cannot receive any CO_2 from ships before the ships have sailed to the loading ports and back again, at the earliest. Hence, since there is no CO_2 in the unloading ports during the first time periods, the model must handle that the flow between unloading ports and permanent storage locations starts later.

We assume that it is possible to operate the system and regulate the flow in a way that handles these start-up effects. To enable this in the model, we establish a set of initial time periods for each node. For the ports, the set of initial time periods has cardinality equal to the minimum number of time periods it takes for a ship to sail from its initial position to a loading port or back to an unloading port, respectively. Thus, if it takes a ship three time periods to sail from its initial position to a loading port, the set of initial time periods for that loading port has cardinality three. Similarly, if it takes a ship seven time periods to sail from its initial position to a loading port, operate in that port, and sail back to an unloading port, the set of initial time periods for that unloading port has cardinality seven. During the initial time periods, the respective ports do not need to handle any flow of CO_2. The flow of CO_2 from the emission sources to a specific loading port starts at the earliest possible arrival of a ship in that loading port. Thus, each emission source has a set of initial time periods where no ship has arrived at any loading port yet. Similarly, the flow out from an unloading port

starts after the initial time periods for that port are over. Since the first flow will not arrive at storage locations before the first flow departures from an unloading port, the set of initial time periods for all storage locations is equal to the shortest set of initial time periods among the unloading ports. After the initial time periods are finished, the operating time periods start. For each node, the sets of initial and operating time periods span all time periods in the planning horizon. Figure 5.4 illustrates how the time periods are associated with the two sets for a loading port and an unloading port.

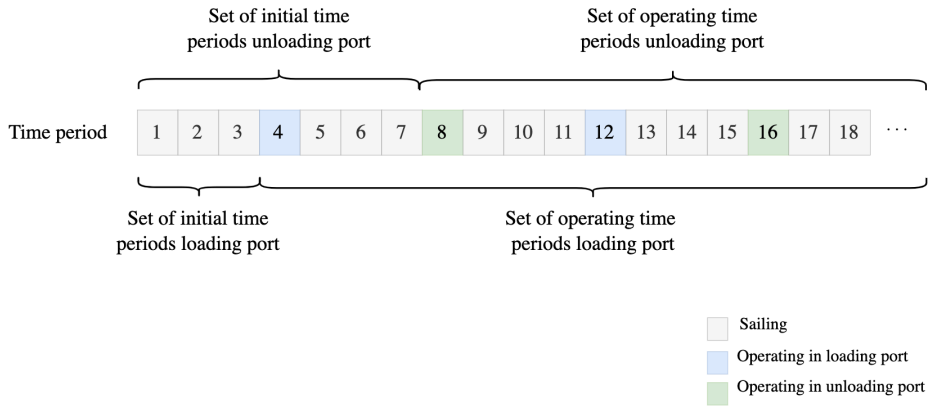

Figure 5.4: Illustration of how the planning horizon is divided into initial and operating time periods for a loading and an unloading port

5.2 Notation

The following section presents the notation used in the model formulation. Section 5.2.1 presents the sets. The parameters and decision variables are presented in Section 5.2.2.

5.2.1 Sets

To formulate the model mathematically, the involved emission sources, ports, storage locations, ships, and pipelines are described as sets. A complete presentation of the sets is found in Table 5.1. The sets $\mathcal{N}^U$ and $\mathcal{N}^L$ denote the unloading ports and loading ports, respectively. Together, they form the set of all ports, denoted $\mathcal{N}^P$. The set of emission sources is denoted $\mathcal{N}^E$, while the permanent storage locations are collected in the set $\mathcal{N}^S$. Together, the sets $\mathcal{N}^P$, $\mathcal{N}^E$ and $\mathcal{N}^S$ compose the set of all ports, emission sources, and storage locations, denoted $\mathcal{N}$. The emission sources, ports, and storage locations may collectively be referred to as *nodes*.

The set of available ships is denoted $\mathcal{V}$. Furthermore, each ship is associated with a ship type, where the set of ship types is denoted $\mathcal{C}$. Finally, $\mathcal{V}_c$ denotes the subset of ships of ship type c.

As a simplification, pipelines are distinguished based on their inner diameter, which in turn determines their capacity to handle the flow of CO_2. The set of pipeline diameters is denoted $\mathcal{D}$.

As the model is based on discrete time, we have defined a set consisting of all time periods in the planning horizon, denoted $\mathcal{T}$. To separate the time periods where the system is operating from the initial time periods, we split them in the subsets $\mathcal{T}_i^O$ and $\mathcal{T}_i^{[init]}$. They represent the *set of operating time periods* and *set of initial time periods* for node i, respectively. As described in Section 5.1, the time needed to start the system is specific for each port and emission source. Thus, both of the subsets are specific for node $i \in \mathcal{N}$. Moreover, $\mathcal{T} = \mathcal{T}_i^{[init]} \cup \mathcal{T}_i^O$, which is true for all i. The last set describing a collection of time periods is denoted $\mathcal{T}^C$, and decribes the *central planning horizon*. The central planning horizon spans the same interval as the most extensive set of operating time periods. Thus, $\mathcal{T}^C = \mathcal{T}_i^O$ where $|\mathcal{T}_i^O| \geq |\mathcal{T}_j^O|, i \in \mathcal{N}, j \in \mathcal{N}, i \neq j$.

Table 5.1: Model sets.

Set	Description
$\mathcal{N}^U$	Set of unloading ports
$\mathcal{N}^L$	Set of loading ports
$\mathcal{N}^P$	Set of ports, $\mathcal{N}^P = \mathcal{N}^U \cup \mathcal{N}^L$
$\mathcal{N}^E$	Set of emission sources
$\mathcal{N}^S$	Set of permanent storage locations
$\mathcal{N}$	Set of ports, emission sources and permanent storage locations, $\mathcal{N} = \mathcal{N}^P \cup \mathcal{N}^E \cup \mathcal{N}^S$
$\mathcal{V}$	Set of ships
$\mathcal{C}$	Set of ship types
$\mathcal{V}_c$	Set of ships of type c, $\mathcal{V}_c \subset \mathcal{V}$
$\mathcal{D}$	Set of candidate pipeline diameters
$\mathcal{T}$	Set of time periods
$\mathcal{T}_i^O$	Set of operating time periods for port i
$\mathcal{T}_i^{[init]}$	Set of initial time periods for port i
$\mathcal{T}^C$	Set of time periods in the central planning horizon

5.2.2 Decision variables and parameters

In this section, we present the parameters and decision variables. A complete presentation of the parameters is found in Table 5.2, while Table 5.3 presents the decision variables.

We begin by introducing the variables and parameters associated with the transportation network. The binary variable x_{ivjt} takes the value 1 if ship v starts operating in port i at the start of time period t. As a result of the assumptions in Section 5.1, this also entails that ship v sails directly towards port j after the operations in port i

are finished. The cost related to the port operation and subsequent sailing is denoted C^T_{ijv}. Ship v uses T^L_v number of time periods to fully load or unload itself in a port. Thus, the ship loads or unloads an amount equal to its load capacity K_v, measured in tonnes of CO_2. T_{ijvt} is the time ship v uses to operate in port i and then sail to port j. The sailing time can vary depending on the sailing conditions, and hence the parameter T_{ijvt} can get different values in different time periods. During sailing, a percentage of a full shipload of CO_2 is released due to boil-off every time period. This is represented by the parameter B. When ships are neither operating nor sailing, they are waiting. Waiting is represented by the binary variable w_{ivt}, which takes the value 1 if ship v waits outside port i in time period t. The cost associated with ship v waiting for one time period is denoted C^W_v. The binary variable h_{ijv} takes the value 1 if ship v is hired, and used to transport CO_2 between loading port i and unloading port j. The cost of hiring a ship for the considered planning horizon is denoted C^H_v.

As described in Chapter 2, ports facilitating CO_2 ship transportation need certain equipment and capacities. The CO_2 needs to be liquefied in loading ports and reconditioned in unloading ports. The cost per tonne for liquefaction is denoted C^L, and the cost per tonne of reconditioning is denoted C^R. When loaded onto ships and unloaded from ships in a given port i, each tonne of CO_2 is assigned the cost of loading or unloading, denoted C^I_i. If ship v is operating in port i during time period t, the binary variable δ_{ivt} gets assigned value 1. This is further used to set the number of docks needed in port i, given by the integer variable d_i. Thus, this is the number of ships port i can serve simultaneously. We assume that every dock in a specific port costs the same to build, and this cost is given by the parameter C^D_i. The intermediate buffer storage is the last port facility that is needed to support ship transportation. The continuous variable b_i represents the maximum buffer storage capacity in port i, given in tonnes. Each tonne of capacity is assigned a cost of C^B. The inventory level in port i in time t is denoted s_{it}, which is also a continuous variable. Due to technical requirements, it is also necessary to determine a lower bound on the inventory through the parameter $\underline{S}_i$. The amount of overspill in port i in time period t is denoted e_{it}. Each tonne of CO_2 emitted due to overspill is punished with the cost C^E. In our model, overspill is only allowed in loading ports.

There are three types of pipelines in our model. Onshore pipelines, connecting emission sources and loading ports on land, offshore pipelines, connecting loading and unloading ports, and storage pipelines, connecting unloading ports and permanent storage locations. The integer variables p^L_{ijd} (superscript L for land, onshore), p^O_{ijd} (superscript O for offshore), and p^S_{ijd} (superscript S for storage) denotes the number of onshore, offshore and storage pipelines on a given link i and j with the inner diameter option d. Each pipeline of diameter option d on the link between i and j is associated with a cost of C^{PL}_{ijd} for onshore pipelines, C^{PO}_{ijd} for offshore pipelines and C^{PS}_{ijd} for storage pipelines. The amounts of CO_2 transported through pipelines between nodes i and j during a time period are assumed to be equal in all time periods and are represented by the continuous variables f^L_{ij}, f^O_{ij}, and f^S_{ij}. Each tonne of CO_2 transported in pipelines between nodes i and j is assigned a variable cost of C^V_{ij}, which is independent of pipeline type. Each pipeline has a maximum feasible flow capacity due to its inner diameter. This is represented by the parameter F_d, given in tonnes per time period.

As we model a full supply chain, we have included the cost of capturing the CO_2 and the cost of storing it after transportation. Emission source i generates P_i tonnes of CO_2 each time period. A share of this may be captured. Thus, the continuous variable c_i represents the amount of CO_2 captured from emission source i each time period. The industrial processes in the emission sources may vary significantly. Hence, the cost of capture may vary as well. Therefore, the cost of capturing one tonne of CO_2 is distinguished between emission sources and denoted C_i^C for emission source i. Since the cheapest solution is to not capture or transport any CO_2, the parameter O^M denotes the percentage share of the total produced CO_2 that must be transported through the supply chain to finally be deposited in a permanent storage location. When the CO_2 is finally stored at the storage location i, it gets assigned a cost of C_i^S per tonne stored.

Table 5.2: Model parameters.

Parameter	Description
C_v^H	Cost of hiring ship v during the central planning horizon, $\mathcal{T}^C$
C_{ijv}^T	Cost of ship v operating in port i and sailing from port i to port j
C_v^W	Cost of waiting outside a port during one time period for ship v
C_i^I	Cost per tonne loaded onto or unloaded from ships in port i
C^B	Cost per tonne of intermediate buffer storage capacity
C^E	Cost per tonne of emitted CO_2 due to overspill
C^L	Cost per tonne liquefied CO_2
C^R	Cost per tonne reconditioned CO_2
C_i^D	Cost per dock in port i, scaled to the length of the central planning horizon
C_{ijd}^{PL}	Cost per onshore pipeline with diameter d between node i and node j, scaled to the length of the central planning horizon
C_{ijd}^{PO}	Cost per offshore pipeline with diameter d between node i and node j, scaled to the length of the central planning horizon
C_{ijd}^{PS}	Cost per storage pipeline with diameter d between node i and node j, scaled to the length of the central planning horizon
C_{ij}^V	Variable cost per tonne of CO_2 flowing through pipelines between node i and node j
C_i^S	Cost per tonne of CO_2 stored permanently at location i
C_i^C	Cost per tonne of CO_2 captured in emission source i
T_v^L	Number of time periods ship v uses to fully load or unload itself
T_{ijvt}	Number of time periods used by ship v to start operating in port i in time period t and, immediately after operating, sailing from port i to port j
K_v	Load capacity of ship v, in tonnes of CO_2
B	Boil-off per time period, as a percentage of a complete shipload
F_d	Maximal flow capacity through a pipeline of diameter d, in tonnes per time period
$\underline{S}_i$	Lower bound on inventory in buffer storage at port i
P_i	Produced CO_2 in emission source i during one time period
O^M	Minimum share of produced CO_2 that is captured and transported to permanent storage

Table 5.3: Model variables.

Variable	Domain	Description
h_{ijv}	Binary	1 if ship v is hired and used on the link (i, j) where i represents a loading port, while j represents an unloading port, 0 otherwise
x_{ijvt}	Binary	1 if ship v starts operating in port i at time period t, and thereafter directly sails from port i to its dedicated port j, 0 otherwise
w_{ivt}	Binary	1 if ship v waits outside port i in time periode t, 0 otherwise
δ_{ivt}	Binary	1 if ship v is operating in port i in time period t
d_i	Integer	Number of docks in port i
b_i	Continuous	Buffer storage capacity in port i, i.e., upper bound on inventory level in port i. Measured in tonnes
s_{it}	Continuous	Inventory level in port i at the end of time period t. Measured in tonnes
e_{it}	Continuous	Emitted CO_2 from port i in time period t due to overspill. Measured in tonnes
c_i	Continuous	Quantity of CO_2 that is captured in emission source i during one time period. Measured in tonnes
p^L_{ijd}	Integer	Number of onshore pipelines with diameter d between emission source i and emission source or loading port j
p^O_{ijd}	Integer	Number of offshore pipelines with diameter d between loading port i and unloading port j
p^S_{ijd}	Integer	Number of storage pipelines with diameter d between unloading port i and storage location j
f^L_{ij}	Continuous	Total flow of CO_2 through onshore pipelines between emission source i and emission source or loading port j, in tonnes per time period
f^O_{ij}	Continuous	Total flow of CO_2 through offshore pipelines between loading port i and unloading port j, in tonnes per time period
f^S_{ij}	Continuous	Total flow of CO_2 through storage pipelines between unloading port i and permanent storage location j, in tonnes per time period

5.3 Model formulation

In the following section, we present the model. Section 5.3.1 presents the objective function and Section 5.3.2 presents the constraints needed to guarantee feasibility of the obtained solutions.

5.3.1 Objective

The objective function (5.1) consists of several terms, specified in terms (5.2) through (5.14). The term $C^{[Hire]}$ is the total cost of hiring ships. The cost of sailing is calculated in the term $C^{[Sail]}$. This is divided into sailing from unloading ports and sailing from loading ports. We cannot sum over all ports in the matrix $\mathcal{N}^P \times \mathcal{N}^P$ because x-variables denoting sailing between a pair of unloading ports or a pair of loading ports are not defined. The term $C^{[Wait]}$ calculates the sum of waiting costs. In (5.5) we calculate the cost of loading and unloading operations in the ports. Note that we adjust the amount of CO_2 unloaded in unloading ports by the boil-off. Liquefaction costs and reconditioning costs are calculated in the terms $C^{[Liq]}$ and $C^{[Rec]}$, respectively. With the term $C^{[Buffer]}$, we calculate the total cost of buffer storage and emission due to overspill, while the cost of docks is represented by $C^{[Docks]}$. The terms $C^{[Pipe-L]}$, $C^{[Pipe-O]}$, and $C^{[Pipe-S]}$ calculate the total pipeline costs for onshore, offshore, and storage pipelines, respectively. Finally, the total capture cost is calculated by the term $C^{[Capture]}$, and $C^{[Store]}$ represents the cost of storing the CO_2 in the permanent storage.

$$\begin{aligned}\min\ w = {} & C^{[Hire]} + C^{[Sail]} + C^{[Wait]} + C^{[L+U]} + C^{[Liq]} + C^{[Rec]} + C^{[Buffer]} \\ & + C^{[Docks]} + C^{[Pipe-L]} + C^{[Pipe-O]} + C^{[Pipe-S]} + C^{[Capture]} + C^{[Store]} \end{aligned} \tag{5.1}$$

where each term is presented below:

$$C^{[Hire]} = \sum_{i \in \mathcal{N}^L} \sum_{j \in \mathcal{N}^U} \sum_{v \in \mathcal{V}} C_v^H h_{ijv} \tag{5.2}$$

$$C^{[Sail]} = \sum_{i \in \mathcal{N}^L} \sum_{j \in \mathcal{N}^U} \sum_{v \in \mathcal{V}} \sum_{t \in \mathcal{T}_i^O} C_{ijv}^T x_{ijvt} + \sum_{i \in \mathcal{N}^U} \sum_{j \in \mathcal{N}^L} \sum_{v \in \mathcal{V}} \sum_{t \in \mathcal{T}_i^O} C_{ijv}^T x_{ijvt} \tag{5.3}$$

$$C^{[Wait]} = \sum_{i \in \mathcal{N}^P} \sum_{v \in \mathcal{V}} \sum_{t \in \mathcal{T}_i^O} C_v^W w_{ivt} \tag{5.4}$$

$$\begin{aligned} C^{[L+U]} = & \sum_{i \in \mathcal{N}^L} \sum_{j \in \mathcal{N}^U} \sum_{v \in \mathcal{V}} \sum_{t \in \mathcal{T}_i^O} C_i^I K_v x_{ijvt} \\ & + \sum_{i \in \mathcal{N}^U} \sum_{j \in \mathcal{N}^L} \sum_{v \in \mathcal{V}} \sum_{t \in \mathcal{T}_i^O} \left(1 - (B \cdot T_{ijvt})\right) C_i^I K_v x_{ijvt} \end{aligned} \tag{5.5}$$

$$C^{[Liq]} = \sum_{i \in \mathcal{N}^L} \sum_{j \in \mathcal{N}^U} \sum_{v \in \mathcal{V}} \sum_{t \in \mathcal{T}_i^O} C^L K_v x_{ijvt} \tag{5.6}$$

$$C^{[Rec]} = \sum_{i \in \mathcal{N}^U} \sum_{j \in \mathcal{N}^L} \sum_{v \in \mathcal{V}} \sum_{t \in \mathcal{T}_i^O} \left(\left(1 - (B \cdot T_{ijvt})\right) C^R K_v x_{ijvt}\right. \tag{5.7}$$

$$C^{[Buffer]} = \sum_{i \in \mathcal{N}^P} C^B b_i + \sum_{i \in \mathcal{N}^L} \sum_{t \in \mathcal{T}_i^O} C^E e_{it} \tag{5.8}$$

$$C^{[Docks]} = \sum_{i \in \mathcal{N}^P} C_i^D d_i \tag{5.9}$$

$$C^{[Pipe-L]} = \sum_{i \in \mathcal{N}^E} \sum_{j \in \mathcal{N}^E \cup \mathcal{N}^L} \sum_{d \in \mathcal{D}} C_{ijd}^{PL} p_{ijd}^L + \sum_{i \in \mathcal{N}^E} \sum_{j \in \mathcal{N}^E \cup \mathcal{N}^L} |\mathcal{T}_i^O| C_{ij}^V f_{ij}^L \tag{5.10}$$

$$C^{[Pipe-O]} = \sum_{i \in \mathcal{N}^L} \sum_{j \in \mathcal{N}^U} \sum_{d \in \mathcal{D}} C_{ijd}^{PO} p_{ijd}^O + \sum_{i \in \mathcal{N}^L} \sum_{j \in \mathcal{N}^U} |\mathcal{T}_i^O| C_{ij}^V f_{ij}^O \tag{5.11}$$

$$C^{[Pipe-S]} = \sum_{i \in \mathcal{N}^U} \sum_{j \in \mathcal{N}^S} \sum_{d \in \mathcal{D}} C_{ijd}^{PS} p_{ijd}^S + \sum_{i \in \mathcal{N}^U} \sum_{j \in \mathcal{N}^S} |\mathcal{T}_i^O| C_{ij}^V f_{ij}^S \tag{5.12}$$

$$C^{[Capture]} = \sum_{i \in \mathcal{N}^E} |\mathcal{T}_i^O| C_i^C c_i \tag{5.13}$$

$$C^{[Store]} = \sum_{i \in \mathcal{N}^U} \sum_{j \in \mathcal{N}^S} |\mathcal{T}_i^O| C_i^S f_{ij}^S \tag{5.14}$$

5.3.2 Constraints

The constraints needed to formulate the problem are presented below. They include sailing conservation constraints, ship hiring constraints, and inventory and flow constraints.

Ship hiring and sailing conservation

Constraints (5.15) ensure that a ship can only be hired to serve one link, namely a bidirectional arc between an unloading port and a loading port. Constraints (5.16) and (5.17) are the general ship sailing constraints, controlling the movements and sequences of sailing, port operations, and waiting. Constraints (5.18) have two effects. First, they ensure that if a ship is used to either operate, sail or wait, it must be hired. Moreover, since h_{ijv} is binary, they also ensure that a ship can only perform one activity during each time period. Constraints (5.19) enforce that a ship needs to start its operations in a loading port. Finally, Constraints (5.20) and (5.21) are needed to ensure that no activity is allowed until the operating time periods start. However, for technical feasibility, they are not defined for the last time period in the set of initial time periods. This allows for waiting in the last time period of the initial time periods. This is necessary for Constraints (5.16) and (5.17) to find feasible solutions in the first time period of the operating time periods, as the terms $w_{jv,t-1}$ and $w_{iv,t-1}$ can get value 1. The variables still need to be defined; otherwise, the model will not accept Constraints (5.16) and (5.17), since the terms $x_{ijv,t-T_{ijvt}}$ could be referring to non-existing variables. We consider this as a necessary start-effect of the ship sailing conservation, whose impact is negligible.

$$\sum_{i \in \mathcal{N}^L} \sum_{j \in \mathcal{N}^U} h_{ijv} \leq 1 \qquad v \in \mathcal{V} \quad (5.15)$$

$$x_{ijv,t-T_{ijvt}} + w_{jv,t-1} = w_{jvt} + x_{jivt} \qquad i \in \mathcal{N}^L, j \in \mathcal{N}^U, v \in \mathcal{V}, t \in \mathcal{T}_j^O \quad (5.16)$$

$$x_{jiv,t-T_{jivt}} + w_{iv,t-1} = w_{ivt} + x_{ijvt} \qquad i \in \mathcal{N}^L, j \in \mathcal{N}^U, v \in \mathcal{V}, t \in \mathcal{T}_i^O \quad (5.17)$$

$$x_{ijvt} + x_{jivt} + w_{ivt} + w_{jvt} \leq h_{ijv} \qquad i \in \mathcal{N}^L, j \in \mathcal{N}^U, v \in \mathcal{V}, t \in \mathcal{T} \quad (5.18)$$

$$\sum_{\tau=1}^{t} x_{ijv\tau} \geq x_{jivt} \qquad i \in \mathcal{N}^L, j \in \mathcal{N}^U, v \in \mathcal{V}, t \in \mathcal{T} \quad (5.19)$$

$$x_{ijvt} + w_{ivt} = 0 \qquad i \in \mathcal{N}^L, j \in \mathcal{N}^U, v \in \mathcal{V}, t \in \{\mathcal{T}_i^{[init]} | t \leq |\mathcal{T}_i^{[init]}|\} \quad (5.20)$$

$$x_{ijvt} + w_{ivt} = 0 \qquad i \in \mathcal{N}^U, j \in \mathcal{N}^L, v \in \mathcal{V}, t \in \{\mathcal{T}_i^{[init]} | t \leq |\mathcal{T}_i^{[init]}|\} \quad (5.21)$$

Inventory and flow management

First, Constraints (5.22) secure that no more CO_2 is captured than what is available in the emission sources in each time period. As an emission source could be part of a cluster, it may receive CO_2 from another emission source. Thus, Constraints (5.23) ensure that, for each emission source, the incoming CO_2 together with the captured CO_2 should equal the outgoing CO_2. Constraints (5.24) apply for loading ports and ensure that the net change in inventory should equal the difference between all incoming CO_2 from onshore pipelines and all non-emitted CO_2 going out to either offshore pipelines or ships. The requirement for unloading ports is similar; however, in this case, there is no option to release excess CO_2 into the atmosphere. The CO_2 may come from offshore pipelines and ships and flow out in storage pipelines heading towards storage locations. This is ensured by Constraints (5.25).

$$c_i \leq P_i \qquad i \in \mathcal{N}^E \quad (5.22)$$

$$\sum_{j \in \mathcal{N}^E \setminus \{i\}} f^L_{ji} + c_i = \sum_{j \in \mathcal{N}^E \cup \mathcal{N}^L \setminus \{i\}} f^L_{ij} \qquad i \in \mathcal{N}^E \quad (5.23)$$

$$s_{i,t-1} + \sum_{j \in \mathcal{N}^E} f^L_{ji} - \sum_{j \in \mathcal{N}^U} f^O_{ij} - \sum_{j \in \mathcal{N}^U} \sum_{v \in \mathcal{V}} K_v x_{ijvt} = e_{it} + s_{it} \qquad i \in \mathcal{N}^L, t \in \mathcal{T}^O_i \quad (5.24)$$

$$s_{i,t-1} + \sum_{j \in \mathcal{N}^L} f^O_{ji} + \sum_{j \in \mathcal{N}^L} \sum_{v \in \mathcal{V}} (1 - (B \cdot T_{ijvt}))\, K_v x_{ijvt} = \sum_{j \in \mathcal{N}^S} f^S_{ij} + s_{it} \qquad i \in \mathcal{N}^U, t \in \mathcal{T}^O_i \quad (5.25)$$

The inventory can never exceed the buffer storage capacity, which is ensured by Constraints (5.26). Furthermore, constraints (5.27) enable us to find a balanced ship transportation solution by ensuring that the inventory in each unloading port is the same at the start and end of the operating time periods. Finally, Constraints (5.28) ensure that the buffer storages are not filled before the operating time periods start for the respective ports.

$$s_{it} \leq b_i \qquad i \in \mathcal{N}^P, t \in \mathcal{T} \quad (5.26)$$

$$s_{i,|\mathcal{T}^{init}_i|} = s_{i,|\mathcal{T}|} \qquad i \in \mathcal{N}^U \quad (5.27)$$

$$s_{it} = 0 \qquad i \in \mathcal{N}^P, t \in \{\mathcal{T}^{[init]}_i | t \leq |\mathcal{T}^{[init]}_i|\} \quad (5.28)$$

Each pipeline has a maximum capacity, given by the inner diameter. Thus, Constraints (5.29) through (5.31) are needed to ensure that the pipeline flow on an arc is below the maximum capacity of that arc.

$$f_{ij}^{L} \leq \sum_{d \in \mathcal{D}} F_d p_{ijd}^{L} \qquad i \in \mathcal{N}^{E}, j \in \mathcal{N}^{E} \cup \mathcal{N}^{L} \setminus \{i\} \tag{5.29}$$

$$f_{ij}^{O} \leq \sum_{d \in \mathcal{D}} F_d p_{ijd}^{O} \qquad i \in \mathcal{N}^{L}, j \in \mathcal{N}^{U} \tag{5.30}$$

$$f_{ij}^{S} \leq \sum_{d \in \mathcal{D}} F_d p_{ijd}^{S} \qquad i \in \mathcal{N}^{U}, j \in \mathcal{N}^{S} \tag{5.31}$$

Constraint (5.32) ensures that at least O^M percentage of the CO_2 that is produced is captured, transported to loading ports, and sent out from loading ports. Furthermore, together with Constraints (5.25) and (5.27), it ensures that the same amount of CO_2 is transported all the way to permanent storage.

$$\sum_{i \in \mathcal{N}^{L}} |\mathcal{T}_i^{O}| \sum_{j \in \mathcal{N}^{U}} f_{ij}^{O} + \sum_{i \in \mathcal{N}^{L}} \sum_{j \in \mathcal{N}^{U}} \sum_{v \in \mathcal{V}} \sum_{t \in \mathcal{T}} K_v x_{ijvt} \geq \sum_{i \in \mathcal{N}^{E}} O^M P_i |\mathcal{T}_i^{O}| \tag{5.32}$$

Constraints (5.33) through (5.36) ensure that each port builds the number of docks needed to handle the ship traffic. Constraints (5.33) ensure that the binary variable δ_{ivt} gets assigned value 1 if ship v is docked in loading port i in time period t. After that, Constraints (5.34) ensure that the variable d_i is greater or equal to the maximum number of ships visiting the loading port in a time period. Thus, it represents the number of docks needed in that port. Similarly, Constraints (5.35) and (5.36) ensure the same behavior for unloading ports.

$$\sum_{j \in \mathcal{N}^{U}} \sum_{\tau = t - T_v^{L}}^{t} x_{ijv\tau} \leq \delta_{ivt} \qquad i \in \mathcal{N}^{L}, v \in \mathcal{V}, t \in \{\mathcal{T} | t \geq T_v^{L}\} \tag{5.33}$$

$$\sum_{v \in \mathcal{V}} \delta_{ivt} \leq d_i \qquad i \in \mathcal{N}^{L}, t \in \mathcal{T} \tag{5.34}$$

$$\sum_{j \in \mathcal{N}^{L}} \sum_{\tau = t - T_v^{L}}^{t} x_{ijv\tau} \leq \delta_{ivt} \qquad i \in \mathcal{N}^{U}, v \in \mathcal{V}, t \in \{\mathcal{T} | t \geq T_v^{L}\} \tag{5.35}$$

$$\sum_{v \in \mathcal{V}} \delta_{ivt} \leq d_i \qquad i \in \mathcal{N}^{U}, t \in \mathcal{T} \tag{5.36}$$

Variable domains

Finally, Constraints (5.37) to (5.52) define the domains of all decision variables. It should be noted that x-variables are only defined for pairs of a loading port and an unloading port. Thus, we do not define variables that represent sailing between two loading ports or between two unloading ports.

$$h_{ijv} \in \{0,1\} \qquad i \in \mathcal{N}^L, j \in \mathcal{N}^U, v \in \mathcal{V} \tag{5.37}$$

$$x_{ijvt} \in \{0,1\} \qquad i \in \mathcal{N}^L, j \in \mathcal{N}^U, v \in \mathcal{V}, t \in \mathcal{T} \tag{5.38}$$

$$x_{ijvt} \in \{0,1\} \qquad i \in \mathcal{N}^U, j \in \mathcal{N}^L, v \in \mathcal{V}, t \in \mathcal{T} \tag{5.39}$$

$$w_{ivt} \in \{0,1\} \qquad i \in \mathcal{N}^P, v \in \mathcal{V}, t \in \mathcal{T} \tag{5.40}$$

$$\delta_{ivt} \in \{0,1\} \qquad i \in \mathcal{N}^P, v \in \mathcal{V}, t \in \mathcal{T} \tag{5.41}$$

$$d_i \in \mathbb{Z}^+ \qquad i \in \mathcal{N}^P \tag{5.42}$$

$$b_i \geq 0 \qquad i \in \mathcal{N}^P \tag{5.43}$$

$$s_{it} \geq \underline{S}_{it} \qquad i \in \mathcal{N}^P, t \in \mathcal{T} \tag{5.44}$$

$$e_{it} \geq 0 \qquad i \in \mathcal{N}^L, t \in \mathcal{T} \tag{5.45}$$

$$c_i \geq 0 \qquad i \in \mathcal{N}^E \tag{5.46}$$

$$p^L_{ijd} \in \mathbb{Z}^+ \qquad i \in \mathcal{N}^E, j \in \mathcal{N}^E \cup \mathcal{N}^L \setminus \{i\}, d \in \mathcal{D} \tag{5.47}$$

$$p^O_{ijd} \in \mathbb{Z}^+ \qquad i \in \mathcal{N}^L, j \in \mathcal{N}^U, d \in \mathcal{D} \tag{5.48}$$

$$p^S_{ijd} \in \mathbb{Z}^+ \qquad i \in \mathcal{N}^U, j \in \mathcal{N}^S, d \in \mathcal{D} \tag{5.49}$$

$$f^L_{ij} \geq 0 \qquad i \in \mathcal{N}^E, j \in \mathcal{N}^E \cup \mathcal{N}^L \setminus \{i\} \tag{5.50}$$

$$f^O_{ij} \geq 0 \qquad i \in \mathcal{N}^L, j \in \mathcal{N}^U \tag{5.51}$$

$$f^S_{ij} \geq 0 \qquad i \in \mathcal{N}^U, j \in \mathcal{N}^S \tag{5.52}$$

5.4 Model enhancements

While the formulation of the model presented in Section 5.3 describes the problem sufficiently, the model may be solved faster by adding some additional constraints. This section presents two types of such constraints, namely symmetry-breaking constraints and valid inequalities.

Symmetry-breaking constraints

A challenge in MIP models such as ours is that two or more mathematically different solutions can be practically identical. Thus, one might use unnecessary computation time to compare such identical solutions. This phenomenon is known as symmetry and can be explained in our model by the following example: If one has 12 available ships of each ship type and a solution that requires nine ships of a ship type, one will need to compare $\frac{12!}{9!(12-9)!} = 220$ practically identical solutions.

Constraints (5.53) and Constraints (5.54) through (5.57) break the ship symmetries in the model. The former ensure that if several ships of the same ship type are used, ship v needs to be used if ship $v+1$ is used. This restricts the model from considering all ships within a ship type each time it investigates solutions with one more ship. Since all ships within a ship type are equal, this does not affect the solution quality.

$$\sum_{i \in \mathcal{N}^L} \sum_{j \in \mathcal{N}^U} (h_{ijv} - h_{ij,v+1}) \geq 0 \qquad c \in \mathcal{C}, v \in \mathcal{V}_c \tag{5.53}$$

Constraints (5.54) through (5.57) ensure that if ship v and ship $v+1$ are used and of the same ship type, ship v needs to start operating and sailing before ship $v+1$. This removes symmetry as one does not need to compare the order in which the ships start sailing. Similarly as for Constraints (5.53), it does not affect the quality of the optimal solution. In Constraints (5.54) through (5.57), the binary variable τ_{vt} is used as a supporting variable; which takes value 1 if the first time ship v starts sailing is in time step t. Thus, only one τ-variable gets assigned 1 for each ship, and the rest gets assigned value zero. The aforementioned properties are ensured through Constraints (5.54), (5.55) and (5.57). Constraints (5.56) break the symmetry as desired.

$$\sum_{t \in \mathcal{T}} \tau_{vt} \leq 1 \qquad v \in \mathcal{V} \tag{5.54}$$

$$x_{ijvt} - \sum_{t_1=0}^{t-1} x_{ijv,t_1} \leq \tau_{vt} \qquad i \in \mathcal{N}^L, j \in \mathcal{N}^U, v \in \mathcal{V}, t \in \mathcal{T} \tag{5.55}$$

$$\sum_{t \in \mathcal{T}} t \cdot \tau_{vt} - \sum_{t \in \mathcal{T}} t \cdot \tau_{v+1,t} + 1 \leq \sum_{i \in \mathcal{N}^L} \sum_{j \in \mathcal{N}^U} h_{ijv} \qquad c \in \mathcal{C}, v \in \{\mathcal{V}_c | v < |\mathcal{V}_c|\} \tag{5.56}$$

$$\tau_{vt} \in \{0,1\} \qquad v \in \mathcal{V}, t \in \mathcal{T} \tag{5.57}$$

Valid inequalities

Valid inequalities are used to make the formulation of the model stronger by tightening the feasible region of the LP-relaxation of the problem. Constraints (5.58) and (5.59) are added as valid inequalities. They ensure that ships only can sail on one link, namely between one loading port and one unloading port. The property is also ensured by defining the variable h_{ijv} for a loading port i and an unloading port j. However, by formulating the same requirement through the variable x_{ijvt}, Constraints (5.58) and (5.59) might strengthen the formulation. The term $\frac{\lceil |\mathcal{T}| \rceil}{T_{ijvt}+T_{jivt}}$ serves the purpose of a Big-M parameter, as it computes the largest possible value that the right hand side of the constraints can take.

$$\frac{\lceil |\mathcal{T}| \rceil}{T_{ijvt} + T_{jivt}} (1 - x_{ijvt}) \geq \sum_{k \in \mathcal{N}^L \setminus \{j\}} \sum_{\tau \in \mathcal{T}} x_{ikv\tau} \quad i \in \mathcal{N}^U, j \in \mathcal{N}^L, v \in \mathcal{V}, t \in \mathcal{T} \quad (5.58)$$

$$\frac{\lceil |\mathcal{T}| \rceil}{T_{ijvt} + T_{jivt}} (1 - x_{ijvt}) \geq \sum_{k \in \mathcal{N}^L \setminus \{j\}} \sum_{\tau \in \mathcal{T}} x_{ikv\tau} \quad i \in \mathcal{N}^L, j \in \mathcal{N}^U, v \in \mathcal{V}, t \in \mathcal{T} \quad (5.59)$$

Chapter 6

Data and Scenarios

As presented in Chapter 1, we choose to apply the model to a case with emission sources in Germany and storage infrastructure in Norway. This chapter presents the input data needed for designing such a German-Norwegian CCS supply chain. This includes a description of the sets in Section 6.1, and the necessary parameter values in Section 6.2. Then, in Section 6.3, we present a set of scenarios based on the available emission sources, loading ports, and unloading ports, which are used for the analyses in the subsequent chapters.

6.1 Input data for the model sets

Unloading ports

This set only contains one port located in Kollsnes, Norway. This is the unloading port used in the Northern Lights project, which offers the world's first CO_2 storage infrastructure that is open to international customers (Northern Lights JV DA 2022). There are no other such projects in Norway that are currently being developed, and therefore, no other ports than Kollsnes are natural to include in this set.

Loading ports

The set of Loading ports only includes the port of Wilhelmshaven, Germany. Other relevant ports near Germany, such as Rotterdam, Antwerp, and Dunkirk, have been considered, as these are deemed to be vital exporting ports for CO_2 in future European CCS development through ongoing European CCS projects (Directorate-General for Energy 2021). However, preliminary testing found that Wilhelmshaven is consistently chosen as the loading port in the model solutions. This also fits well with the newly announced German combined hydrogen and CCS project, described in Section 2.4, where Wilhelmshaven plays a central role as the planned exporting hub for CO_2 from German industrial emitters (Wintershall Dea 2022). Therefore, we only include Wilhelmshaven in this set to avoid redundant loading ports and align with the German CCS strategy.

Emission sources

Emission sources are chosen from a dataset of German pollution in 2018 provided by The Federal Environment Agency (2018). The dataset contains information about major polluting facilities in Germany in 2018 and can be filtered by type of pollution. The 337 emission sources that emit CO_2 are illustrated in Figure 6.1, and are presented in Appendix D.

Figure 6.1: Map of German emission sources. The locations are retrieved from The Federal Environment Agency (2018).

Storage locations

In this thesis, we use one storage location. This is the Northern Lights exploitation permit EL001 "Aurora" in the saline aquifer known as the Johansen formation, south in the Troll field. The location is illustrated in Figure 6.2. The storage capacity of the permit is based on the initial phase of Northern Lights aiming at 1.5 Mtpa CO_2 through one injection point over 25 years, which results in a total of 37.5 Mt CO_2 stored. However, the theoretical capacity of the Johansen formation is 1 Gt (Eigestad et al. 2009). Thus, with a successful initial phase, we assume that Northern Lights will seek to extend the allowed storage capacity as CCS demand increases. This extension will likely happen through additional injection points and exploitation permits within and nearby the Johansen formation. This will enable Northern Lights to exploit the

already existing infrastructure and use the full storage potential of the Johansen formation and the additional storage capacity of surrounding saline aquifers. With this reasoning, and for simplicity, EL001 is modeled as the storage location for all volume scenarios throughout this thesis.

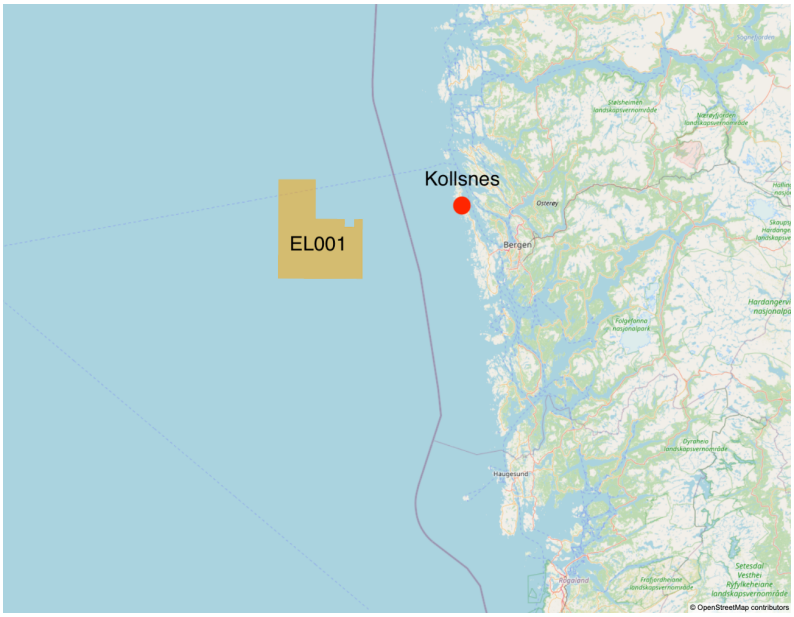

Figure 6.2: The location and surroundings of EL001

Ships

Each ship is associated with a ship type $c \in \mathcal{C}$, where the load capacities of the ships distinguish the types. Table 6.1 presents the capacities and thus the ship types. Hence, the parameter K_v refers to one of the elements in the column "Ship capacity", depending on which ship type ship v represents. Based on the discussions in Chapter 2.2.2, we have included six ship capacities, ranging from 50 000 tonnes to 100 000 tonnes.

For our analyses, we include 12 indexed ships of each type, which makes the cardinality $|\mathcal{V}_c| = 12$, $c \in \mathcal{C}$, and the cardinality $|\mathcal{V}| = |\mathcal{V}_c| \times |\mathcal{C}| = 12 \times 6$.

Pipeline diameters

The set of pipeline diameters are defined as $\mathcal{D} = \{0.2, 0.3, 0.4, 0.5, 0.6, 0.7, 0.8, 0.9, 1.0\}$, where diameters are defined as inner diameter measured in meters. Calculations of optimal pipeline diameters are complex, where flow rates, density, viscosity, pipe roughness, topography, bends, and pressure drop impact the design (Vandeginste and Piessens n.d.). However, diameters of current and considered CO_2 transportation pipelines typically range from 0.2 meters to slightly below 1 meter (Peletiri et al. 2018; Serpa et al. 2011).

Table 6.1: Fuel consumption for different ship capacities when sailing at the service speed of 14 knots (Roussanaly et al. 2021).

Ship capacity (tonnes)	Fuel consumption (tonne/km)
50 000	0.260
60 000	0.287
70 000	0.308
80 000	0.320
90 000	0.325
100 000	0.328

Time periods

The model is solved over a defined planning horizon, where the set of time periods is denoted $\mathcal{T}$. The set includes indexed time periods $t \in \mathcal{T}$, with an equal length of 12 hours. The number of time periods included in the planning horizon is yet to be decided. As we solve a strategic problem, the length of the planning horizon must be sufficiently long to find a stable solution, where the impact of start and stop effects are negligible. As discussed in 5.1, such a planning horizon will also provide solutions representative of longer planning horizons.

6.2 Parameter values

Time

Three time-related parameters have not been introduced so far. The first parameter is T_v^L, which is the number of time periods ship v uses to complete one operation in a port. Here, $T_v^L = 1$, meaning that it takes one time period, or 12 hours, to load or unload. 12-hour loading and unloading time is considered to apply for all ship types (ZEP 2021). Secondly, the parameter T_{ijvt} represents the number of time periods ship v uses to operate in port i and sail from port i to port j. Thus, it includes T_v^L. The parameter is indexed by t to allow for varying sailing times, so that seasonality or daily variations in weather can be incorporated into the model. The final parameter, H, is not introduced in the model. However, it is needed when pre-calculating the cost parameters. The parameter H represents the length of the project horizon, which in turn represents a reasonable lifetime for the physical equipment used, such as ships and pipelines. As seen later in this section, it is used to scale the investment costs down to the length of the planning horizon. Here, it is set to 20 years, so $H = 20$.

Distances

The distance D_{ij} on the arc between two nodes i and j is calculated by the Haversine formula, which calculates the great-circle distance between nodes. This applies to both sailing legs and pipelines. Since straight lines underestimate the actual distances to some degree, we have adjusted for this by scaling the distances by a factor of 1.1. This means that we assume that all transportation follows a path that is 10% longer than the straight line.

6.2.1 Ship costs

Ship hiring cost

The cost of hiring ship v for the planning horizon is calculated based on its capacity and the length of the planning horizon. Hiring costs consist of two components: a share of the investment cost for the ship and a fixed OPEX. The latter include, amongst others, regular maintenance, insurance, and the cost of the crew. To calculate the share of investment cost to assign to the planning horizon, we assume linear depreciation of investment costs over the length of the project horizon, H. Thus, the 20-year project horizon implies a yearly depreciation of 5%. Hence, the annual CAPEX is 5% of the investment costs. The next part of the hiring cost is the fixed OPEX. Based on Roussanaly et al. (2021), this is set to 5% of the construction costs. Thus, the yearly hiring cost is 10% of the initial investment cost. This is further scaled up or down to the length of the planning horizon by the term $\frac{\overline{T}}{365}$, where $\overline{T}$ is the length of the planning horizon in the number of days.

The construction cost for ship v, here named I_v, depends on the ship type. Based on construction costs found in the literature, Amlie et al. (2018) made a non-linear regression to estimate the construction cost in GBP as a function of capacity. This function, presented in Equation (6.1), is used in our cases and converted to euro using a currency exchange rate of 1.18 EUR/GBP. Finally, Equation (6.2) expresses the hiring costs for ship v.

$$I_v = 1.18 \left(198\ 100 \cdot K_v^{V(0.5369)}\right) \tag{6.1}$$

$$C_v^H = \left(\frac{I_v}{H} + 0.05 I_v\right) \frac{\overline{T}}{365} = \left(\frac{I_v}{20} + 0.05 I_v\right) \frac{\overline{T}}{365} = 0.1 I_v \cdot \frac{\overline{T}}{365} \tag{6.2}$$

Ship costs

The ship costs are divided into three elements, namely sailing costs, port fees, and waiting costs. The cost of sailing a route is calculated by multiplying the route distance in kilometers by the cost per kilometer sailed. The cost per kilometer sailed depends on the cost of fuel and the ship's fuel consumption. Based on the average fuel price for Very Low Sulfur Fuel Oil (VLSFO) since 2019, the cost of fuel is set to 500 euro per tonne (Ship & Bunker 2022). Fuel consumption for each ship type is based on the work of Roussanaly et al. (2021) and presented in Table 6.1. It should be noted that the fuel consumption is based on an assumed service speed of 14 knots, and is only dependent on distance. The cost of sailing from port i to port j with ship v is represented by Equation (6.3). D_{ij} is the distance between the ports, F_v is the fuel consumption as presented in Table 6.1, and 500 is the fuel price in euro per tonne.

$$C_{ijv}^{[sail]} = D_{ij} \cdot F_v \cdot 500 \tag{6.3}$$

Port fees for using space and facilities occur when ships moor at docks. Based on the works from Amlie et al. (2018), we use a regression model as presented in Equation (6.4) to calculate the port fees. The term in the numerator is the port costs per round

trip, denoted in GBP. Thus, we divide by two to get the cost per port visit and multiply it with an assumed exchange rate of 1.18 EUR/GDP. It should be noted that this calculation assumes equal port fees for all ports.

$$C_{iv}^{[fee]} = 1.18 \cdot \frac{0.4635K_v + 5559.3}{2} \tag{6.4}$$

The sailing cost and port cost parameters are merged into the parameter C_{ijv}^{T} for readability.

$$C_{ijv}^{T} = C_{ijv}^{[sail]} + C_{iv}^{[fee]} \tag{6.5}$$

The last part of the ship costs is the cost of waiting, denoted C_v^W, and given in euro per time step. As the propulsion engine is not required during stationary waiting, the fuel consumption when waiting is approximated by the fuel consumption of the auxiliary engine. Based on the works from Li and Jia (2020) and Global Maritime Energy Efficiency Partnerships (2022), this is assumed to be equal to 15% of the total fuel consumption during sailing. Equation 6.6 presents the calculation of the waiting cost. The fuel cost is $500 \cdot F_v$ euro per km. By multiplying with the speed of 14 knots and adjusting that one nautical mile is 1.852 km, we get the cost in euro per hour. Finally, we find the waiting cost per time period by multiplying by the number of hours in a time period, namely 12.

$$C_v^W = 0.15 \cdot 500 \cdot F_v \cdot 1.852 \cdot 14 \cdot 12 \tag{6.6}$$

6.2.2 Port facility costs

The following section presents the port facility costs specific to ship transportation. They comprise the buffer storage cost, docks construction cost, the cost of loading and unloading facilities, and liquefaction and reconditioning costs.

Buffer storage cost

The buffer storage costs, C^B, are calculated based on the storage capacity. They have two components: a depreciated share of the investment costs and some fixed OPEX. The investment costs are proportional to storage capacity and are 478 euro per tonne of storage capacity according to (Bjerketvedt et al. 2022). Yearly fixed OPEX is set to a share of the investment costs here as well, namely 6%. Both investment costs and fixed OPEX are scaled linearly to the length of the planning horizon. In the same way, as for ship hiring costs, this results in yearly costs of 11% (5% + 6%) of the investment costs. Equation (6.7) expresses the total buffer costs per tonne of storage capacity.

$$C^B = \left(\frac{478}{H} + 0.06 \cdot 478\right) \frac{\overline{T}}{365} = \left(\frac{478}{20} + 0.06 \cdot 478\right) \frac{\overline{T}}{365} = 52.6 \cdot \frac{\overline{T}}{365} \tag{6.7}$$

Liquefaction cost

Liquefaction cost is calculated based on the throughput of CO_2 and the length of the planning horizon. The throughput affects the required capacity of the liquefaction facility, which in turn affects the construction cost. As for ships and buffer storages, the liquefaction facility investment cost is linearly depreciated over the project horizon, and yearly fixed OPEX is a share of the initial investment cost. While Roussanaly et al. (2021) use a cost power-law (Chauvel et al. 2003) to approximate the investment costs as a function of yearly throughput, we approximate the investment costs as a linear function of annual throughput to keep our model linear. This implies a slight overestimation of the liquefaction costs, especially for large volumes. The investment cost is approximated to 17.3 euro per tonne CO_2 of yearly liquefaction capacity (Roussanaly et al. 2021). Note that this cost assumes that the CO_2 is pressurized to approximately 90 bar when it arrives at the liquefaction facility, which is the case when the CO_2 comes in pipelines from inland emitters. The second part of the fixed cost is the yearly fixed OPEX, which is 6% of the investment cost (Roussanaly et al. 2021). Both the investment cost and the fixed annual OPEX are scaled down to the length of the planning horizon.

As the liquefaction process is energy-intensive, there are also some variable costs. These costs are estimated based on electricity consumption and the unit price of electricity. As Roussanaly et al. (2021), we estimate the electricity consumption to be 20 kWh per liquefied tonne of CO_2 and assume the electricity price to be 0.08 euro per kWh.

Based on the discussion above, the total liquefaction cost is presented by Equation (6.8). As the parameters are multiplied with the quantity throughput during the planning horizon, not yearly throughput, we need to scale the throughput to the length of a year by the expression $\frac{365}{\overline{T}}$.

$$C^L = \frac{365}{\overline{T}} \left(\frac{17.3}{H} + 0.06 \cdot 17.3 \right) \frac{\overline{T}}{365} + 20 \cdot 0.08 = \left(\frac{17.3}{20} + 1.038 \right) + 1.6 = 3.50 \quad (6.8)$$

Reconditioning cost

The calculation of the reconditioning costs is similar to that of liquefaction, including facility investment costs, fixed OPEX, and variable OPEX. Based on the work by Bjerketvedt et al. (2020), the investment cost is 9 euro per tonne of CO_2 in yearly reconditioning capacity. Moreover, the fixed OPEX is 4.6% of the investment costs, and the variable cost is 0.41 euro per tonne of reconditioned CO_2. As for liquefaction, the reconditioning cost is scaled down to the length of the planning horizon. The cost, denoted C^R, is presented in Equation (6.9).

$$C^R = \frac{365}{\overline{T}} \left(\frac{9}{H} + 0.046 \cdot 9 \right) \frac{\overline{T}}{365} + 0.41 = \left(\frac{9}{20} + 0.41 \right) + 0.41 = 1.27 \quad (6.9)$$

Dock cost

When estimating the dock cost, C_i^D we assume that one dock can host and serve one ship simultaneously and that all considered ship types can moor to the dock. Furthermore, we consider the dock cost to exclude specific CCS-related equipment handled independently, such as facilities for buffer storage, liquefaction, reconditioning, and loading and unloading, as these are handled independently. Based on the works from Andhra Pradesh Gas Distribution Cooperation Ltd. (2012), the investment cost for one dock is estimated to be 90 million euro. The dock cost does not include any operational costs, as these are included in the loading and unloading costs. The parameter value is presented in Equation (6.10).

$$C_i^D = \frac{90\ 000\ 000}{H} \cdot \frac{\overline{T}}{365} = \frac{90\ 000\ 000}{20} \cdot \frac{\overline{T}}{365} = 4\ 500\ 000 \cdot \frac{\overline{T}}{365} \tag{6.10}$$

Cost of loading and unloading facilities

The final port facility cost, C_i^I, is the cost of the loading and unloading facilities in the port docks. This includes the loading arms, pipe systems, pumps, and other equipment and operations needed to transfer the CO_2 to and from the ships in the docks. The costs are set equal for all ports in our model, as done by Roussanaly et al. (2021). This cost has two components. The first is the investment cost, related to the required port facilities to handle the amounts loaded or unloaded, while the second component is the fixed operational cost. According to Roussanaly et al. (2021), the investment cost is 2.33 euro per tonne CO_2 of yearly throughput, while the yearly fixed operational cost is 2% of the investment cost for the facility. Equation (6.11) presents the parameter value, denoted per tonne of CO_2 loaded or unloaded. The investment costs are depreciated over the project horizon in the same way as for ships.

As we see from the objective function in Equation (5.3), C_i^I is multiplied by the total amount of loaded/unloaded CO_2 over the planning horizon, which is given by the terms $K_v x_{ijvt}$ and $(1 - (B \cdot T_{ijvt}))\, K_v x_{ijvt}$ for loading and unloading ports, respectively. Since the investment cost of 2.33 euro is defined per tonne of yearly throughput, we need to multiply with $\frac{365}{\overline{T}}$ to scale the amount loaded/unloaded up to a year. The inverse term, $\frac{\overline{T}}{365}$ is needed to scale the yearly costs to the length of the planning horizon. In total, these two terms cancel out.

$$C_i^I = \frac{365}{\overline{T}} \left(\frac{2.33}{H} + 0.02 \cdot 2.33 \right) \frac{\overline{T}}{365} = \frac{2.33}{20} + 0.0466 = 0.163 \tag{6.11}$$

6.2.3 Pipeline costs

Pipeline investment and fixed cost

Pipelines require large initial investments and both fixed and variable operational costs. The underlying drivers for the investment cost are the required CO_2 flow capacities, the pipeline length, and the terrain that the pipeline crosses. In the model, we apply a set of pipeline diameter options when constructing pipelines. The calculation of the CO_2 flow capacity given a pipeline diameter is non-trivial. However, it can be

simplified by applying a widely used velocity-based equation (Knoope et al. 2013), seen in Equation (6.12). D_d is the inner diameter of the pipeline with diameter option d, in meters. With CO_2 pressurized to supercritical state, the density is typically 850 kg/m^3 (Serpa et al. 2011) and the velocity is around 2 m/s (Knoope et al. 2013). Thus, the flow capacity parameter F'_d is given as kg CO_2 per second. Furthermore, Equation (6.13) presents parameter F_d, as used in the model, where the flow is converted from kg/s to tonnes per time step. T^P is the number of days in one time period.

$$F'_d = \frac{density \cdot velocity \cdot \pi}{4} \cdot D_d^2 = \frac{850 \cdot 2 \cdot \pi}{4} \cdot D_d^2 = 425\pi D_d^2 \tag{6.12}$$

$$F_d = \frac{F'_d \cdot 86\ 400 \cdot T^P}{1000} \tag{6.13}$$

Equation (6.14) presents the conversion of flow from tonnes per time step, F_d, to Mtpa, F_d^Y, as this is used in further calculations.

$$F_d^Y = \frac{F_d \cdot 365}{T^P} \cdot \frac{1}{1\ 000\ 000} = \frac{F_d \cdot 365}{0.5 \cdot 1\ 000\ 000} = \frac{F_d \cdot 365}{500\ 000} \tag{6.14}$$

The investment cost per kilometer of pipeline is derived based on a simplifying heuristic developed by Serpa et al. (2011), as presented in Equation (6.15). The heuristic is based on empirical data on the investment costs of previous natural gas pipeline projects, and is thus assumed to include all cost aspects related to constructing pipelines. There, α and β are found through independent estimation to be 0.533 and 0.019, respectively. As the heuristic estimates the cost in million euro, we multiply by 1 000 000 to obtain the cost in euro.

$$C_d = \left(\alpha + \beta \cdot F_d^Y\right) \cdot 1\ 000\ 000 = \left(0.533 + 0.019 \cdot F_d^Y\right) \cdot 1\ 000\ 000 \tag{6.15}$$

Finally, the calculation of the parameter C_{ijd}^{PL} is presented in Equations (6.16) and (6.17). Equation (6.16) presents the total investment cost for pipelines between nodes i and j. As this is based on the cost for onshore pipelines traversing flat terrain, T_{ij}^F represents an adjusting terrain factor for the pipeline path between nodes i and j. The terrain factor adjusts for higher costs due to complicating terrain along the path, such as densely populated or mountainous terrain, or offshore paths. Here, T_{ij}^F is assigned the value 1.2 for all onshore pipelines and 2.0 for all offshore and storage pipelines (Serpa et al. 2011). Equation (6.17) concludes the discussion of pipeline costs. With the same approach as for ship hiring costs, the total CAPEX and fixed OPEX are scaled down to the length of the planning horizon. Here, fixed OPEX represents 2.5% of the investment cost. While Equation (6.17) presents the calculation of C_{ijd}^{PL}, it should be noted that the same calculation applies to the cost of offshore pipelines, C_{ijd}^{PO}, and storage pipelines, C_{ijd}^{PS}, where only the terrain factor in Equation (6.16) differentiates the calculations.

$$C_{ijd}^I = C_d \cdot D_{ij} \cdot T_{ij}^F \tag{6.16}$$

$$
\begin{aligned}
C_{ijd}^{PL} &= \left(\frac{C_{ijd}^{I}}{H} + 0.025 \cdot C_{ijd}^{I} \right) \frac{\overline{T}}{365} \\
\Rightarrow C_{ijd}^{PL} &= \left(\frac{C_{ijd}^{I}}{20} + 0.025 \cdot C_{ijd}^{I} \right) \frac{\overline{T}}{365} \\
\Rightarrow C_{ijd}^{PL} &= 0.075 C_{ijd}^{I} \cdot \frac{\overline{T}}{365}
\end{aligned} \tag{6.17}
$$

Table 6.2 presents the parameter values F_d and C_d, as well as yearly flow capacity, for the pipeline options included in our model.

Table 6.2: Flow capacities and cost for the chosen pipeline diameters.

d	$\mathbf{D}_d$ **(m)**	$\mathbf{F}_d$ **(tonnes/time step)**	**Capacity (Mtpa)**	$\mathbf{C}_d$ **(€/km)**
1	0.2	2 307	1.7	565 001
2	0.3	5 191	3.8	605 001
3	0.4	9 229	6.7	661 003
4	0.5	14 420	10.5	733 004
5	0.6	20 765	15.2	821 006
6	0.7	28 263	20.6	925 008
7	0.8	36 915	26.9	1 045 011
8	0.9	46 721	34.1	1 181 013
9	1.0	57 680	42.1	1 333 017

Pipeline variable operational cost

The variable operational pipeline costs, C_{ij}^{V}, are essentially the costs of energy consumption required to maintain the desired transportation conditions of the CO_2 in the pipelines. The onshore pipelines are equipped with booster stations that take care of pressure drops along the pipeline and keep the pressure above the critical point of 73.8 bar. The offshore pipelines cannot have booster stations due to technical restrictions. Instead, they must pressurize the flow to a sufficient pressure at the inlet of the pipeline, such that the outlet conditions after the pressure drop along the pipeline are sufficient. For storage pipelines, the equipment of booster stations depends on whether they are onshore or offshore. For simplicity, we assume that the energy consumption is equal for all types of pipelines. The variable costs are therefore the cost of electricity needed to boost the pressure along these pipelines and keep the CO_2-flow above the critical point. Knoope et al. (2013) finds that most papers regarding variable operations cost of CO_2 pipelines use an equation derived by McCollum and Ogden (2006) to determine the pumping power requirement for the boosters given a daily flow of CO_2. We also apply this equation to determine the pumping power requirement of the boosters, and the equation is shown in (6.18).

$$
W_b = \left(\frac{1000}{24 \cdot T^P \cdot 36} \right) \cdot \left[\frac{m(P_{out} - P_{in})}{\rho \eta_p} \right] = \left(\frac{1000}{24 \cdot 0.5 \cdot 36} \right) \cdot \left[\frac{m(130 - 90)}{817 \cdot 0.75} \right] = 0.151 \cdot m \tag{6.18}
$$

In the formula above, W_b represents the booster pumping power requirement in kW. In the first multiplicator of the formula, 1000 represents kilograms per tonne, and 24 is hours per day. T^P is the number of days per time period, which in our case is 0.5. 36 is a parameter set by McCollum and Ogden (2006) whose unit of measurement is $m^3 \cdot$ bar/hr per kW. In the bracket, m is the CO_2 flow rate in tonnes per time period. P_{out} is the outlet pressure of the booster in bar, which in our case is set to 130 bar. P_{in} is the inlet pressure of the booster in bar, which is set to 90 bar. The difference $P_{out} - P_{in}$ represents the pressure drop between the booster stations. ρ is the density of the pressurized CO_2 in kg/m^3 which is 817 kg/m^3 at the highest operating pressure of 130 bar. η_p is the pump efficiency, which usually is set to 75% (Knoope et al. 2013). The parameters used are also summarized in Table 6.3.

Table 6.3: Parameters used to calculate the variable costs of pipeline flow.

Parameter	Value
T^P	0.5 days
P_{out}	130 bar
P_{in}	90 bar
ρ	817 kg/m^3
η_p	75 %

The flow per time period is the variable associated with the power requirement. The equation must be divided by the flow m to apply to our pipeline flows. Assuming an electricity cost of 0.08 euro per kWh, the variable cost associated with a given flow m through a booster over a time period is given by Equation (6.19). Note that $24 \cdot T^P$ represents the operating hours of the booster over a time period.

$$C^V = \frac{W_b}{m} \cdot 24 \cdot T^P \cdot 0.08 = \frac{m \cdot 0.151}{m} \cdot 24 \cdot 0.5 \cdot 0.08 = 0.145 \tag{6.19}$$

Knoope et al. (2013) also states that the literature agrees with the assumption that booster stations are needed roughly every 200 km of pipeline to maintain the desired operating pressure. We linearize the pressure drop along the pipeline to model the energy consumption costs for pipelines of lengths that are not a multiplier of 200. We scale the pumping power requirement to the length of the pipeline. Thus, the variable cost parameter C^V_{ij} for a pipeline with distance D_{ij} for each time period is given in Equation (6.20).

$$C^V_{ij} = C^V \cdot \frac{D_{ij}}{200km} = 0.145 \cdot \frac{D_{ij}}{200km} \tag{6.20}$$

6.2.4 Capture and storage costs

Capture costs

Capture costs are primarily dependent on the type of combustion process that releases the CO_2 and may vary significantly between different emission sources. Bains et al. (2017) and the IEA (2022) have estimated the costs of carbon capture for a set of industrial processes. Their estimated costs vary from 15-25 euro per tonne CO_2 for

processes producing highly concentrated CO_2 streams, such as ethanol production, to 40-120 euro per tonne CO_2 for processes with dilute gas streams, such as cement production and power generation from fossil fuels. As evident from these ranges, the cost of capture is uncertain. The emitters presented in Section 6.1 represent various sectors and industrial processes, which translate to different requirements regarding capture technologies. Every emission source has an associated NACE sector, a standardized classification of economic activities in the EU. To estimate their capture costs, the emission sources have been mapped to a set of industry-specific CO_2 capture processes provided by Bains et al. (2017) and the IEA (2022) through their NACE sector. The capture cost estimate is set to the average of the given capture cost range. An overview of the mapping from NACE sector to capture process and costs can be seen in Table 6.4.

Table 6.4: Examples of our mapping of NACE sector to industrial process and capture costs. The NACE sectors are collected from Federal Environment Agency Germany (2022), and the industrial processes and capture costs are collected from Bains et al. (2017) and IEA (2022).

NACE sector	Industrial process	Cost range (€)	Cost estimate (€)
Manufacture of industrial gases	Refinery	35-100	67.5
Manufacture of man-made fibres	Refinery	35-100	67.5
Manufacture of oils and fats	Refinery	35-100	67.5
Manufacture of plastics in primary forms	Refinery	35-100	67.5
Manufacture of paper and paperboard	Refinery	35-100	67.5
Manufacture of refined petroleum products	Refinery	35-100	67.5
Treatment and coating of metals	Refinery	35-100	67.5
Manufacture of flat glass	Refinery	35-100	67.5
Distribution of gaseous fuels through mains	Power generation	50-100	75
Production of electricity	Power generation	50-100	75
Steam and air conditioning supply	Power generation	50-100	75
Casting of iron	Iron and steel	40-100	70
Copper production	Iron and steel	40-100	70
Manufacture of basic iron and steel and of ferro-alloys	Iron and steel	40-100	70
Aluminium production	Iron and steel	40-100	70
Manufacture of cement	Cement	60-120	90
Manufacture of lime and plastic	Cement	60-120	90
Manufacture of fertilisers and nitrogen compounds	Ammonia	25-35	30
Mining of chemical and fertiliser minerals	Ammonia	25-35	30
Manufacture of other inorganic basic chemicals	Ethylene oxide	25-35	30
Manufacture of other organic basic chemicals	Ethylene oxide	25-35	30
Manufacture of coke oven products	Coal	41-51	46

Storage costs

The cost of storage, C_i^S, is based on the work of ZEP (2011), which provide realistic cost estimates of CO_2 storage based on ZEP members' extensive knowledge and experience. They divide the storage opportunities into six cases, differentiated by the type of geological storage reservoir, which is either depleted oil and gas fields (DOGF) or saline aquifers (SA), whether the storage reservoir is offshore or onshore, and if there exist legacy wells, which only applies to DOGF. The type of storage considered in this thesis is offshore SA, such as the Johansen formation in the Norwegian North Sea shelf used in the Northern Lights project.

Through a sensitivity analysis of the most important cost drivers such as field capacity, well injection rate, well depth, well completion costs, and the number of observation wells and exploration wells, ZEP (2011) estimates a range for the storage costs in offshore SA. The range is divided into low-, medium-, and high-cost scenarios, mainly

based on the economies of scale which can be achieved with higher field capacity. The low-cost scenario applies to storage fields greater than 200Mt. As the Johansen formation has a theoretical capacity of 1 Gt (Eigestad et al. 2009), the low-cost scenario is a reasonable assumption for the costs associated with storing CO_2 in the Johansen formation. The cost summary provided by ZEP (2011) is shown in Table 6.5.

Table 6.5: Summary of parameters in the low-cost scenario from ZEP (2011) for storage in an offshore SA

Attribute	**Value**
CO_2 stored	200 Mt
Lifetime	40 years
CO_2 injection rate	5 Mtpa
CAPEX	M€ 238
Annualized CAPEX	M€ 20
OPEX	M€ 8
CAPEX	€ 1 per tonne
Annualized CAPEX	€ 4 per tonne
OPEX	€ 2 per tonne
Cost of storage	**€ 6 per tonne**

From Table 6.5 we see that the cost parameter for storage, C_i^S, equals 6 euro per tonne CO_2 stored for the storage location considered in our thesis. However, one must note that this cost may be an overestimation of the actual cost, as higher capacity and CO_2 injection rates may amplify economies of scale. Since the Johansen formation is of even greater capacity than the 200 Mt capacity discussed by ZEP (2011), and the injection rate in some scenarios will be higher than 5 Mtpa, the costs could be lower.

6.2.5 Miscellaneous parameters

In this section, we present values for various parameters which do not fit in the structure of the previous subsections. The parameters and their values are all presented in Table 6.6. The first one, P_i, is the amount of CO_2 produced in the inland emission sources (Federal Environment Agency Germany 2022). All emission sources and their corresponding values for P_i are presented in Appendix D. In short, the emissions vary between 0.1 Mtpa and 11.7 Mtpa, with an average of 0.60 Mtpa and a median of 0.26 Mtpa. One should note that, while the data is fetched from the Federal Environment Agency in Germany, it was collected in 2018. Thus, it could already be outdated. Furthermore, while we use this data for all current and future scenarios, it will not necessarily represent future emissions. Some factories will shut down, some new factories will be built, and some will continue operations, but possibly with changed emissions. Lastly, we have assumed that all of the emissions can be captured. Despite being a significant simplification, it works well to estimate which current and future inland emissions are available for capture in Germany.

The second parameter is the overspill cost, C^E, which is the cost per tonne emitted due to overspill in loading ports. Based on historical prices for CO_2 emission allowances in the Emission Trading System in the EU (EU ETS), this is set as 80 euro per tonne.

The third parameter, B, is the boil-off rate. This is the percentage of a full shipload of CO_2 that is lost due to evaporation during a time period of 12 hours of sailing. Based on the works from IEA (2004), this is set to 0.1% of the full shipload. $\underline{S}_i$ represents the inventory lower bound of the buffer storages and is set to zero. Finally, the parameter O^M represents the percentage of the supplied CO_2 from the inland emission sources that the system needs to transport all the way to storage. This parameter can not be 100% due to end of horizon effects concerning ship transportation. However, through testing, we have found that 97% is a reasonable value for O^M.

Table 6.6: The miscellaneous parameters and their values.

Parameter	Value
P_i	0.1-11.7 Mtpa
C^E	€ 80 per tonne
B	0.1 % per time period
$\underline{S}_i$	0
O^M	97%

6.3 Basic scenarios

The following section presents the scenarios used for the computational study. The scenarios are prepared based on what is assumed to be a realistic future development of the European CCS logistics infrastructure. Each scenario in this thesis consists of a combination of emission sources with associated yearly CO_2 emission rates, a loading port, an unloading port, and a storage site. The purpose of the scenarios is to see how the system changes with an increasing number of emission sources and amounts of CO_2 to be handled. All scenarios have Wilhelmshaven in Germany as the only loading port, and Kollsnes in Norway as the only unloading port. The storage site is EL001.

The amounts of CO_2 to be handled by the model set the basis of the scenarios. Here, we present scenarios with amounts 5, 20, 50, and 100 Mtpa. These amounts can be seen in context with anticipated demand for CCS in the years 2030, 2040, and 2050, and with the loosely planned capacity expansion of the Northern Lights project. Northern Lights already plans to have capacities of 1.5 and 5 Mtpa, where the 1.5 Mtpa capacity system is scheduled to be operational by 2024. If proven successful, the demand for CCS may increase rapidly. After the initialization of phase two with 5 Mtpa, CO_2 amounts of 20, 50, and 100 Mtpa are natural starting points for simulating this rapid increase and may as well represent the demand for CCS in the basic scenarios in this thesis.

When the amount of CO_2 to be handled by the model is decided, we must determine what emission sources to include in the scenario. When choosing amongst the set of emission sources to form the basic scenarios, we prioritize on the amount that the sources emit. When prioritizing on amount emitted only, we choose the subset of the largest German emission sources whose emissions sum up to a target amount of either 5, 20, 50, or 100 Mtpa. The largest emission source emits about 11.7 Mtpa. Thus, in the 5 Mtpa scenario, we model with a 5 Mtpa fraction of the 11.7 Mtpa emission source being captured. The map of the 100 Mtpa scenario where emission sources are prioritized based on size only can be seen in Figure 6.3. A rationale for the prioritiza-

tion of the amount emitted is that we restrict the onshore infrastructure possibilities sensibly and thus ease the computational burden of the model. Furthermore, large point sources with a significant supply of CO_2 are sensible to include as they are more likely to make the transportation system efficient. The largest emitters are also the ones who are most likely to have the financial strength needed to invest in retrofitting their plants with CO_2 capture facilities, which in turn makes the prioritization reasonable from a microeconomic perspective.

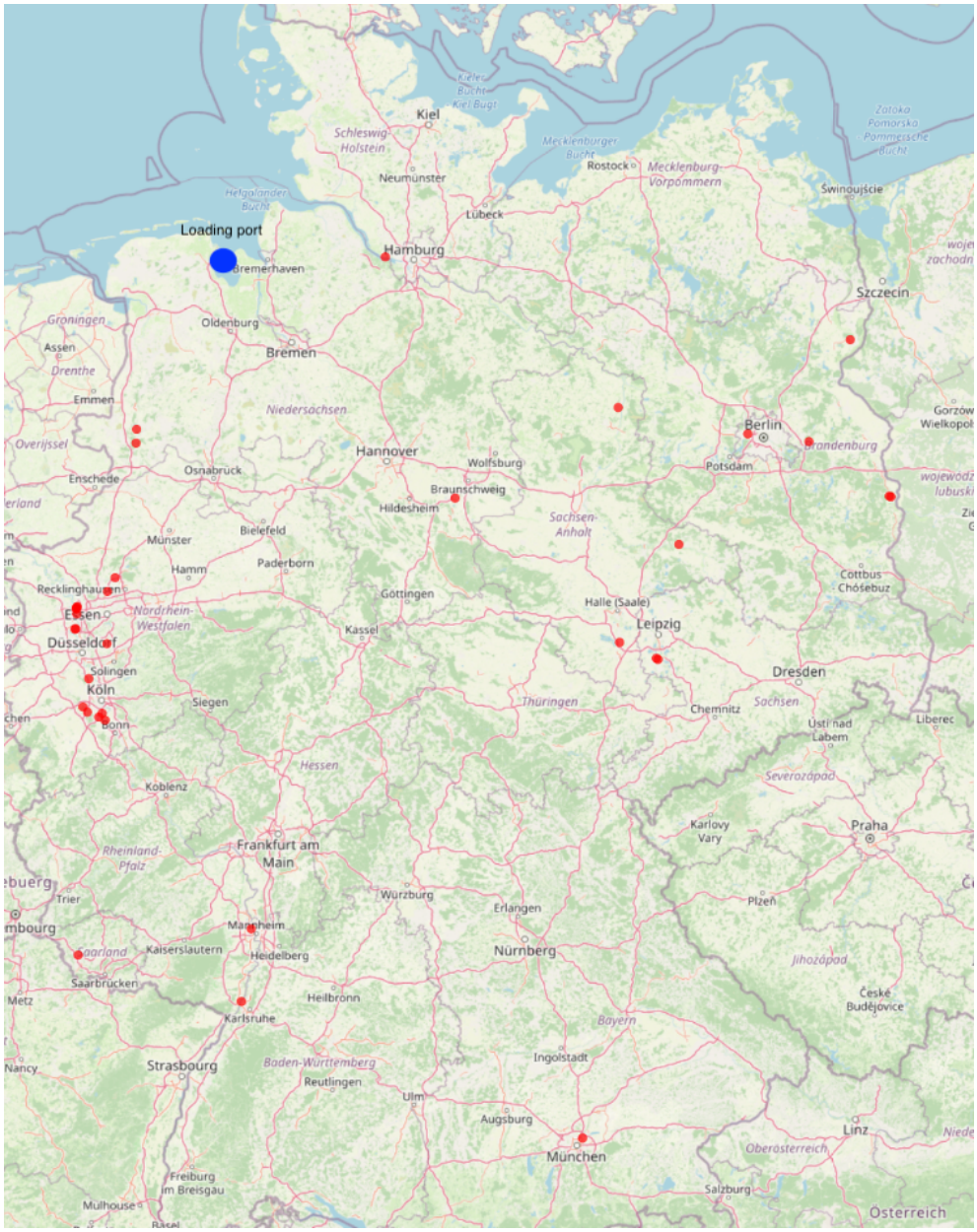

Figure 6.3: Emission sources in 100 Mtpa scenario when prioritizing on size.

The scenarios are summarized in Table 6.7. Together with the model and its sets and parameters, they make up the basis for the computational and economic analysis in the following chapters. For simplicity, the scenarios are named S5, S20, S50, and S100. The mapping from scenario names to actual scenarios can be derived from the table.

Table 6.7: The basic scenarios and the number of emission sources in each scenario, the average emissions per source and the average capture cost for the chosen emission sources.

Scenario	**Amount**	# **Emission sources**	**Avg. emissions per source**	**Avg. capture cost per tonne**
S5	5 Mtpa	1	5 Mtpa	€ 75.00
S20	20 Mtpa	2	9.82 Mtpa	€ 72.50
S50	50 Mtpa	9	5.56 Mtpa	€ 65.43
S100	100 Mtpa	34	2.93 Mtpa	€ 64.28

Chapter 7

Computational Study

In this chapter, we present a computational study on our model of the CCS-SCDP, consisting of a technical analysis and several economic analyses. In Section 7.1, we aim to find the optimal configuration of the model. After that, Section 7.2 presents the solutions to our basic scenarios, which represent CO_2 volumes of 5, 20, 50, and 100 Mtpa. In Section 7.3, we compare ships and pipelines as the offshore transportation mode. One should note that the offshore transportation mode refers to the transportation mode between a loading port and an unloading port. The only transportation mode between unloading ports and storage locations is pipelines. Then, we present sensitivity analyses in Section 7.4 and 7.5, both aiming to discuss the optimal offshore transportation mode. The former concerns the model's sensitivity to cost deviations for essential supply chain components. The latter examines the impact of offshore transportation distance. Then, in Section 7.6, we discuss the effects of the choice of emission sources. We construct three new scenarios where the emission sources in each scenario are from the same industry sector. Finally, we summarize the most critical insights from our economic analyses in Section 7.7.

7.1 Technical analysis

In this section, we aim to identify the optimal configuration of the model, both in terms of the length of the planning horizon and which model enhancement methods to use. First, in Section 7.1.1, we analyze and discuss the impact of applying the valid inequalities and symmetry-breaking constraints presented in Section 5.4. Then, in Section 7.1.2, we discuss what length of planning horizon is needed to get valid and representative solutions.

The impact of the changes is measured through the model's solving time, the optimality gap (also referred to as the gap), and the objective value of the solutions. To improve the accuracy of the gaps, costs that do not affect the structure of the solution have been removed from the objective value in this analysis. These include the injection cost and the sunk capture cost, which is the minimum capture cost among the emission sources. Therefore, the objective values in the technical analysis are lower than the actual supply chain costs.

For the technical analyses, we only use scenario S100, with 100 Mtpa CO_2 and emission sources ordered by size. The scenario is chosen based on its size, and preliminary testing has shown that this is the most challenging scenario to solve out of the four basic scenarios. If this scenario is solved, the other scenarios are also solved, as they are only simpler variants of the same scenario. Thus, S100 is a sound basis for a comparative analysis of possible enhancements of the model formulation.

The model is implemented using the solver Gurobi v.9.1.2 and Python v. 3.8. All computations are run on a Dell PowerEdge R640 with the following capacities: 2 × 2.4GHz Intel Xeon Gold 5115 CPU with ten cores; 96Gb RAM; 55Gb SATA SSD.

7.1.1 Test of model enhancement methods

The starting point of this analysis is a test run of the basic model, which is the model without any enhancement methods, as described in Section 5.3. The basic model is run on scenario S100 over a planning horizon of 30 days. A graph representation of the run with information about the gap and elapsed time can be seen in Figure 7.1, where the orange line represents the run from the basic model. When run with a time limit of 24 hours, the model reaches its lowest gap of 0.5147% after approximately 20 hours. A gap of under 1% is reached after 1 hour. The solution corresponding to the lowest gap, 0.5147%, has an objective value of 328.4599 million euro. The solution corresponding to the gap just below 1% has an objective value of 328.5449 million euro. The additional 19 hours of run time, which reduces the gap from 1% to 0.5147%, has a minimal impact (0.02%) on the overall cost of the system. Hence, the primary contributor to the gap reduction is a lower dual bound.

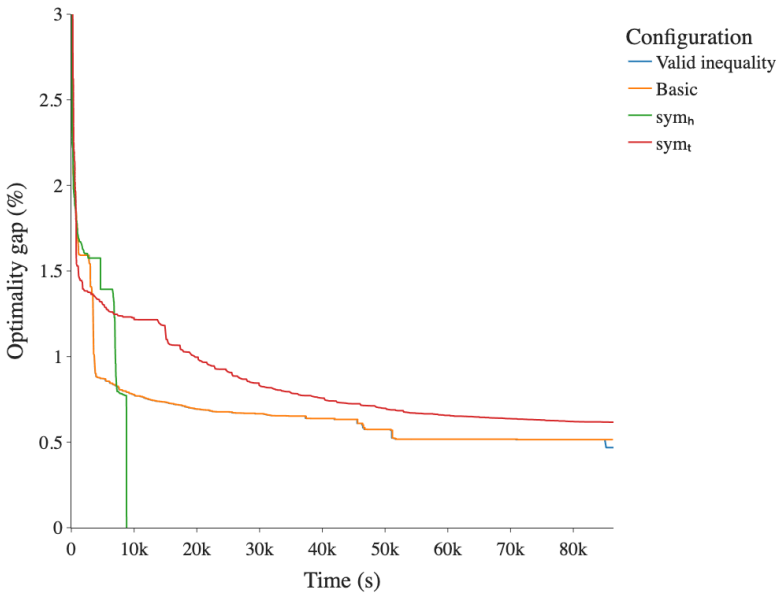

Figure 7.1: Plot of gap and elapsed time for model runs with basic model configuration (red), symmetry-breaking constraints sym_h (green) and sym_t (red) and valid inequalities (blue) with a planning horizon of 30 days.

As presented in Section 5.4, the solutions of the basic model may contain symmetries or have large feasible regions in the LP relaxation, which are factors that may increase the solving time. Therefore, two types of symmetry-breaking constraints and one valid inequality, all presented in detail in Section 5.4, are added to the model to evaluate their effects on the computational performance.

We name the first set of symmetry-breaking constraints sym_h. sym_h refers to Constraints (5.53), which ensure that the ships are hired in specific order decided by their index in the list of ships. The effect of sym_h on the computational solving time of S100 over 30 days is visualized through the green line in Figure 7.1. Here, the model finds the optimal solution after approximately 2.5 hours. We also see that the model does not reach a 1% gap before almost 2 hours have passed. Thus, sym_h contribute to faster convergence to the optimal solution, although it uses more time to reach a gap below 1%. The optimal solution corresponds to an objective value of 328.3238 million euro, which is a cost improvement of 226 000 euro, or 0.04%, compared to the best solution found in the 24-hour run of the basic model.

Another way to break the ship symmetry is to add constraints that help arrange the ship deployments. We call this set of symmetry-breaking constraints sym_t, which refers to Constraints (5.54) through (5.57). The plot of the model's gap with sym_t implemented instead of sym_h can be seen from the red line in Figure 7.1. The graph shows that the model does not reach a proven optimal solution and terminates after 24 hours with a gap of 0.62%. Moreover, it does not reach a gap of 1% until 5.5 hours have elapsed.

The last model enhancement method applied to the model is the valid inequalities as presented in Constraints (5.58)-(5.59). The valid inequalities are used to strengthen the model formulation by tightening the feasible region of the LP-relaxed problem. As for the previous model versions, these are also tested on S100 with a planning horizon of 30 days. The blue line in Figure 7.1 represents the model run when valid inequalities are added. The figure shows that the valid inequalities do not affect the solution time compared to the basic model until about 23 hours have elapsed. It follows almost the same pattern as the basic model until that point. Around 23.5 hours, it drops to a gap of approximately 0.47%, resulting in an objective value of 328.4599 million euro. Despite the lower gap, this is precisely the same solution as the best solution found in the basic model run.

Based on the results presented above, the model configuration used for the further economic analyses should include symmetry-breaking constraints sym_h.

7.1.2 Length of the planning horizon

Due to start-of-horizon and end-of-horizon effects from ship transportation, the length of the planning horizon might impact the cost of the optimal solutions. Therefore, to determine if 30 days is a sufficiently long planning horizon to represent a steady-state system, we run the model for a planning horizon of 50 days and compare the costs. We start with running all four configurations from Section 7.1.1, meaning the basic model, and the models with sym_h, sym_t, and the valid inequalities implemented. Similarly, as for the test of model enhancements, we run them on scenario S100, but with a planning horizon of 50 days. Figure 7.2 gives a summary of the gap and time consumption for the different runs.

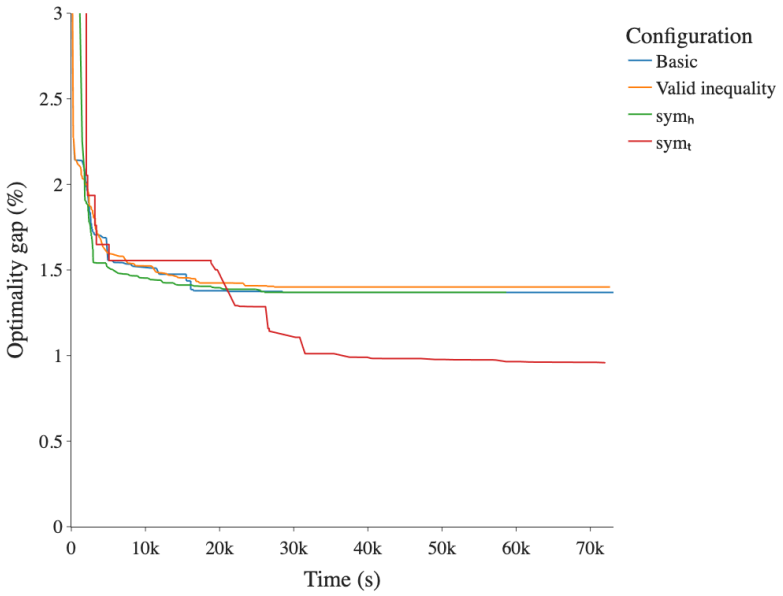

Figure 7.2: Plot of gap and elapsed time for model runs with basic model configuration (blue), symmetry-breaking constraints sym_h (green) and sym_t (red) and valid inequalities (yellow) with a planning horizon of 50 days.

As can be concluded from Figure 7.2, sym_t provides the lowest gap of just below 1% after 20 hours of run time. The better performance of the model with sym_t implemented can be explained by the increase in time-dependent sailing variables from the 30-day to the 50-day planning horizon. This gap corresponds to a solution with an objective value of 544.8011 million euro. To compare this with the optimal solution from the 30-day planning horizon, we divide the objective value by the number of days in the planning horizons to get a per-day cost. The planning horizon of 50 days corresponds to a daily cost of 10.8960 million euro. On the other hand, the cost for the optimal solution with a planning horizon of 30 days is 10.9441 million euro. Thus, the best solution found for the 50-day planning horizon corresponds to a daily cost that is 0.44% lower than the optimal solution for the 30-day planning horizon. With such a slight difference, we can conclude that 30 days is a sufficiently long planning horizon to represent a steady-state system, given the strategic perspective of the CCS-SCDP.

7.2 Analysis of basic scenarios

In this section, we solve the CCS-SCDP for the basic scenarios S5, S20, S50, and S100. The costs of the solutions are presented in Table 7.1, while Table 7.2 presents a summary of the key supply chain components of the scenario solutions. In the following subsections, we present and discuss the optimal CCS supply chains for the different scenarios in greater detail.

Table 7.1: Cost summary of optimal solutions in scenarios S5-S100.

Scen.	Supply chain cost	Volume	Supply chain cost per tonne	Transportation cost per tonne	Transportation cost/ Total cost
S5	M€ 41.4	0.4 Mt	€ 103.1	€ 22.1	21.5%
S20	M€ 137.9	1.6 Mt	€ 87.3	€ 8.3	9.6%
S50	M€ 323.9	4.1 Mt	€ 79.0	€ 7.9	10.0%
S100	M€ 619.7	8.1 Mt	€ 76.5	€ 7.0	9.2%

Table 7.2: Summary of key supply chain components of the optimal solutions in scenarios S5-S100.

Scen.	# Emission sources	Total length of pipelines	# Pipelines	# Ships	# Round trips	# Docks in each port	Buffer storage capacity in Kollsnes	Buffer storage capacity in Wilhelmshaven
S5	1	458.3 km	2	2	5	1	91.2 kt	113.1 kt
S20	2	1265.2 km	4	-	-	-	-	-
S50	9	2993.2 km	13	-	-	-	-	-
S100	33	4270.6 km	39	-	-	-	-	-

7.2.1 Scenario S5

The first scenario we present is S5, where CO_2 emissions of 5 Mtpa are considered. The requirement to capture, transport, and store 97% of the emissions implies that the model needs to handle emissions of 30 days, equivalent to 4.85 Mtpa. The only emission source is the Lausitz Energy coal power plant in Lippendorf, Germany. Based on Federal Environment Agency Germany (2022), this power plant has yearly emissions of 11.7 Mtpa CO_2. Thus, this scenario represents a possible initial CCS capture project for the powerplant, where about 40% of the plant's total CO_2 emissions are captured, transported, and stored. The optimal solution for this scenario uses ships for offshore transportation, resulting in a total supply chain cost of 41.4 million euro, corresponding to 103.1 euro per tonne captured, transported, and stored. Transportation costs sum up to 22.1 euro per tonne. Thus, the transportation costs make up about 21% of the supply chain cost, which is dominated by the capture cost of 75 euro per tonne. A visual representation of the transportation network can be seen in Figure 7.3.

The optimal solution includes two ships, one with 50 kt load capacity and one with 90 kt load capacity. During the planning horizon of 30 days, the 50 kt ship only makes one round trip, while the 90 kt ship does four. The solution has two pipeline connections, one from the emission source to Wilhelmshaven and one from Kollsnes to storage. The two pipelines have a diameter of 0.4 m and a capacity of 6.7 Mtpa. Both Kollsnes and Wilhelmshaven have only one dock, and the routing of the two ships between Kollsnes and Wilhelmshaven results in buffer storage capacity requirements of 91.2 kt and 113.1 kt, respectively. Figure 7.4 shows how the inventory of the buffer storages develop over the planning horizon. The required buffer storage capacity equals the maximum inventory throughout the period.

The total CO_2 emissions from the ship engines during the planning horizon of 30 days sum up to about 5.8 kt, or 1.4% of the transported amount. This is calculated based on the amount transported and numbers from Faber et al. (2020), which report that LNG ships with load capacities 50-100kt emit 16.3 gCO_2 per tonne of load per nautical mile.

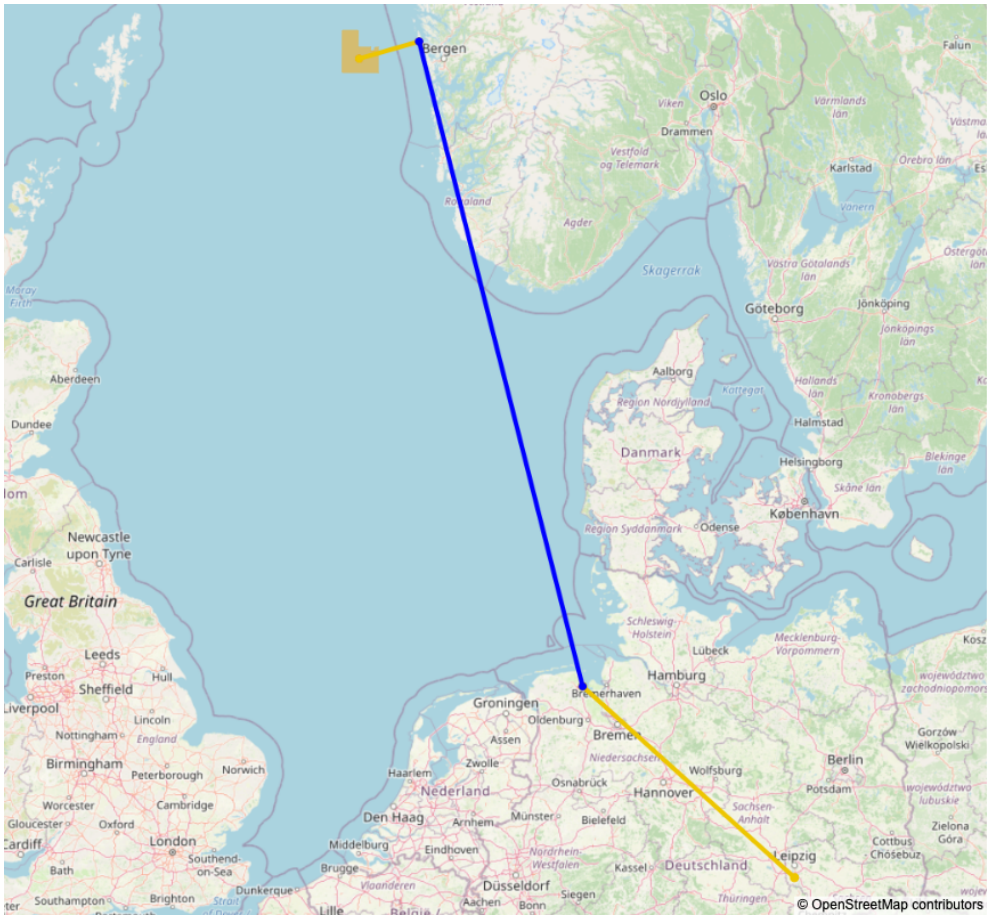

Figure 7.3: Optimal transportation network for scenario S5. The blue line represents ship connections between the ports, while the yellow lines represent pipeline connections with a yearly flow of 5 Mt.

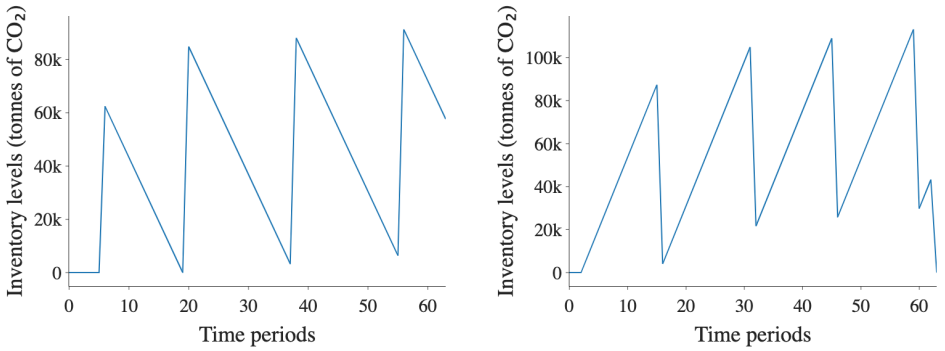

(a) Kollsnes **(b)** Wilhelmshaven

Figure 7.4: Development of inventory levels for buffer storages in **(a)** Kollsnes and **(b)** Wilhelmshaven in S5 during planning horizon of 30 days, i.e., 60 time periods. The inventory levels are given in tonnes of CO_2.

The cost structure of the S5 solution is summarized in Figure 7.5. The onshore pipeline investment costs, cost of hiring ships, and liquefaction costs are the three primary cost components, followed by buffer storage costs, sailing costs, and dock costs.

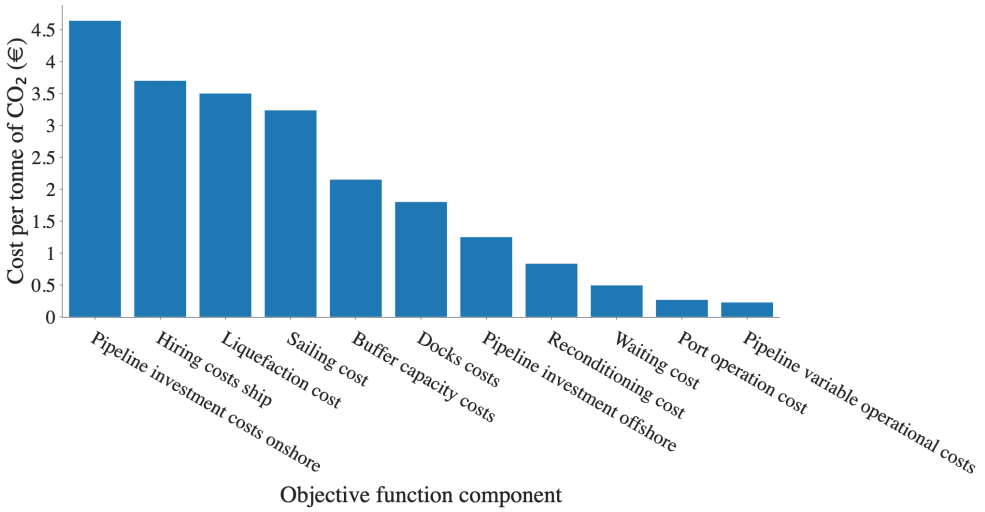

Figure 7.5: The cost composition for the S5 scenario supply chain without capture and storage costs.

7.2.2 Scenario S20

The second scenario, S20, considers CO_2 emissions of 20 Mtpa. The 97% requirement implies that the model must handle 30 days of emission equivalent to 19.4 Mtpa. S20 can be viewed as a natural development from scenario S5, where the remaining emissions of the Lausitz powerplant and the emissions from a major steel manufacturer are captured. As opposed to S5, the solution in S20 includes pipelines as the optimal

offshore transportation mode. The supply chain cost per tonne is reduced to 87.3 euro per tonne. Transportation costs are 8.3 euro per tonne, or 9.6% of the supply chain cost per tonne. The dominating cost is still the capture costs, at 73 euro per tonne. The transportation network can be seen in Figure 7.6.

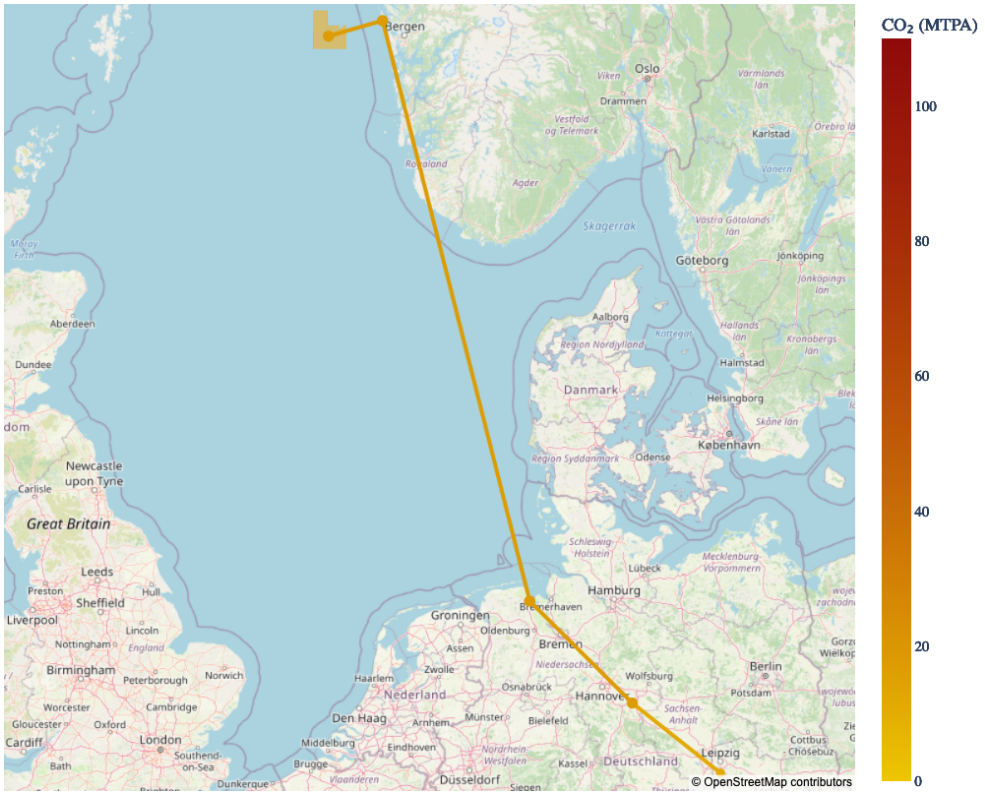

Figure 7.6: Optimal transportation network for scenario S20. All lines represent pipeline connections. As shown by the colored bar to the right of the map, the more red the pipeline lines, the higher the flow.

A summary of the pipeline network for scenario S20 is shown in Table 7.3. Compared to S5, ships are replaced by an offshore pipeline with a diameter of 0.7 m and a corresponding capacity of 20.6 Mtpa. The onshore pipeline network also utilizes a 0.6 m pipeline between the emission sources, with a corresponding capacity of 15.2 Mtpa. The latter pipeline is needed to serve the whole flow from the Lausitz power plant of 11.7 Mtpa. Hence, its capacity is only 76% utilized. Conversely, the pipelines with a capacity of 20.6 Mtpa serve a flow of 19.64 Mtpa, implying a utilization of 95%.

Table 7.3: Pipeline summary for optimal solution in scenario S20.

	Onshore pipelines		Offshore pipelines (W.haven - Kollsnes)		Storage pipelines (Kollsnes - Storage)	
Pipeline diameter	**# Pipelines**	**Total pipeline length**	**# Pipelines**	**Total pipeline length**	**# Pipelines**	**Total pipeline length**
0.6 m	1	173.4 km	-	-	-	-
0.7 m	1	216.9 km	1	806.0 km	1	68.9 km
Total	**2**	**390.3 km**	**1**	**806.0 km**	**1**	**68.9 km**

7.2.3 Scenario S50

In scenario S50, we consider 50 Mtpa of CO_2 emissions. Thus, the model requires handling a 30-day equivalent of 48.5 Mtpa. The scenario includes nine emissions sources, with yearly emissions ranging from 3.6 to 11.7 Mtpa. Compared to S20, S50 represents a further expansion of the CCS activity in Germany. Seven emission sources are added to the onshore network, five of which are steel manufacturers. The resulting optimal supply chain uses only pipeline transportation and has a total cost of 323.9 million euro, corresponding to a supply chain cost of 79.0 euro per tonne. Of this, 7.9 euro, or 10%, comes from transportation. The optimal transportation network is illustrated in Figure 7.7.

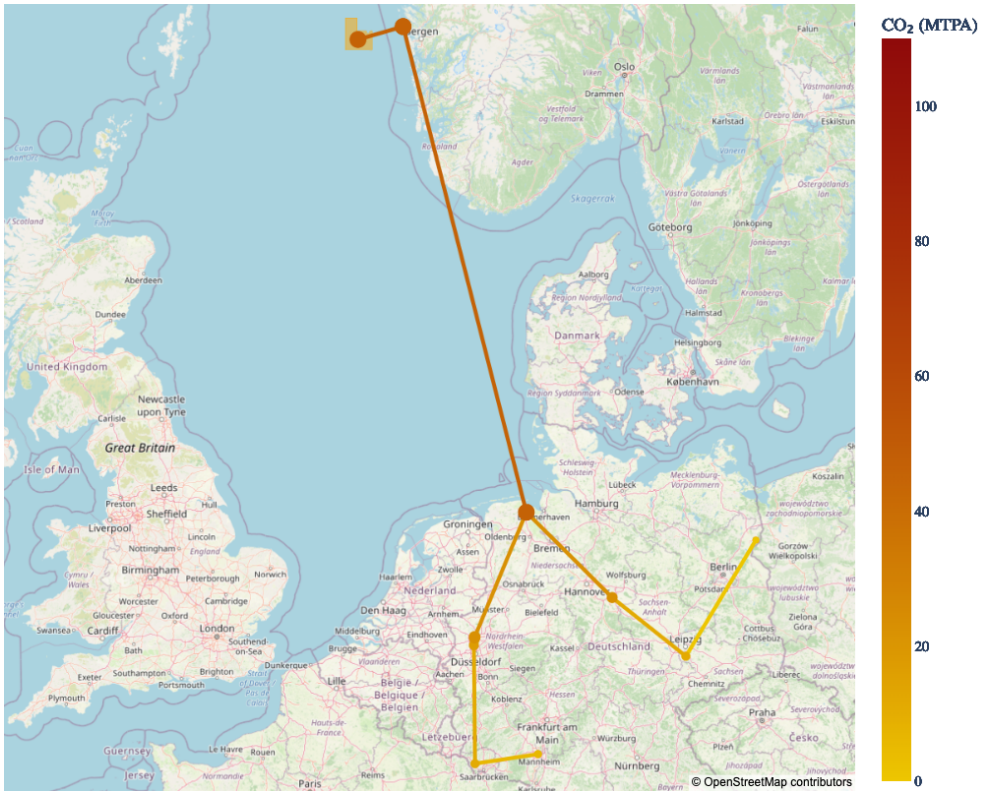

Figure 7.7: Optimal transportation network for scenario S50. All lines represent pipeline connections. There is a cluster of 4 emission sources in the Düsseldorf area, which is barely visible in the figure.

As can be seen from Table 7.4, the optimal pipeline transportation network in S50 has a wider variety of pipeline dimensions than the previous scenarios, ranging from 0.3 m to 1.0 m. There are now 13 pipelines stretched over a total distance of 2993.2 km. Two pipelines serve both types of offshore connections; one pipeline with a diameter of 1.0 m and a capacity of 42.1 Mtpa and one pipeline with a diameter of 0.4 m and a capacity of 6.7 Mtpa. The largest pipeline is fully utilized, while the smaller has a utilization of 95%.

Table 7.4: Pipeline summary for optimal solution in scenario S50.

	Onshore pipelines		**Offshore pipelines (W.haven - Kollsnes)**		**Storage pipelines (Kollsnes - Storage)**	
Pipeline diameter	# **Pipelines**	**Total pipeline length**	# **Pipelines**	**Total pipeline length**	# **Pipelines**	**Total pipeline length**
0.3 m	1	247.0 km	-	-	-	-
0.4 m	-	-	1	806.0 km	1	68.9 km
0.5 m	1	122.8 km	-	-	-	-
0.6 m	2	397.6 km	-	-	-	-
0.7 m	2	13.8 km	-	-	-	-
0.8 m	3	462.2 km	-	-	-	-
1.0 m	-	-	1	806.0 km	1	68.9 km
Total	**9**	**1243.4 km**	**2**	**1612.0 km**	**2**	**137.8 km**

7.2.4 Scenario S100

Scenario S100 includes a total of 34 emission sources. The emissions per source range from 1.17 Mtpa to 11.7 Mtpa and sum up to 100 Mtpa. The model enforces that a 30-day equivalent of 97 Mtpa is handled. A wide selection of CO_2-emitting industries are included, and the scenario represents a situation where CCS has become a regular part of the business for major CO_2-emitting German companies. As for S20 and S50, pipelines are the only transportation mode in the optimal solution for scenario S100. The total cost of the supply chain is now 619.7 million euro. Thus, the supply chain cost per tonne has decreased to 76.5 euro. Moreover, the transportation cost per tonne is reduced to 7.0 euro per tonne, 9.2 % of the supply chain cost. The onshore transportation network is visualized in Figure 7.8. For visibility purposes, the offshore and storage part of the transportation network is left out of the figure. However, they look the same as in the other scenarios, but with darker lines representing the higher capacity of these pipeline connections compared to scenarios S20 and S50.

From Table 7.5, we see that the optimal transportation network in S100 includes all pipeline diameters available. There are 39 pipelines in total, stretching a total distance of 4720.6 km. There are now ten pipelines of the highest capacity, where four of them serve the two offshore connections. Hence, both offshore pipeline connections need two pipelines of the highest capacity. These are fully utilized. In addition, the offshore connections also have a pipeline with a diameter of 0.6 m and a capacity of 15.2 Mtpa. These pipelines are 85% utilized.

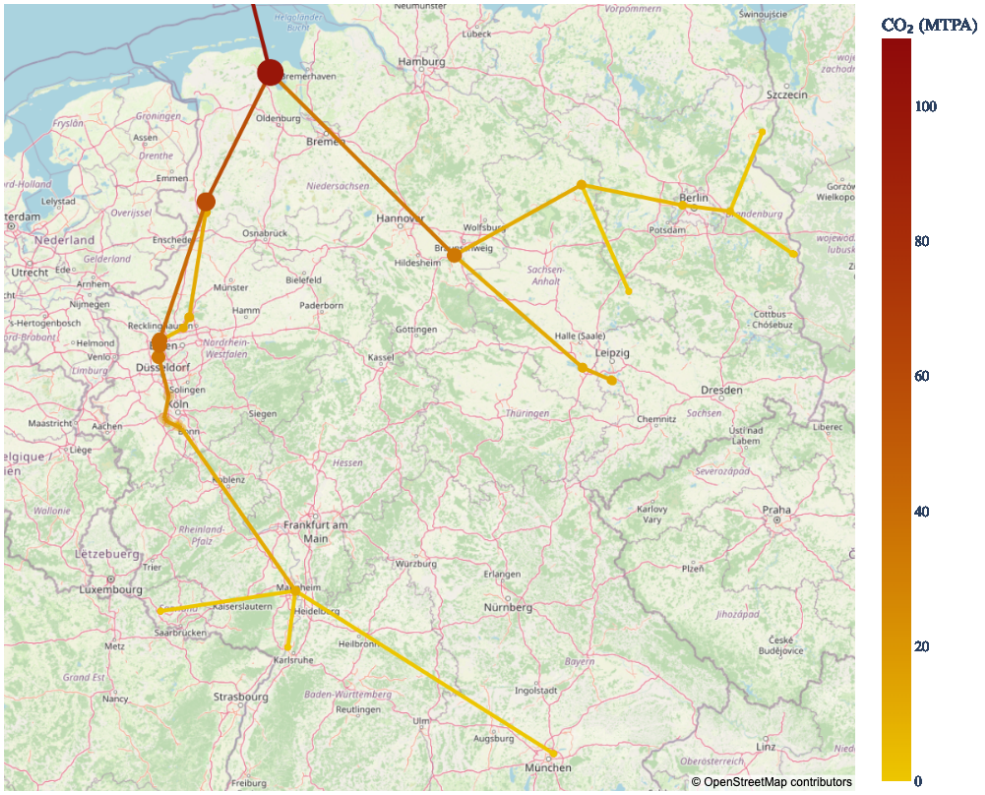

Figure 7.8: Optimal transportation network for scenario S100. All lines represent pipeline connections. In this network, several clusters and aggregating trunk lines can be identified.

Table 7.5: Pipeline summary for optimal solution in scenario S100.

	Onshore pipelines		Offshore pipelines (W.haven - Kollsnes)		Storage pipelines (Kollsnes - Storage)	
Pipeline diameter	**# Pipelines**	**Total pipeline length**	**# Pipelines**	**Total pipeline length**	**# Pipelines**	**Total pipeline length**
0.2 m	1	3.4 km	-	-	-	-
0.3 m	4	429.8 km	-	-	-	-
0.4 m	4	259.3 km	-	-	-	-
0.5 m	3	151.1 km	-	-	-	-
0.6 m	6	398.3 km	1	806.0 km	1	68.9 km
0.7 m	3	189.8 km	-	-	-	-
0.8 m	4	152.9 km	-	-	-	-
0.9 m	2	155.1 km	-	-	-	-
1.0 m	6	356.2 km	2	1612.0 km	2	137.8 km
Total	**33**	**2095.9 km**	**3**	**2418.0 km**	**3**	**206.7 km**

7.2.5 Insights from basic scenario solutions

With the current EU ETS price of about 80 euro per tonne (Ember 2022), only scenarios S50 and S100 provide supply chain costs that make CCS profitable. However, since the estimated capture costs vary from 30 to 90 euro per tonne for different

emission sources, CCS may be profitable in S5 and S20, but only for specific emission sources with low capture costs. Our model solutions provide only the direct cost of capture, transportation, and storage. Providers of these services might need to charge a price above their direct costs to be profitable. Thus, from the perspective of an individual emission source, considering the implementation of carbon capture in its facility, the actual price of CCS may be higher.

There are clear economies of scale within the transportation network with increasing volumes. When the solution switch from ships to pipelines between Wilhelmshaven and Kollsnes from S5 to S20, the transportation cost decreases from 22.1 per tonne to 8.3 euro per tonne. From S20 to S100, pipelines are consistently used, and the transportation cost is further reduced to 7.0 euro per tonne. A comparison of the cost breakdown of S20, S50, and S100, is presented in Figure 7.9. It shows that the economies of scale from S20 to S100 come from the offshore pipelines, which we know have higher capacities and degrees of utilization with the increasing volumes.

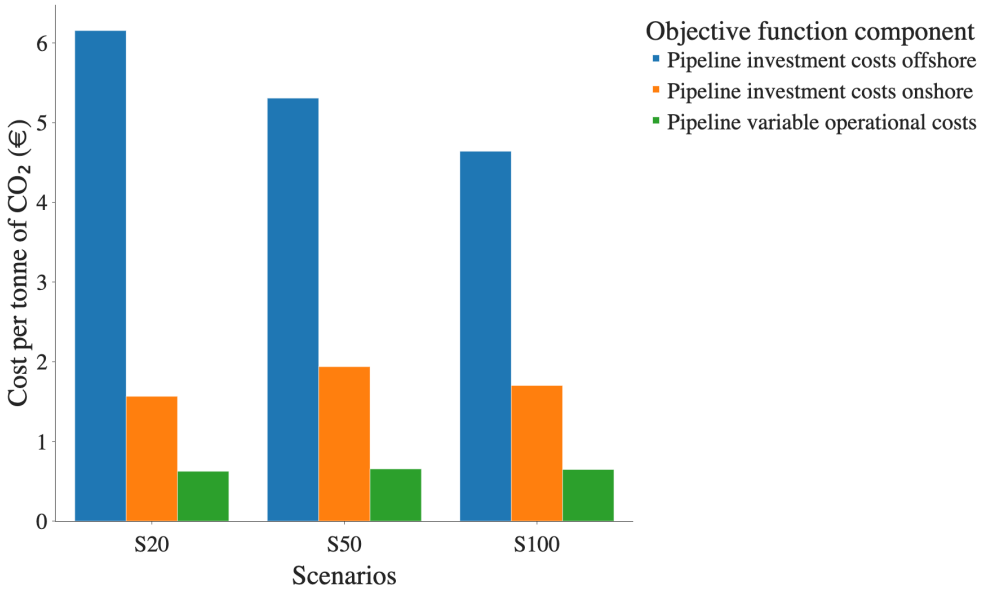

Figure 7.9: Cost breakdown for transportation cost in the scenarios S20, S50, and S100.

As the four scenarios correspond to a ramp-up of the captured volumes, we may also obtain insights on how to gradually develop the transportation network. By examining the offshore transportation solutions between Wilhelmshaven and Kollsnes, we see that in S20, a 0.7 m pipeline is required. In S50, one 1.0 m and one 0.4 m pipeline is needed. Finally, in S100, the optimal solution includes two pipelines of 1.0 m and one of 0.6 m. However, this implies replacing the 0.7 m pipeline with a 0.4 m pipeline in S50 and the 0.4 m pipeline with a 0.6 m pipeline in S100. A more sensible way to solve this might be to invest in a pipeline of 0.7 m in S20 and then add a pipeline of 1.0 m in S50 and an additional 1.0 m pipeline in S100. The pipeline network would then be oversized in S50 and S100, but considerable construction work, resources, and costs

are also avoided. However, providing solutions with the optimal development in such ramp-up scenarios generally requires an extended model. Regardless, this example shows how our model can inform decision-makers considering a gradual development of the CCS supply chain.

7.3 Ships vs. pipelines: the cost of flexibility

Ship transportation is inherently more flexible than pipeline transportation. First and foremost, ships provide cheaper and easier relocation to other geographical locations if needed. Additionally, they may be more easily adjusted or rebuilt for other purposes, such as LNG transportation. This section discusses the monetary cost of the flexibility that the ships offer. This is done by comparing the costs from the optimal solutions in Section 7.2 with solutions where the model is forced to use ship transportation between Wilhelmshaven and Kollsnes, referred to as *ships only*. As we have seen in Section 7.2, ships are the preferred transportation mode in scenario S5. Therefore, we briefly discuss what happens in scenario S5 when we force the model to use pipelines (*pipelines only*) instead of ships. Table 7.6 summarizes the cost differences between the optimal solutions of S5-S100 from Section 7.2 and the solutions where pipelines are forced in S5 and ships are forced in S20-S100. For a more detailed presentation and discussion of the underlying solutions for this analysis, see Appendix B.

Table 7.6: Comparison of the key costs of basic scenarios solutions when an unpreferred offshore transportation mode is forced to be used. The columns named Δ represent the cost increase by forcing an unpreferred offshore transportation mode.

Scen.	Force transp. mode	Supply chain cost	Volume	Supply chain cost per tonne	Δ	Isolated offsh. transp. cost per tonne	Δ	Isolated transp. cost share
S5	-	M€ 4.1	0.4 Mt	€ 103.1	-	€ 16.0	-	15.5 %
S5	Pipelines	M€ 4.1	0.4 Mt	€ 103.7	0.6%	€ 16.6	3.8%	16.0 %
S20	-	M€ 137.9	1.6 Mt	€ 87.3	-	€ 6.1	-	7.0 %
S20	Ships	M€ 147.8	1.6 Mt	€ 92.4	5.8%	€ 11.1	82.0%	12.0 %
S50	-	M€ 323.9	4.1 Mt	€ 79.0	-	€ 5.3	-	6.7 %
S50	Ships	M€ 343.6	4.1 Mt	€ 83.8	6.1%	€ 10.1	90.6%	12.1 %
S100	-	M€ 619.7	8.1 Mt	€ 76.5	-	€ 4.7	-	6.1 %
S100	Ships	M€ 662.58	8.1 Mt	€ 81.8	6.9%	€ 9.9	110.6%	12.1 %

When forcing pipeline transportation from Wilhelmshaven and Kollsnes in S5, the total supply chain cost per tonne only increases from 103.1 to 103.7 euro per tonne, corresponding to an increase of 0.6%. Considering uncertainty in the cost input parameters, the costs are equal for all practical purposes. The cost increase is reflected in the cost of offshore transportation between Wilhelmshaven and Kollsnes. As this cost is a part of the total transportation costs in the supply chain, we refer to it as the *isolated offshore transportation cost*. The isolated offshore transportation cost increases from 16.0 to 16.6 euro per tonne, corresponding to a 3.8% increase.

Compared to S5, we find a significantly greater increase in the costs when enforcing ships in S20, S50, and S100. By forcing ships in scenario S20, the total supply chain cost increases from 87.3 to 92.4 euro per tonne, corresponding to a 5.8% cost increase. Moreover, the isolated offshore transportation cost increases from 6.1 euro per tonne to 11.1 euro per tonne, corresponding to an 82.0% increase. A similar pattern is

found for S50 and S100, but with slightly more negative impacts of forcing ships. For instance, the isolated transportation costs increase by 110.6% in S100.

Forcing ship transportation also results in emissions from the ship engines. These emissions sum up to approximately 1.4% of the transported amount of CO_2 during the 30-day planning horizon (Faber et al. 2020). Thus, in the S100 scenario, forcing ships leads to emissions of about 114kt CO_2 over a period of 30 days, or almost 1.4 Mt per year.

In conclusion, choosing ship transportation between ports significantly increases isolated offshore transportation costs for scenarios with 20 Mtpa, 50 Mtpa, and 100 Mtpa. The increase in isolated offshore transportation costs ranges from 4.8 to 5.2 euro per tonne, representing relative increases of around 82.0% to 110.6%. Since the increase in transportation cost is quite similar for the three scenarios, both in absolute terms and percentage-wise, it is natural to conclude that the cost of the flexibility that the ships offer is around 5 euro per tonne for CO_2 supplies in the 20-100 Mtpa range. Furthermore, we have discovered that when considering emissions of 5 Mtpa, the cost difference between pipeline and ship transportation is small. Thus, it seems that volumes of 5 Mtpa are close to a switching point for the choice of offshore transportation mode. For higher volumes than 5 Mtpa, pipeline transportation is optimal. For lower volumes, ship transportation is the optimal offshore transportation mode.

7.4 Cost parameter sensitivity

The cost estimates related to ships and pipelines used for the model parameters affect the choice of offshore transportation mode between loading and unloading ports, which is an important strategic decision. To identify how sensitive the solutions are to changes in cost estimates, we perform a sensitivity analysis on key cost components with a significant degree of uncertainty. The cost components analyzed are ship hiring, offshore pipeline investment, and ship fuel costs. In our analyses, we allow ships with load capacities of up to 100 kt of CO_2. Such ships are not in use nor built up to now, but are found to be a plausible and cost-effective option for large-scale CO_2 ship transportation in the future (Roussanaly et al. 2021). Therefore, with no empirical data, the estimates for both hiring cost and fuel consumption are subject to uncertainty. For pipelines, the cost estimates are based on the heuristic proposed by Serpa et al. (2011), where we have included terrain factors to adjust for cost changes between offshore pipelines and onshore pipelines. While being based on actual CO_2 pipeline projects, these costs are also subject to uncertainty and may have increased since the heuristic was developed. Lastly, fuel prices vary significantly over time. Combined with the uncertain fuel consumption for large ships, it is a natural cost component to include in such an analysis.

Table 7.7 presents the sensitivities for each cost parameter and scenario. The *switching point* is the deviation from the original parameter values, at which the optimal transportation mode switches from the mode which was optimal under the original parameter value.

Table 7.7: Summary of cost sensitivities.

	Offshore pipeline investment cost		Ship hiring cost		Fuel cost	
Scen.	**Sensitivity for pipeline solutions**	**Switching point**	**Sensitivity for ship solutions**	**Switching point**	**Sensitivity for ship solutions**	**Switching point**
S5	€ 1.8	-10%	€ 0.4	16%	€0.4	18%
S20	€ 0.6	90%	-	-	-	-
S50	€ 0.4	150%	-	-	-	-
S100	€ 0.4	160%	-	-	-	-

Looking at the offshore pipeline investment cost parameter, the switching point for S5 is at -10%. Hence, the optimal solution switches from ships to pipelines at a 10% decrease in offshore pipeline investment costs. On average, each ten percentage point increase in offshore pipeline investment cost increases the transportation costs by 1.8 euro per tonne. Thus, the "sensitivity for pipeline solutions" is 1.8 euro per tonne. The switching point for S20 is at 90%, with a sensitivity of 0.6 euro. Thus, the optimal mode shifts to ship transportation when offshore pipeline investment cost increases by 90%. Furthermore, we see that the switching point is reached at 150% and 160% for S50 and S100, respectively. The switching points support the results from 7.2, where pipelines are preferred for higher volumes transported. Conversely, the sensitivities for pipeline solutions decrease with larger emission scenarios. This is because the offshore pipeline networks benefit from economies of scale, as larger pipelines are cheaper per unit of capacity. Thus, the offshore pipeline costs per tonne of CO_2 flow are smaller for larger emission scenarios. One should note that the sensitivities only apply for cost ranges where pipelines are the preferrable transportation mode. This is because the transportation costs are unaffected by increased pipeline costs from the point where ships are the chosen offshore transportation mode.

When we reach a 16% increase in ship hiring costs in scenario S5, the optimal transportation mode shifts from ships to pipelines. Until that point, the transportation costs increase by 0.4 euro per tonne for each ten percentage point increase in ship hiring cost. Interestingly, we cannot find any switching point for scenarios S20, S50, or S100. Hence, pipeline transportation is preferred even if ship hiring is free. The same results are found for deviations in fuel costs; despite free ship fuel, pipelines are preferable over ships in all scenarios except S5, where pipelines are chosen when the fuel cost is increased by 18%.

To conclude, we have found that the optimal transportation mode in S5 depends on our estimated parameter values to a large degree. Conversely, for larger emission scenarios, the optimal transportation mode is, to a small degree, sensitive to the estimated parameter values for relevant costs. Even more so for ship hiring and fuel costs, which could be costless without changing the conclusion.

7.5 The impact of offshore transportation distances

This section aims at analyzing how the optimal offshore transportation mode changes if the distance between loading and unloading ports is changed. Hence, the results may be generalized to cases outside Northern Europe. We still use the basic scenarios with Wilhelmshaven as the loading port and Kollsnes as the unloading port. However, the results can be interpreted as if the infrastructure in Kollsnes was located at a different

place - either further away from or closer to Wilhelmshaven, depending on what scenario we analyze. The analysis can also be seen in the context of the term *switching distance*, which was introduced in the work of Roussanaly et al. (2013). The switching distance is the offshore transportation distance for a given volume of CO_2 from where ship transportation becomes more economical than pipeline transportation.

In the S5 scenario, the optimal solution includes ships for the actual distance of 806.0 km between Wilhelmshaven and Kollsnes. To identify the distance where pipelines become preferable over ships, we run the model on shorter distances than the actual distance. We also analyze if ship transportation continues to be the preferred mode when the distance increases. Hence, we perform a sensitivity analysis where we change the distance in 20 percentage point intervals from -60% to +60% deviation from the original distance. The resulting transportation cost per tonne for these stepwise changes in offshore transportation distance and the resulting transportation modes are visualized in Figure 7.10.

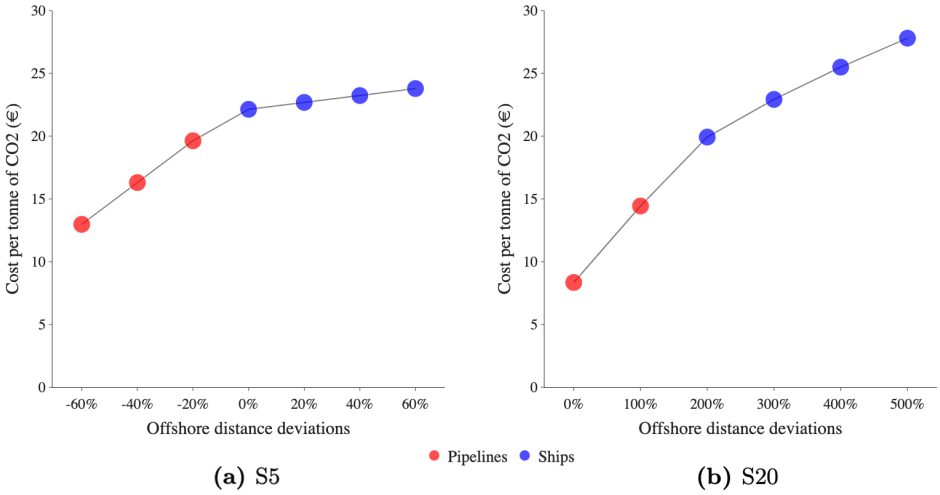

(a) S5 **(b)** S20

Figure 7.10: Offshore distance sensitivity analysis for **(a)** S5 and **(b)** S20.

As presented by Figure 7.10, the optimal offshore transportation mode switches from ships to pipelines at a 20% decrease in distance. A more granular analysis of what happens between -20% and 0%, presented in Appendix C shows that the switching distance is approximately 800 km. Moreover, the optimal transportation mode is consistent on both sides of the switching distance. Thus, ship transportation is the most economical offshore transportation option for a supply chain that handles 5 Mtpa of CO_2 with an offshore transportation distance longer than 800 km.

In scenarios S20, S50, and S100, the optimal solutions include pipelines as offshore transportation mode between Wilhelmshaven and Kollsnes. With the results from the distance analysis of S5 in mind, which proved to be consistent in the solutions with pipelines when the distance was decreased from the switching point, we only increase the distance in the analysis of S20, S50, and S100. To which extent we deviate from the baseline distance differs between scenarios, as the switching distance increases for

higher volumes.

For S20, the distance is increased at steps of 100%, from 0% to +500%. The results from this analysis are presented in Figure 7.10. The figure shows that the model starts choosing ships when the distance is increased between 100% and 200%. By a more granular analysis presented in Appendix C, we find that the switching distance is at 195%, which corresponds to approximately 2400 km. As in the S5 offshore distance analysis, the model is consistent with choosing ships beyond the switching point.

Figure 7.11 presents the results for scenario S50. Two distances are identified where the optimal offshore transportation modes change. First, at a 100% increase in offshore distance, it is optimal to switch from pure pipeline transportation to a combination of ships and pipelines. From the analysis in Appendix C, we find that the switching distance is at a 20% increase, corresponding to approximately 970 km. Hence, when the distance gets longer than 970 km, both pipelines and ships are utilized as offshore transportation modes between the loading and unloading ports. Compared to the solutions found in Section 7.2.3, this solution uses one ship of 90 kt instead of pipelines to transport the excess CO_2 not transported by the largest pipeline with a capacity of 42.1 Mtpa. The substituted pipeline has a 0.4 m diameter with a capacity of 6.7 Mtpa and is 95% utilized in the original solution. The second distance at which the optimal transportation mode changes is found at a 510% increase, corresponding to approximately 4100 km, see Appendix C. From this point onwards, the remaining pipeline with a diameter of 1.0 m is substituted by ships. A comparison of key metrics between the optimal solution for S50 at the two switching intervals (+10%,+20%) and (+500%,+510%) can can be seen in Table 7.8.

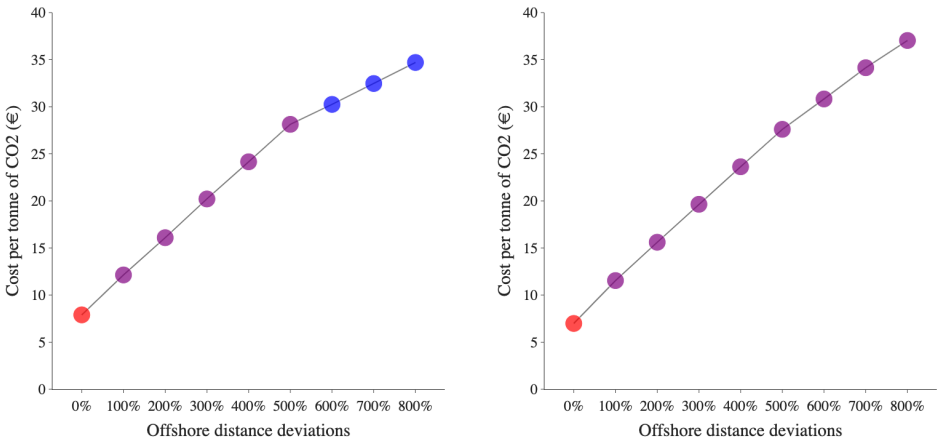

(a) S50 **(b)** S100

Figure 7.11: Offshore distance sensitivity analysis for **(a)** S50 and **(b)** S100.

As also shown by Figure 7.11, scenario S100 reaches its switching distance somewhere between 0 and 100% increase. From the analysis in Appendix C we find that a combination of ships and pipelines is optimal from 90%, corresponding to approximately

1500 km. At this distance, ships substitute the smallest pipeline with a diameter of 0.6 m. In the basic scenario, this pipeline handles the flow exceeding the capacity of the two pipelines of 1.0 m, implying an 85% utilization. A combination of ships and pipelines is chosen up to an increase of 1300%, representing a distance of over 11 000 km. Distances above this are probably not relevant for CO_2 transportation, and a further search for the switching distance is not performed.

Table 7.8: Key metrics of solutions on both sides of the two switching points in the offshore distance analysis for scenario S50.

Switching point	**Deviation (offshore distance)**	**Total pipeline length**	**Offshore pipelines used**	# **Ships used**	# **Round trips**
Pipelines → Combinantion	+10% (886.6 km)	3154.4 km	1 x 0.4 m 1 x 1.0 m	-	-
	+20% (967.2 km)	2348.4 km	1 x 1.0 m	1 x 90 kt	6
Combination → Ships	+500% (4030.0 km)	6218.7 km	1 x 1.0 m	3 x 100 kt 1 x 70 kt	6
	+510% (4110.6 km)	1313.8 km	-	12 x 100 kt 11 x 90 kt 5 x 80 kt	43

The general tendency in this analysis is that ships are preferable to pipelines for longer distances. At what distance ships become more economical than pipelines depends on the capacity and utilization of the pipelines. The higher the capacity and utilization of a pipeline, the longer the switching distance, where ships become preferable. For S5, ships are already more economical at the original distance of 806.0 km, which is also the switching distance. If pipelines are enforced as the only offshore transportation mode, the optimal solution would be a pipeline with a diameter of 0.4 m. With a capacity of 6.7 Mtpa, it would only be 73% utilized. For S20, which uses one 0.7 m diameter pipeline with 20.6 Mtpa capacity and 95% utilization in the original solution, ships become more economical at around 2400 km. For S50, a 0.4 m pipeline is switched with ships at about 970 km, providing a combined solution. The longer switching distance compared to S5 is due to the pipeline having a higher utilization of 95% in S50. Furthermore, ships are the only offshore transportation mode in S50 at about 4100 km. Thus, this is the switching distance of the fully utilized 1.0 m pipeline with 42.1 Mtpa capacity. For S100, a 0.6 m pipeline with 85% utilization is substituted by ships at about 1500 km.

When comparing our results from the distance sensitivity analysis with the results from Roussanaly et al. (2014), we find that our results tend more towards using pipeline transportation. They present switching distances of 400 km at 5 Mtpa and 625 km at 20 Mtpa, which means that from these distances at the given volumes, ships are the preferred offshore transportation mode. However, the results are not directly comparable to ours. They investigate ship transportation to an offshore site, meaning that the injection to storage happens at sea, right above the storage location. This is a less mature concept than ship transportation between two onshore ports, which is used in this thesis.

7.6 Industry-specific supply chains

The scenarios studied so far have been formed based on annual volumes of either 5, 20, 50, or 100 Mt, where the emission sources are chosen based on their CO_2 emission rates. The capture costs differ within the scenarios, as the emission sources are chosen regardless of their industrial sector. However, the relevance of CCS differs from one industry sector to another. An important argument for deploying CCS is to reduce emissions from sectors with otherwise limited abatement options. A typical example of an industry where CCS might not be an essential measure is the electricity-producing part of the energy sector, as there are several alternative renewable energy sources. Other industries, like the cement industry, rely on chemical processes that release CO_2 either way. Thus, CCS might be more relevant to the cement industry than the electricity-producing industry. In this analysis, we make three new scenarios representing the German cement, steel, and organic chemicals industries, which are sectors deemed reliant on CCS to meet carbon reduction requirements (IEA 2019). Each scenario includes all available emissions within the sector it represents. The resulting solutions show the optimal design and cost of CCS supply chains within the specific sectors. Thus, they give insights into what a CCS collaboration between actors within the same German industry sector might look like. The scenarios are summarized in Table 7.9. Here, the corresponding NACE sectors are added to describe the core activities of the emission sources within each scenario. The scenario solutions are presented in Table 7.10.

Table 7.9: Characteristics of the industry-specific scenarios Steel, Cement, and Organic chemicals (Orgchem).

Scenario	**NACE sector**	# **Emission sources**	**Total CO_2 emissions**	**Capture cost per tonne**
Steel	Manufacture of basic iron and steel and ferro alloys	13	38.1 Mtpa	€ 70
Cement	Manufacture of cement	30	19.7 Mtpa	€ 90
Orgchem	Manufacture of other organic basic chemicals	12	15.8 Mtpa	€ 30

Table 7.10: Summary of the model solutions for industry-specific scenarios.

Scenario	**Supply chain cost per tonne**	**Transportation cost per tonne**	% **Transportation cost**	**Total length of pipelines**	# **Pipelines**
Steel	€ 83.0	€ 7.0	8.5	1867.3 km	15
Cement	€ 108.7	€ 12.7	11.7	2797.2 km	32
Orgchem	€ 49.3	€ 13.3	27.0	2111.9 km	14

7.6.1 Steel

The majority of CO_2 produced in the steel industry comes from the process of heating iron ore and coke in a blasting furnace. The coke absorbs oxygen from the iron ore and

produces CO_2 (Argus Media 2019). While being subject to a decarbonization strategy using green hydrogen instead of coke in the heating process, CCS is still relevant for the steel sector as an already mature abatement option (IEA 2019). Moreover, with Germany being the largest steel manufacturer in the European Union (EUROFER 2021), the steel industry is considered to be a relevant basis for a scenario.

The solutions for the Steel scenario are summarized in Table 7.10, and the onshore transportation network is presented in Figure 7.12. Including a capture cost of 70 euro per tonne, the supply chain cost is 83 euro per tonne. The high number of steel factories in the Düsseldorf area contributes to relatively low transportation costs of 7 euro per tonne.

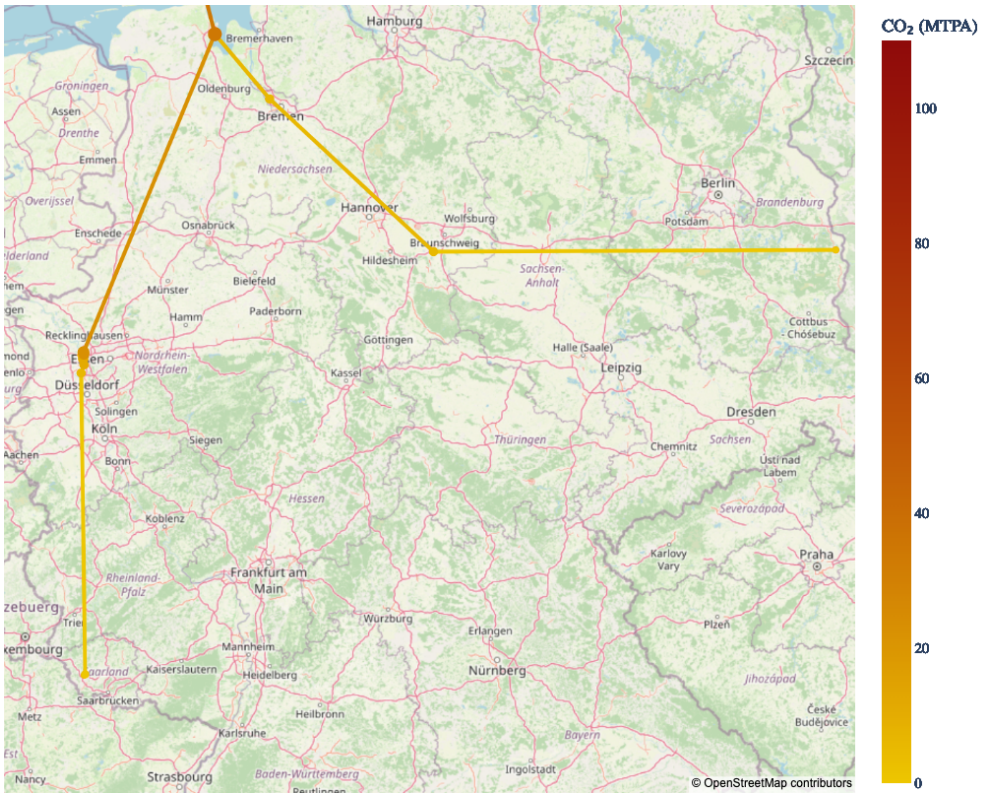

Figure 7.12: Onshore pipeline network for the Steel scenario.

7.6.2 Cement

Two-thirds of the emissions from cement production come from the production of clinker. In order to produce cement clinker, limestone is heated to above 800 °C, causing CO_2 in the stone to be released. These emissions are hard to abate, and CCS is so far the most promising option for decarbonizing the cement industry (Argus Media 2019). Moreover, Germany is the second largest cement producer in Europe according to Garside (2022), emphasizing the relevance of the Cement scenario.

Table 7.10 summarizes the results for the Cement scenario, and the onshore transportation network is presented in Figure 7.13. With high capture costs compared to

other industries, the German cement industry faces a supply chain cost of 108.7 euro per tonne. The transportation costs are 55% higher than for the Steel scenario due to lower volumes, more emission sources, and a substantial increase in the total length of pipelines within the onshore transportation networks.

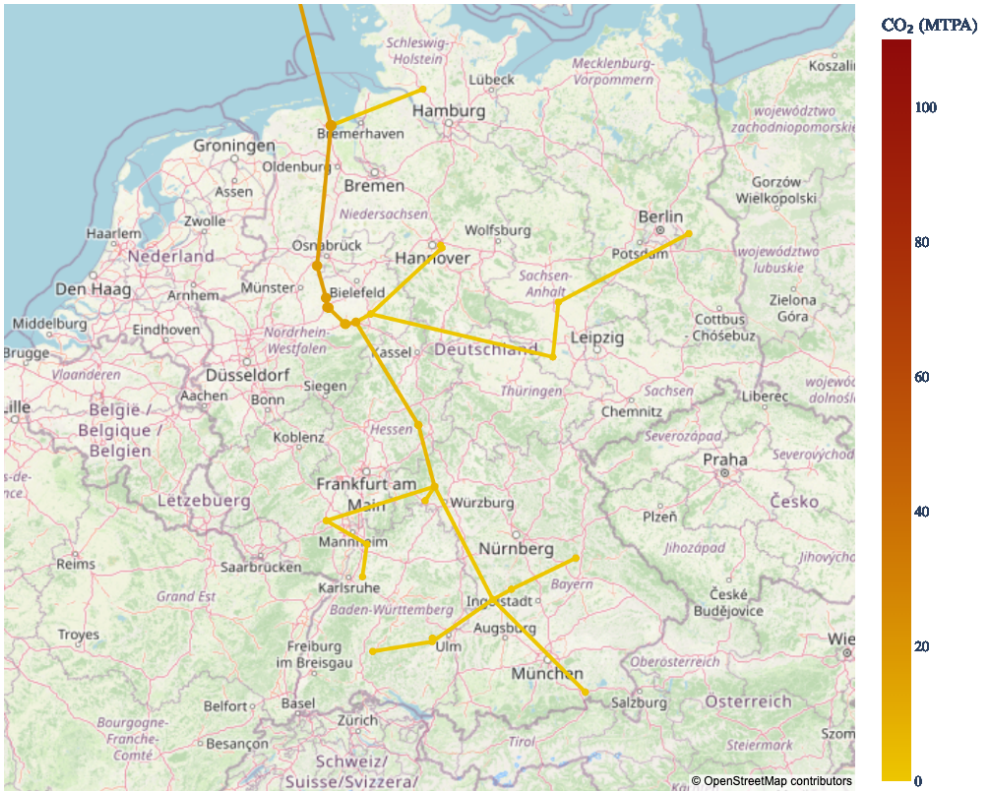

Figure 7.13: Onshore pipeline network for the Cement scenario.

7.6.3 Organic chemicals

In the organic chemicals industry, around half of the CO_2 emissions are due to the manufacturing of chemicals using basic processes such as thermal cracking and distillations with fossil fuels as feedstock (IEA 2019). In some chemical processes, this share can be reduced by using biomass as feedstock, but CO_2 emissions will still be present. Thus, CCS is an appropriate measure to reduce emissions from the organic chemicals industry as well.

With a much lower capture cost than the other industries, of only 30 euro per tonne, the organic chemicals industry's supply chain cost is 49.3 euro per tonne. As in the steel scenario, many industry actors are located in the Düsseldorf area, forming an efficient capture cluster. However, low volumes and two remotely located emission sources result in the highest transportation cost per tonne of the three scenarios, at 13.3 euro per tonne.

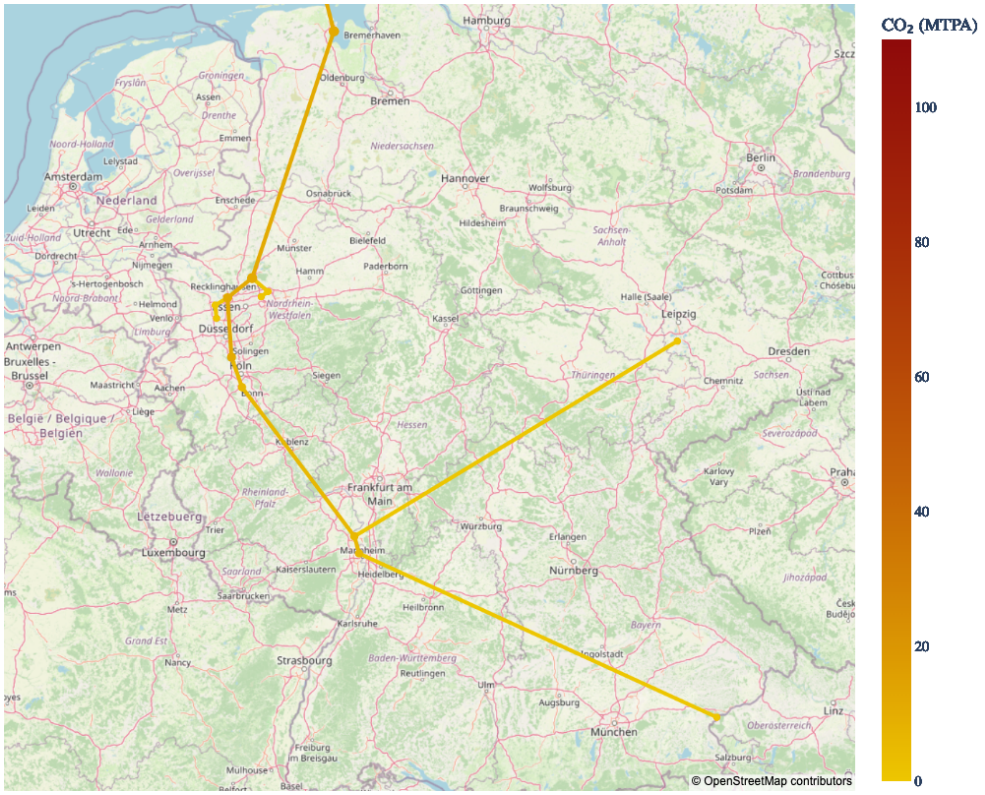

Figure 7.14: Onshore pipeline transportation network for the Organic chemicals scenario.

In conclusion, the costs of CCS vary significantly between industrial sectors. However, if actors within the sectors collaborate, the transportation costs might decrease to 7.0 euro per tonne transported. The organic chemicals sector has a supply chain cost far below the current EU ETS price, indicating that CCS is already significantly cheaper than emitting the CO_2. For the steel industry, the supply chain cost is about equal to the current carbon price, while the cost for the cement industry is more than 30% higher. However, with the anticipated increase in carbon prices in the coming years, as described in Section 2.5, CCS might soon be economically desirable for all vital industry sectors.

7.7 Summary of results

To conclude and summarize the results of the economic analysis, we present a list of essential managerial insights that can be drawn from the analyses. These insights are meant to guide policy-makers and companies, particularly those faced with the task of designing a cross-border maritime CCS supply chain between Germany and Norway with critical transportation and storage infrastructure in the ports of Wilhelmshaven and Kollsnes.

- A German-Norwegian CCS supply chain can soon provide CCS costs well below the price of EU ETS CO_2 allowances, especially if the increasing price trend of the allowances continues.
- Transportation costs decrease significantly when the volumes of CO_2 to be transported increase. For example, they are reduced from 22.1 euro per tonne to 7.0 euro per tonne when volumes increase from 5 Mtpa to 100 Mtpa. The decrease is due to large shared pipelines with a high degree of utilization, which offer economies of scale in the transportation of captured CO_2.
- Ship transportation is the more flexible offshore transportation mode but comes at a cost for volumes higher than 5 Mtpa. We have shown that ship transportation is feasible for volumes up to 100 Mtpa, but this leads to a transportation cost increase of around 5 euro per tonne transported compared to pipelines.
- Ships powered by fuel oil lead to transport-related emissions corresponding to 1.4% of the transported amount of CO_2. Using ships as the offshore transportation mode in S100 thus results in transport-related CO_2 emissions of 1.4 Mtpa.
- Independent of the offshore transportation mode, high capture volumes result in a need for extensive onshore pipeline networks to transport the CO_2 from the emission sources to Wilhelmshaven. For example, when capturing 100 Mtpa from the largest emission sources, over 2000 km of onshore pipelines must be built across Germany. Building such a network is capital- and labor-intensive and requires political and societal support.
- What is the cheapest offshore transportation mode to connect the CCS infrastructure of the two countries depends on three main factors: volume, distance, and pipeline utilization. For volumes under 5 Mtpa, ships are the most economical option by default. For higher volumes, pipelines provide the lowest cost per tonne. With increasing distance and low pipeline utilization, ships become more competitive at higher volumes, especially compared to the smallest pipelines.
- Among industrial sectors where CCS is an important measure to avoid emissions, the cost of CCS varies significantly. The estimated cost of CCS is already far below the EU ETS price for the organic chemicals industry due to a low capture cost. Moreover, the steel and cement industries might as well reach viable supply chain costs soon, bearing in mind the anticipated increase in carbon allowance prices.
- CCS supply chain collaboration within industrial sectors such as Cement, Steel, and Organic chemicals can provide transportation costs in the same range as supply chains based on emission source size. A CCS supply chain with emission sources from the steel industry only can provide transportation costs of 7.0 euro per tonne with CO_2 volumes of 38.1 Mtpa. This is the same transportation cost as in the 100 Mtpa country-wide scenario.

Chapter 8

Concluding Remarks

In this thesis, we have investigated the strategic problem referred to as the CCS-Supply Chain Design Problem (CCS-SCDP). The CCS-SCDP is about designing a multimodal supply chain, utilizing both ships and pipelines to transport CO_2 captured from inland emission sources to suitable storage locations at the lowest possible cost. It is solved with a new MIP model, encapsulating the most important CCS supply chain design decisions. The decisions include the following: which emissions sources to capture from; the number, capacity, and placement of pipelines; the flow through the pipelines; which ships to use and how to route them; the capacities and equipment needed for the infrastructure of the loading and unloading ports.

Our main contribution to the existing literature is our MIP model, which aims at bridging the gap between models for small but detailed, unimodal CCS supply chains and large but simplified multimodal supply chains. By including both onshore and offshore transportation, the model enables inland emissions sources to connect to available storage facilities, independent of location. Thus, the model is applicable to a variety of potential CCS supply chains. Furthermore, by introducing time-discrete ship routing and detailed cost modeling of supply chain components, the model can provide precise indications of the optimal transportation modes. Time discretization ensures operationally feasible ship routing and optimal sizing of essential port infrastructure. The detailed cost modeling enhances the validity of the model solutions and makes the model's supply chain components adaptable to changing cost estimates. Our modeling approach has also enabled circumstantial analyses of the CCS-SCDP, giving policy-makers valuable insights. These contributions bridge the gap in the reviewed literature, and we have shown that the model can provide sufficiently detailed solutions to large, cross-border CCS supply chain design problems with CO_2 volumes of up to 100 Mtpa.

The model is tested on scenarios representing different CO_2 volumes for a German-Norwegian CCS supply chain. With Northern Lights' transportation and storage infrastructure in Kollsnes under construction and the plans for Wilhelmshaven as a CO_2 collecting hub in Germany, these ports were included in each scenario as the unloading and loading ports, respectively. We developed seven scenarios where German emission sources were chosen based on attributes such as size and industrial sector. The results from running the model on these scenarios show that ships are preferable for offshore

transportation for CO_2 volumes under 5 Mtpa. For higher volumes, pipelines provide lower costs. The transportation costs are subject to economies of scale with increasing volumes, and the transportation cost is reduced from 22.1 euro per tonne to 7.0 euro per tonne when the volume of CO_2 increases from 5 to 100 Mtpa. The economies of scale are mainly due to emission sources sharing high-capacity offshore pipelines that are well-utilized. The supply chain cost per tonne is highly influenced by the capture costs, which are estimated to range from 30 to 90 euro per tonne, dependent on the industry. For the scenarios where the emission sources are prioritized on size and thus have affiliations to various industries and capture costs, supply chain costs vary from 103.1 euro per tonne at 5 Mtpa to 79 euro per tonne at 100 Mtpa. These costs are in the range of the current EU ETS price of about 80 euro per tonne and show that it is probable that CCS could soon be a beneficial alternative for emission-intensive industries, given a continuation of the trend with increasing EU ETS prices. Finally, we have designed supply chains for three specific industrial sectors: organic chemicals, cement, and steel. As these sectors have inherent CO_2 emissions from chemical processes, CCS is considered a vital measure to abate their emissions. Through collaboration within its industry sector, the German organic chemical industry can reach a supply chain cost of 49.3 euro per tonne. At this cost, CCS is already desirable compared to the current EU ETS prices. The supply chain costs for the steel and cement industries are 83.0 and 108.7 euro per tonne, respectively. Anticipating higher carbon prices in the coming years, CCS might be a viable alternative for those sectors as well.

Through the economic analysis in Chapter 7, we have illustrated the usability of our model as a CCS supply chain design tool. More specifically, our model can provide technical details and economic implications of the optimal design of a German-Norwegian CCS supply chain for different capture scenarios.

Our results regarding offshore transportation modes coincide with the studied literature, as the optimal offshore transportation mode in the model solutions switches from ships to pipelines with increasing CO_2 volumes. Moreover, our results align with Northern Lights' ambition of transporting 5 Mtpa through ship transportation. Although pipelines are the most economical offshore transportation mode for volumes of 20 to 100 Mtpa, they might not be the preferred option due to their limited flexibility compared to ships. By forcing ship transportation, we have indicated that this is an operationally feasible offshore transportation mode for volumes up to 100 Mtpa. Furthermore, we have discovered that choosing ships at volumes between 20 and 100 Mtpa would increase the transportation cost per tonne by about 5 euro. Moreover, ships become more cost-competitive at greater distances. This insight is generalizable to other scenarios and shows that ships could be economically beneficial for volumes higher than 5 Mtpa if offshore distances surpass 800 km. Furthermore, we have seen that the choice of offshore transportation mode is relatively insensitive to changes in uncertain cost parameters.

Finally, by studying scenarios with an increasing volume of CO_2, the model can provide insights into how a possible ramp-up of the German-Norwegian CCS supply chain may occur.

Chapter 9

Future Research

In this chapter, we briefly discuss suggestions for future research within the domain of the CCS-SCDP. The suggestions concern the input data to our model, handling uncertainty, and gradual build-up of the supply chain over time.

Improved model input data

Our model constructs an optimal network of pipelines between emission sources and loading ports. However, this optimality is implicitly relying on some simplifying assumptions. We assume that it is possible to lay pipelines anywhere. In practice, this may not be the case. For instance, laying pipelines through the Ruhr area, which is densely populated, might become very expensive or practically impossible. To model this, one could remove infeasible or undesired arc options between emission sources or adjust the path if the straight path is infeasible or undesired. Technically, these adjustments are made to the input data, not the model itself.

All scenarios analyzed in this thesis used Wilhelmshaven as the only loading port, Kollsnes as the only unloading port, and EL001 as the only storage site. These choices were based on the currently ongoing CCS projects. However, the model formulation can handle several loading ports, unloading ports, and storage sites. As new CCS projects occur and new locations become relevant for CCS supply chains, analyzing larger scenarios can provide insight into developing a future multi-national, European CCS cooperation.

Since CCS is currently an immature industry, and the costs of several of the elements present in a full-scale CCS supply chain are uncertain, the cost of the supply chain is subject to significant uncertainties. As discussed in Chapter 7, the most significant cost component is CO_2 capture. Moreover, as illustrated by IEA (2022), the estimated capture costs are uncertain. Thus, more thorough research on capture cost is needed to get accurate cost estimations for the supply chain. Furthermore, as discussed in Section 7.4, the costs of pipeline and ship transportation affect not only the cost of the supply chain but also the optimal choice of offshore transportation mode. Therefore, future research may benefit from acquiring even more accurate cost estimates for elements connected to transportation, especially as the relevant technologies are further developed.

Handling uncertainty

As a result of potential rapid development in CCS deployment in the coming years, there is inherently much uncertainty as the range of possible outcomes is ample for several parts of the supply chain. For instance, there is much uncertainty connected to which emission sources will adopt CO_2 capture technology. However, in our deterministic model formulation, there are no uncertainties regarding the emission sources, so its onshore pipeline network does not take into account the fact that some of the emission sources might supply different amounts of CO_2 or none at all. Therefore, a model formulation that includes this uncertainty will probably have a different, more practically sound onshore pipeline network. To expand the model formulation towards the generation of more robust solutions, one could construct several scenarios for each basic scenario, where each scenario considers a variation in the amounts of captured CO_2 and at different locations.

Following the magnitude and variety of elements in the CCS supply chain, there are many other sources of uncertainty that may affect the preferred solutions as well. A couple of examples are uncertain weather conditions affecting the sailing speed or power consumption and changes in geological or political circumstances that require reinforcements or removal of certain facilities or equipment. Our model can handle the former, although it has not been discussed in our thesis. However, we consider these uncertainties to be of less magnitude, and hence importance, than the uncertain amounts and locations of captured CO_2.

Modeling build-up over time

We have discussed the build-up of the supply chain by analyzing four basic scenarios that differ in the amount of CO_2 emitted. These scenarios correspond to *what if*-analyses, where we can present solutions for only one scenario at a time. However, by extending the model into a multi-period model, one can plan for future system requirements. For instance, each of the basic scenarios could correspond to a single period within a sequence of periods that altogether cover a given time horizon. A multi-period extension could be combined with modeling supply uncertainty by having scenarios with variations in emission sources and their supplies for each period. Such a model would be able to produce solutions with a cost-efficient ramp-up of the CCS supply chain over time. For instance, early investment in infrastructure with higher capacity than needed in the low supply scenarios could result in less need for later readjustments to the supply chain configuration and, thus, reduce the total long-term costs of the system.

Bibliography

Amlie, H. C., M. Hay, A. Markussen, R. de Kler, T. Mikunda, A. Scott, A. Campbell, B. Dolek, D. McGlashan, F. Ollerhead, M. Gilks and S. Murphy (2018). *Shipping* CO_2 *- UK Cost Estimation Study*. Element Energy.

Andhra Pradesh Gas Distribution Cooperation Ltd. (2012). *Development of Offshore LNG FSRU Facility at Kakinada Deep Water Port, Kakinada, Andhra Pradesh*. Tech. rep. Andhra Pradesh Gas Distribution Cooperation Ltd.

Apeland, S., H. Dale, S. Decarre, N. Eldrup, H. Hansen, J. Nilsson, A. Rennie, R. Skagestad and T. Wendt (2011). *The cost of CO2 Transport*. European Technology Platform for Zero Emission Fossil Fuel Power Plants.

Aramis (2022). *About the Aramis Project*. URL: https://www.aramis-ccs.com/project (visited on 25th Mar. 2022).

Argus Media (2019). *Argus White Paper: German industrial emissions*. Argus Media Group.

Aspelund, A., M. Mølnvik and G. De Koeijer (2006). 'Ship Transport of CO2: Technical Solutions and Analysis of Costs, Energy Utilization, Exergy Efficiency and CO2 Emissions'. In: *Chemical Engineering Research and Design* 84.9, pp. 847–855.

Bains, P., P. Psarras and J. Wilcox (2017). 'CO2 capture from the industry sector'. In: *Progress in Energy and Combustion Science* 63, pp. 146–172.

Bennæs, A., M. Skogset and T. Svorkdal (2021). 'Optimization of a Ship-based Logistics System For Carbon Capture and Storage'. Project report. Trondheim, Norway: Norwegian University of Science and Technology.

Bittante, A. and H. Saxen (2020). 'Design of Small LNG Supply Chain by Multi-Period Optimization'. In: *Energies* 13, pp. 1–19.

Bjerketvedt, V. S., A. Tomasgard and S. Roussanaly (2020). 'Optimal design and cost of ship-based CO2 transport under uncertainties and fluctuations'. In: *International Journal of Greenhouse Gas Control* 103, pp. 190–203.

— (2022). 'Deploying a shipping infrastructure to enable carbon capture and storage from Norwegian industries'. In: *Journal of Cleaner Production* 333, pp. 586–601.

Bohlsen, M. (2021). *CCS companies to consider*. URL: https://seekingalpha.com/article/4438777-carbon-capture-and-storage-companies-to-consider (visited on 20th May 2022).

Budinis, S. (2021). *Direct Air Capture*. URL: https://www.iea.org/reports/direct-air-capture (visited on 4th Feb. 2022).

Chandel, M. K., L. F. Pratson and E. Williams (2010). 'Potential economies of scale in CO2 transport through use of a trunk pipeline'. In: *Energy Conversion and Management* 51.12, pp. 2825–2834.

Chauvel, A., G. Fournier and C. Raimbault (2003). *Manual of process economic evaluation*. Editions Technip.

d'Amore, F., M. C. Romano and F. Bezzo (2021). 'Optimal design of European supply chains for carbon capture and storage from industrial emission sources including pipe and ship transport'. In: *International Journal of Greenhouse Gas Control* 109, pp. 372–386.

Debarre, R., P. Gahlot, C. Grillet and M. Plaisant (2021). *Carbon Capture Utilization and Storage, Towards Net-Zero*. Kearney Energy Transition Institute.

Directorate-General for Energy (2021). *Candidate PCI projects in cross-border carbon dioxide (CO_2) transport networks*.

Eigestad, G., H. Dahle, B. Hellevang, F. Riis, W. Johansen and E. Øian (2009). 'Geological modeling and simulation of CO2 injection in the Johansen formation'. In: *Computational Geosciences* 13, pp. 435–450.

Ember (2022). *Carbon Pricing*. URL: https://ember-climate.org/data/data-tools/carbon-price-viewer/ (visited on 20th May 2022).

Environmental and Energy Study Institute (2022). *Fossil Fuels*. URL: https://www.eesi.org/topics/fossil-fuels/description (visited on 7th June 2022).

Equinor (2019). *Northern Lights Concept Report*. Equinor.

EUROFER (2021). *European Steel in Figures 2021*. Tech. rep. The European Steel Association.

Faber, J., S. Hanayama, S. Zhang, P. Pereda, B. Comer and E. Hauerhuf (2020). 'Fourth IMO GHG Study 2020'. In: *International Maritime Organization*, p. 184.

Federal Environment Agency Germany (2022). *Pollutant Release and Transfer Register*. https://www.thru.de/thrude/downloads/?L=3#c1318. (Visited on 7th May 2022).

Garcia, D. J. and F. You (2015). 'Supply chain design and optimization: Challenges and opportunities'. In: *Computers Chemical Engineering* 81, pp. 153–170.

Garside, M. (2022). *Production volume of cement in Europe in 2020, by country*. https://www.statista.com/statistics/1291068/european-cement-production-volume-by-country/. (Visited on 1st June 2022).

Gasnova and Gassco (2016). *Mulighetsstudier av fullskala CO2-håndtering i Norge [Studies of potential full-scale carbon capture and storage in Norway]*. Norwegian Oil and Gas Department.

Gassnova (2019). *Technology status for CO2 capture, transport and storage*. Gassnova.

Global CCS Institute (2016). *Fact Sheet - Capturing* CO_2. Global CCS Institute.

Global Maritime Energy Efficiency Partnerships (2022). *Improved Auxiliary Engine Load*. https://glomeep.imo.org/technology/improved-auxiliary-engine-load/. (Visited on 14th Apr. 2022).

Hofstad, K. (2022). *Karbonfangst og -lagring [Carbon Capture and Storage]*. URL: https://snl.no/karbonfangst_og_-lagring (visited on 14th May 2022).

Holz, F., T. Scherwath, P. Crespo del Granado, C. Skar, L. Olmos, Q. Ploussard, A. Ramos and A. Herbst (2021). 'A 2050 perspective on the role for carbon capture and storage in the European power system and industry sector'. In: *Energy Economics* 104, pp. 631–649.

IEA (2004). *Ship Transport of* CO_2. Tech. rep. International Energy Agency Greenhouse Gas RD Programme.

— (2019). *Transforming Industry through CCUS*. International Energy Agency.

— (2021). *Net Zero by 2050*. International Energy Agency.

— (2022). *Is carbon capture too expensive*. URL: https://www.iea.org/commentaries/is-carbon-capture-too-expensive (visited on 20th Apr. 2022).

IPCC (2022). 'Summary for Policymakers'. In: *Climate Change 2022: Mitigation of Climate Change. Contribution of Working Group III to the Sixth Assessment Report of the Intergovernmental Panel on Climate Change*. Ed. by P. Shukla, J. Skea, R. Slade, A. A. Khourdajie, R. van Diemen, D. McCollum, M. Pathak, S. Some, P. Vyas, R. Fradera, M. Belkacemi, A. Hasija, G. Lisboa, S. Luz and J. Malley. Cambridge, United Kingdom and New York, NY, USA: Cambridge University Press.

Kearns, D., E. Tamme, C. Staib, T. Zhang, J. Burrows, A. Gillespie, I. Havercroft, D. Rassool, C. Consoli and H. Liu (2021). *Global status of CCS 2021*. Clobal CCS Institute.

Kjärstad, J., R. Skagestad, N. H. Eldrup and F. Johnsson (2016). 'Ship transport—A low cost and low risk CO2 transport option in the Nordic countries'. In: *International Journal of Greenhouse Gas Control* 54, pp. 168–184.

Knoope, M., A. Ramırez and A. Faaij (2013). 'A state-of-the-art review of techno-economic models predicting the costs of CO2 pipeline transport'. In: *International Journal of Greenhouse Gas Control* 16, pp. 241–270.

Li, J. and Y. Jia (2020). 'Calculation Method of Marine Ship Fuel Consumption'. English. In: *IOP Conference Series.Earth and Environmental Science* 571.1.

McCollum, D. and J. Ogden (2006). 'Techno-Economic Models for Carbon Dioxide Compression, Transport, and Storage Correlations for Estimating Carbon Dioxide Density and Viscosity'. In: *Institute of Transportation Studies, UC Davis, Institute of Transportation Studies, Working Paper Series*.

Metz, B., J. C. Abanades, M. Akai, S. Benson, K. Caldeira, P. Cook, O. Davidson, R. Doctor, J. Dooley, P. Freund, J. Gale, W. Heidug, H. Herzog, D. Keith, M. Mazzotti, B. Osman-Elasha, A. Palmer, R. Pipatti, K. Smekens, M. Soltanieh, K. Thambimuthu and B. van der Zwaan (2005). *IPCC Special Report on Carbon Dioxide Capture and Storage*. Intergovernmental Panel on Climate Change.

Middleton, R. S. and J. M. Bielicki (2009). 'A scalable infrastructure model for carbon capture and storage: SimCCS'. In: *Energy Policy* 37.3, pp. 1052–1060.

Morbee, J., J. Serpa and E. Tzimas (2012). 'Optimised deployment of a European CO2 transport network'. In: *International Journal of Greenhouse Gas Control* 7, pp. 48–61.

Nam, H., T. Lee, J. Lee, J. Lee and H. Chung (2013). 'Design of carrier-based offshore CCS system: Plant location and fleet assignment'. In: *International Journal of Greenhouse Gas Control* 12, pp. 220–230.

Noothout, P., F. Wiersma, O. Hurtado, P. Roelofsen and D. Macdonald (2013). CO_2 *Pipeline Infrastructure*. IEAGHG.

Northern Lights (2022). *Cory and Northern Lights announce pioneering international carbon partnership*. URL: https://norlights.com/news/cory-and-northern-lights-announce-pioneering-international-carbon-partnership (visited on 23rd May 2022).

Northern Lights JV DA (2022). *Acceleratiоng decarbonisation*. URL: https://norlights.com/ (visited on 29th May 2022).

Ogden, J. and N. Johnson (2010). '2 - Techno-economic analysis and modeling of carbon dioxide (CO2) capture and storage (CCS) technologies'. In: *Developments and Innovation in Carbon Dioxide (CO2) Capture and Storage Technology*. Ed. by M. M. Maroto-Valer. Vol. 1. Woodhead Publishing, pp. 27–63.

Onyebuchi, V., A. Kolios, D. Hanak, C. Biliyok and V. Manovic (2018). 'A systematic review of key challenges of CO2 transport via pipelines'. In: *Renewable and Sustainable Energy Reviews* 81, pp. 2563–2583.

Peletiri, S., N. Rahmanian and I. Mujtaba (2018). 'CO2 Pipeline design: A review'. In: *Energies* 11, pp. 1–25.

Ritchie, H. and M. Roser (2020). 'CO_2 and Greenhouse Gas Emissions'. In: *Our World in Data*. https://ourworldindata.org/co2-and-other-greenhouse-gas-emissions.

Roussanaly, S., A. L. Brunsvold and E. S. Hogne (2014). 'Benchmarking of CO2 transport technologies: Part II – Offshore pipeline and shipping to an offshore site'. In: *International Journal of Greenhouse Gas Control* 28, pp. 283–299.

Roussanaly, S., H. Deng, G. Skaugen and T. Gundersen (2021). 'At what Pressure Shall CO_2 Be Transported by Ship? An in-Depth Cost Comparison of 7 and 15 Barg Shipping'. In: *Energies* 14.18, pp. 1–27.

Roussanaly, S., O. J. P. Jakobsen, E. H. Hognes and A. L. Brunsvold (2013). 'Benchmarking of CO2 transport technologies: Part I—Onshore pipeline and shipping between two onshore areas'. In: *International Journal of Greenhouse Gas Control* 19, pp. 584–594.

Sandberg, P., E. Yde Aasen, I. Pacevicuiute, F. Nebell and V. Kjersti (2019). *Plan for long-term use of the Northern Lights infrastructure*. Equinor.

Serpa, J., J. Morbee and E. Tzimas (2011). 'Technical and Economic Characteristics of a CO2 Transmission Pipeline Infrastructure'. In: European Commision Joint Research Center.

Ship & Bunker (2022). *Rotterdam Bunker Prices*. URL: https://shipandbunker.com/prices/emea/nwe/nl-rtm-rotterdam (visited on 2nd May 2022).

Skagestad, R., K. Onarheim and A. Mathisen (2014). 'Carbon Capture and Storage (CCS) in Industry Sectors – Focus on Nordic Countries'. In: *Energy Procedia* 63, pp. 6611–6622.

Summit Carbon Solutions (2022). *Project Footprint*. URL: https://summitcarbonsolutions.com/project-footprint/ (visited on 23rd May 2022).

The Federal Environment Agency (2018). *Deutschland Freisetzungen*. URL: https://www.thru.de/thrude/downloads/?L=3#c1318 (visited on 17th Feb. 2022).

The Norwegian Government (2020). *Climate plan for 2021 to 2030 [Klimaplan for 2021-2030]*. https://www.regjeringen.no/no/dokumenter/meld.-st.-13-20202021/id2827405/?ch=1. Available at 2022-05-21. (Visited on 27th May 2022).

The World Bank (2022). *Carbon Pricing Dashboard*. https://carbonpricingdashboard.worldbank.org/. (Visited on 25th May 2022).

Vandeginste, V. and K. Piessens (n.d.). 'Pipeline design for a least-cost router application for CO2 transport in the CO2 sequestration cycle'. In: *International Journal of Greenhouse Gas Control* 2.4 (). TCCS-4: The 4th Trondheim Conference on CO2 Capture, Transport and Storage, pp. 571–581.

Vermeulen, T. (2011). *Knowledge Sharing Report – CO2 Liquid Logistics Shipping Concept (LLSC) Overall Supply Chain Optimization*. Tebodin Netherlands B.V.

Wang, Z., G. Fimbres Weihs, G. Cardenas and D. Wiley (2014). 'Optimal pipeline design for CCS projects with anticipated increasing CO2 flow rates'. In: *International Journal of Greenhouse Gas Control* 31, pp. 165–174.

Wang, Z. (2018). '1.23 Energy and Air Pollution'. In: *Comprehensive Energy Systems*. Elsevier, pp. 909–949.

Wintershall Dea (2022). *Wintershall Dea helps shape the Wilhelmshaven Energy Hub*. URL: https://wintershalldea.no/en/newsroom/wintershall-dea-helps-shape-wilhelmshaven-energy-hub (visited on 23rd May 2022).

Witkowski, A., M. Majkut and S. Rulik (2014). 'Analysis of pipeline transportation systems for carbon dioxide sequestration'. In: *Archives of Thermodynamics* 35, s. 117–140.

Yoo, B.-Y. (2017). 'The development and comparison of CO2 BOG re-liquefaction processes for LNG fueled CO2 carriers'. In: *Energy* 127, pp. 186–197.

Yoo, B.-Y., D.-K. Choi, H.-J. Kim, Y.-S. Moon, H.-S. Na and S.-G. Lee (2013). 'Development of CO2 terminal and CO2 carrier for future commercialized CCS market'. In: *International Journal of Greenhouse Gas Control* 12, pp. 323–332.

Zero Emissions Platform (2011). *The Costs of* CO_2 *Storage Post-demonstration CCS in the EU*.

— (2021). *Candidate PCI projects in cross-border* CO_2 *transport networks*.

Appendix A

Complete mathematical model

Sets, parameters and decision variables

Table A.1: Model sets.

Set	Description
$\mathcal{N}^U$	Set of unloading ports
$\mathcal{N}^L$	Set of loading ports
$\mathcal{N}^P$	Set of ports, $\mathcal{N}^P = \mathcal{N}^U \cup \mathcal{N}^L$
$\mathcal{N}^E$	Set of emission sources
$\mathcal{N}^S$	Set of permanent storage locations
$\mathcal{N}$	Set of ports, emission sources and permanent storage locations $\mathcal{N} = \mathcal{N}^P \cup \mathcal{N}^E \cup \mathcal{N}^S$
$\mathcal{V}$	Set of ships
$\mathcal{C}$	Set of ship types
$\mathcal{V}_c$	Set of ships of type c, $\mathcal{V}_c \subset \mathcal{V}$
$\mathcal{D}$	Set of candidate pipeline diameters
$\mathcal{T}$	Set of time periods
$\mathcal{T}_i^O$	Set of operating time periods for port i
$\mathcal{T}_i^{[init]}$	Set of initial time periods for port i
$\mathcal{T}^C$	Set of time periods in the central planning horizon

Table A.2: Model parameters.

Parameter	Description
C_v^H	Cost of hiring ship v during the central planning horizon, $\mathcal{T}^C$
C_{ijv}^T	Cost of ship v operating in port i and sailing from port i to port j
C_v^W	Cost of waiting outside a port during one time period for ship v
C_i^I	Cost per tonne loaded onto or unloaded from ships in port i
C^B	Cost per tonne of intermediate buffer storage capacity
C^E	Cost per tonne of emitted CO_2 due to overspill
C^L	Cost per tonne liquefied CO_2
C^R	Cost per tonne reconditioned CO_2
C_i^D	Cost per dock in port i, scaled to the length of the central planning horizon
C_{ijd}^{PL}	Cost per onshore pipeline with diameter d between node i and node j, scaled to the length of the central planning horizon
C_{ijd}^{PO}	Cost per offshore pipeline with diameter d between node i and node j, scaled to the length of the central planning horizon
C_{ijd}^{PS}	Cost per storage pipeline with diameter d between node i and node j, scaled to the length of the central planning horizon
C_{ij}^V	Variable cost per tonne of CO_2 flowing through pipelines between node i and node j
C_i^S	Cost per tonne of CO_2 stored permanently at location i
C_i^C	Cost per tonne of CO_2 captured in emission source i
T_v^L	Number of time periods ship v uses to fully load or unload itself
T_{ijvt}	Number of time periods used by ship v to start operate in port i in time period t and, immediately after operating, sail from port i to port j
K_v	Load capacity of ship v, in tonnes of CO_2
B	Boil-off per time period, as a percentage of a complete shipload
F_d	Maximal flow capacity through a pipeline of diameter d, in tonnes per time period
$\underline{S}_i$	Lower bound on inventory in buffer storage at port i
P_i	Produced CO_2 in emission source i during one time period
O^M	Minimum share of produced CO_2 that is captured and transported to permanent storage

Table A.3: Model variables.

Variable	Domain	Description
h_{ijv}	Binary	1 if ship v is hired and used on the link (i, j) where i represents a loading port, while j represents an unloading port, 0 otherwise
x_{ijvt}	Binary	1 if ship v starts operating in port i at time period t, and thereafter directly sails from port i to its dedicated port j, 0 otherwise
w_{ivt}	Binary	1 if ship v waits outside port i in time periode t, 0 otherwise
δ_{ivt}	Binary	1 if ship v is operating in port i in time period t
d_i	Integer	Number of docks in port i
b_i	Continuous	Buffer storage capacity in port i, i.e., upper bound on inventory level in port i. Measured in tonnes
s_{it}	Continuous	Inventory level in port i at the end of time period t. Measured in tonnes
e_{it}	Continuous	Emitted CO_2 from port i in time period t due to overspill. Measured in tonnes
c_i	Continuous	Quantity of CO_2 that is captured in emission source i during one time period. Measured in tonnes
p^L_{ijd}	Integer	Number of onshore pipelines with diameter d between emission source i and emission source or loading port j
p^O_{ijd}	Integer	Number of offshore pipelines with diameter d between loading port i and unloading port j
p^S_{ijd}	Integer	Number of storage pipelines with diameter d between unloading port i and storage location j
f^L_{ij}	Continuous	Total flow of CO_2 through onshore pipelines between emission source i and emission source or loading port j, in tonnes per time period
f^O_{ij}	Continuous	Total flow of CO_2 through offshore pipelines between loading port i and unloading port j, in tonnes per time period
f^S_{ij}	Continuous	Total flow of CO_2 through storage pipelines between unloading port i and permanent storage location j, in tonnes per time period

Objective

$$\begin{aligned}\min\ w = {} & C^{[Hire]} + C^{[Sail]} + C^{[Wait]} + C^{[L+U]} + C^{[Liq]} + C^{[Rec]} + C^{[Buffer]} \\ & + C^{[Docks]} + C^{[Pipe-L]} + C^{[Pipe-O]} + C^{[Pipe-S]} + C^{[Capture]} + C^{[Store]}\end{aligned} \tag{A.1}$$

where each term is presented below:

$$C^{[Hire]} = \sum_{i\in\mathcal{N}^L}\sum_{j\in\mathcal{N}^U}\sum_{v\in\mathcal{V}} C_v^H h_{ijv} \tag{A.2}$$

$$C^{[Sail]} = \sum_{i\in\mathcal{N}^L}\sum_{j\in\mathcal{N}^U}\sum_{v\in\mathcal{V}}\sum_{t\in\mathcal{T}_i^O} C_{ijv}^T x_{ijvt} + \sum_{i\in\mathcal{N}^U}\sum_{j\in\mathcal{N}^L}\sum_{v\in\mathcal{V}}\sum_{t\in\mathcal{T}_i^O} C_{ijv}^T x_{ijvt} \tag{A.3}$$

$$C^{[Wait]} = \sum_{i\in\mathcal{N}^P}\sum_{v\in\mathcal{V}}\sum_{t\in\mathcal{T}_i^O} C_v^W w_{ivt} \tag{A.4}$$

$$\begin{aligned}C^{[L+U]} = {} & \sum_{i\in\mathcal{N}^L}\sum_{j\in\mathcal{N}^U}\sum_{v\in\mathcal{V}}\sum_{t\in\mathcal{T}_i^O} C_i^I K_v x_{ijvt} \\ & + \sum_{i\in\mathcal{N}^U}\sum_{j\in\mathcal{N}^L}\sum_{v\in\mathcal{V}}\sum_{t\in\mathcal{T}_i^O} \left(1-(B\cdot T_{ijvt})\right) C_i^I K_v x_{ijvt}\end{aligned} \tag{A.5}$$

$$C^{[Liq]} = \sum_{i\in\mathcal{N}^L}\sum_{j\in\mathcal{N}^U}\sum_{v\in\mathcal{V}}\sum_{t\in\mathcal{T}_i^O} C^L K_v x_{ijvt} \tag{A.6}$$

$$C^{[Rec]} = \sum_{i\in\mathcal{N}^U}\sum_{j\in\mathcal{N}^L}\sum_{v\in\mathcal{V}}\sum_{t\in\mathcal{T}_i^O} \left(\left(1-(B\cdot T_{ijvt})\right) C^R K_v x_{ijvt}\right. \tag{A.7}$$

$$C^{[Buffer]} = \sum_{i\in\mathcal{N}^P} C^B b_i + \sum_{i\in\mathcal{N}^L}\sum_{t\in\mathcal{T}_i^O} C^E e_{it} \tag{A.8}$$

$$C^{[Docks]} = \sum_{i\in\mathcal{N}^P} C_i^D d_i \tag{A.9}$$

$$C^{[Pipe-L]} = \sum_{i\in\mathcal{N}^E}\sum_{j\in\mathcal{N}^E\cup\mathcal{N}^L}\sum_{d\in\mathcal{D}} C_{ijd}^{PL} p_{ijd}^L + \sum_{i\in\mathcal{N}^E}\sum_{j\in\mathcal{N}^E\cup\mathcal{N}^L} |\mathcal{T}_i^O| C_{ij}^V f_{ij}^L \tag{A.10}$$

$$C^{[Pipe-O]} = \sum_{i\in\mathcal{N}^L}\sum_{j\in\mathcal{N}^U}\sum_{d\in\mathcal{D}} C_{ijd}^{PO} p_{ijd}^O + \sum_{i\in\mathcal{N}^L}\sum_{j\in\mathcal{N}^U} |\mathcal{T}_i^O| C_{ij}^V f_{ij}^O \tag{A.11}$$

$$C^{[Pipe-S]} = \sum_{i\in\mathcal{N}^U}\sum_{j\in\mathcal{N}^S}\sum_{d\in\mathcal{D}} C_{ijd}^{PS} p_{ijd}^S + \sum_{i\in\mathcal{N}^U}\sum_{j\in\mathcal{N}^S} |\mathcal{T}_i^O| C_{ij}^V f_{ij}^S \tag{A.12}$$

$$C^{[Capture]} = \sum_{i\in\mathcal{N}^E} |\mathcal{T}_i^O| C_i^C c_i \tag{A.13}$$

$$C^{[Store]} = \sum_{i\in\mathcal{N}^U}\sum_{j\in\mathcal{N}^S} |\mathcal{T}_i^O| C_i^S f_{ij}^S \tag{A.14}$$

Model constraints

$$\sum_{i \in \mathcal{N}^L} \sum_{j \in \mathcal{N}^U} h_{ijv} \leq 1 \qquad v \in \mathcal{V} \quad \text{(A.15)}$$

$$x_{ijv,t-T_{ijvt}} + w_{jv,t-1} = w_{jvt} + x_{jivt} \quad i \in \mathcal{N}^L, j \in \mathcal{N}^U, v \in \mathcal{V}, t \in \mathcal{T}_j^O \quad \text{(A.16)}$$

$$x_{jiv,t-T_{jivt}} + w_{iv,t-1} = w_{ivt} + x_{ijvt} \quad i \in \mathcal{N}^L, j \in \mathcal{N}^U, v \in \mathcal{V}, t \in \mathcal{T}_i^O \quad \text{(A.17)}$$

$$x_{ijvt} + x_{jivt} + w_{ivt} + w_{jvt} \leq h_{ijv} \qquad i \in \mathcal{N}^L, j \in \mathcal{N}^U, v \in \mathcal{V}, t \in \mathcal{T} \quad \text{(A.18)}$$

$$\sum_{\tau=1}^{t} x_{ijv\tau} \geq x_{jivt} \qquad i \in \mathcal{N}^L, j \in \mathcal{N}^U, v \in \mathcal{V}, t \in \mathcal{T} \quad \text{(A.19)}$$

$$x_{ijvt} + w_{ivt} = 0 \qquad i \in \mathcal{N}^L, j \in \mathcal{N}^U, v \in \mathcal{V}, t \in \{\mathcal{T}_i^{[init]} | t \leq |\mathcal{T}_i^{[init]}|\} \quad \text{(A.20)}$$

$$x_{ijvt} + w_{ivt} = 0 \qquad i \in \mathcal{N}^U, j \in \mathcal{N}^L, v \in \mathcal{V}, t \in \{\mathcal{T}_i^{[init]} | t \leq |\mathcal{T}_i^{[init]}|\} \quad \text{(A.21)}$$

$$c_i \leq P_i \qquad i \in \mathcal{N}^E \quad \text{(A.22)}$$

$$\sum_{j \in \mathcal{N}^E \setminus \{i\}} f_{ji}^L + c_i = \sum_{j \in \mathcal{N}^E \cup \mathcal{N}^L \setminus \{i\}} f_{ij}^L \qquad i \in \mathcal{N}^E \quad \text{(A.23)}$$

$$s_{i,t-1} + \sum_{j \in \mathcal{N}^E} f_{ji}^L - \sum_{j \in \mathcal{N}^U} f_{ij}^O - \sum_{j \in \mathcal{N}^U} \sum_{v \in \mathcal{V}} K_v x_{ijvt} = e_{it} + s_{it} \qquad i \in \mathcal{N}^L, t \in \mathcal{T}_i^O \quad \text{(A.24)}$$

$$s_{i,t-1} + \sum_{j \in \mathcal{N}^L} f_{ji}^O + \sum_{j \in \mathcal{N}^L} \sum_{v \in \mathcal{V}} (1 - (B \cdot T_{ijvt})) K_v x_{ijvt} = \sum_{j \in \mathcal{N}^S} f_{ij}^S + s_{it} \qquad i \in \mathcal{N}^U, t \in \mathcal{T}_i^O \quad \text{(A.25)}$$

$$s_{it} \leq b_i \qquad i \in \mathcal{N}^P, t \in \mathcal{T} \quad \text{(A.26)}$$

$$s_{i,|\mathcal{T}_i^{init}|} = s_{i,|\mathcal{T}|} \qquad i \in \mathcal{N}^U \quad \text{(A.27)}$$

$$s_{it} = 0 \qquad i \in \mathcal{N}^P, t \in \{\mathcal{T}_i^{[init]} | t \leq |\mathcal{T}_i^{[init]}|\} \quad \text{(A.28)}$$

$$f_{ij}^{L} \leq \sum_{d \in \mathcal{D}} F_d p_{ijd}^{L} \qquad i \in \mathcal{N}^{E}, j \in \mathcal{N}^{E} \cup \mathcal{N}^{L} \setminus \{i\} \tag{A.29}$$

$$f_{ij}^{O} \leq \sum_{d \in \mathcal{D}} F_d p_{ijd}^{O} \qquad i \in \mathcal{N}^{L}, j \in \mathcal{N}^{U} \tag{A.30}$$

$$f_{ij}^{S} \leq \sum_{d \in \mathcal{D}} F_d p_{ijd}^{S} \qquad i \in \mathcal{N}^{U}, j \in \mathcal{N}^{S} \tag{A.31}$$

$$\sum_{i \in \mathcal{N}^{L}} |\mathcal{T}_i^{O}| \sum_{j \in \mathcal{N}^{U}} f_{ij}^{O} + \sum_{i \in \mathcal{N}^{L}} \sum_{j \in \mathcal{N}^{U}} \sum_{v \in \mathcal{V}} \sum_{t \in \mathcal{T}} K_v x_{ijvt} \geq \sum_{i \in \mathcal{N}^{E}} O^{M} P_i |\mathcal{T}_i^{O}| \tag{A.32}$$

$$\sum_{j \in \mathcal{N}^{U}} \sum_{\tau = t - T_v^{L}}^{t} x_{ijv\tau} \leq \delta_{ivt} \qquad i \in \mathcal{N}^{L}, v \in \mathcal{V}, t \in \{\mathcal{T} | t \geq T_v^{L}\} \tag{A.33}$$

$$\sum_{v \in \mathcal{V}} \delta_{ivt} \leq d_i \qquad i \in \mathcal{N}^{L}, t \in \mathcal{T} \tag{A.34}$$

$$\sum_{j \in \mathcal{N}^{L}} \sum_{\tau = t - T_v^{L}}^{t} x_{ijv\tau} \leq \delta_{ivt} \qquad i \in \mathcal{N}^{U}, v \in \mathcal{V}, t \in \{\mathcal{T} | t \geq T_v^{L}\} \tag{A.35}$$

$$\sum_{v \in \mathcal{V}} \delta_{ivt} \leq d_i \qquad i \in \mathcal{N}^{U}, t \in \mathcal{T} \tag{A.36}$$

Symmetry breaking constraints

$$\sum_{i \in \mathcal{N}^{L}} \sum_{j \in \mathcal{N}^{U}} (h_{ijv} - h_{ij,v+1}) \geq 0 \qquad c \in \mathcal{C}, v \in \mathcal{V}_c \tag{A.37}$$

$$\sum_{t \in \mathcal{T}} \tau_{vt} \leq 1 \qquad v \in \mathcal{V} \tag{A.38}$$

$$x_{ijvt} - \sum_{t_1 = 0}^{t-1} x_{ijv,t_1} \leq \tau_{vt} \qquad i \in \mathcal{N}^{L}, j \in \mathcal{N}^{U}, \; v \in \mathcal{V}, t \in \mathcal{T} \tag{A.39}$$

$$\sum_{t \in \mathcal{T}} t \cdot \tau_{vt} - \sum_{t \in \mathcal{T}} t \cdot \tau_{v+1,t} + 1 \leq \sum_{i \in \mathcal{N}^{L}} \sum_{j \in \mathcal{N}^{U}} h_{ijv} \qquad c \in \mathcal{C}, v \in \{\mathcal{V}_c | v < |\mathcal{V}_c|\} \tag{A.40}$$

$$\tau_{vt} \in \{0, 1\} \qquad v \in \mathcal{V}, t \in \mathcal{T} \tag{A.41}$$

Valid inequalities

$$\frac{\lceil|\mathcal{T}|\rceil}{T_{ijvt}+T_{jivt}}(1-x_{ijvt}) \geq \sum_{k\in\mathcal{N}^L\setminus\{j\}}\sum_{\tau\in\mathcal{T}} x_{ikv\tau} \quad i\in\mathcal{N}^U, j\in\mathcal{N}^L, v\in\mathcal{V}, t\in\mathcal{T} \tag{A.42}$$

$$\frac{\lceil|\mathcal{T}|\rceil}{T_{ijvt}+T_{jivt}}(1-x_{ijvt}) \geq \sum_{k\in\mathcal{N}^L\setminus\{j\}}\sum_{\tau\in\mathcal{T}} x_{ikv\tau} \quad i\in\mathcal{N}^L, j\in\mathcal{N}^U, v\in\mathcal{V}, t\in\mathcal{T} \tag{A.43}$$

Variable domains

$$h_{ijv}\in\{0,1\} \qquad i\in\mathcal{N}^L, j\in\mathcal{N}^U, v\in\mathcal{V} \tag{A.44}$$

$$x_{ijvt}\in\{0,1\} \qquad i\in\mathcal{N}^L, j\in\mathcal{N}^U, v\in\mathcal{V}, t\in\mathcal{T} \tag{A.45}$$

$$x_{ijvt}\in\{0,1\} \qquad i\in\mathcal{N}^U, j\in\mathcal{N}^L, v\in\mathcal{V}, t\in\mathcal{T} \tag{A.46}$$

$$w_{ivt}\in\{0,1\} \qquad i\in\mathcal{N}^P, v\in\mathcal{V}, t\in\mathcal{T} \tag{A.47}$$

$$\delta_{ivt}\in\{0,1\} \qquad i\in\mathcal{N}^P, v\in\mathcal{V}, t\in\mathcal{T} \tag{A.48}$$

$$d_i\in\mathbb{Z}^+ \qquad i\in\mathcal{N}^P \tag{A.49}$$

$$b_i\geq 0 \qquad i\in\mathcal{N}^P \tag{A.50}$$

$$s_{it}\geq \underline{S}_{it} \qquad i\in\mathcal{N}^P, t\in\mathcal{T} \tag{A.51}$$

$$e_{it}\geq 0 \qquad i\in\mathcal{N}^L, t\in\mathcal{T} \tag{A.52}$$

$$c_i\geq 0 \qquad i\in\mathcal{N}^E \tag{A.53}$$

$$p^L_{ijd}\in\mathbb{Z}^+ \qquad i\in\mathcal{N}^E, j\in\mathcal{N}^E\cup\mathcal{N}^L\setminus\{i\}, d\in\mathcal{D} \tag{A.54}$$

$$p^O_{ijd}\in\mathbb{Z}^+ \qquad i\in\mathcal{N}^L, j\in\mathcal{N}^U, d\in\mathcal{D} \tag{A.55}$$

$$p^S_{ijd}\in\mathbb{Z}^+ \qquad i\in\mathcal{N}^U, j\in\mathcal{N}^S, d\in\mathcal{D} \tag{A.56}$$

$$f^L_{ij}\geq 0 \qquad i\in\mathcal{N}^E, j\in\mathcal{N}^E\cup\mathcal{N}^L\setminus\{i\} \tag{A.57}$$

$$f^O_{ij}\geq 0 \qquad i\in\mathcal{N}^L, j\in\mathcal{N}^U \tag{A.58}$$

$$f^S_{ij}\geq 0 \qquad i\in\mathcal{N}^U, j\in\mathcal{N}^S \tag{A.59}$$

Appendix B

Detailed solution information when forcing transportation modes in scenarios S5-S100

Here we present and discuss the solution details from Chapter 7.3. The solutions are summarized in Tables B.1 and B.2.

Table B.1: Ship solution details when ships are forced to be the transportation mode between loading ports and unloading ports in S20-S100.

	S20		**S50**		**S100**	
Ship capacity	**# Ships**	**# Round trips**	**# Ships**	**# Round trips**	**# Ships**	**# Round trips**
50 kt	1	4	-	-	-	-
60 kt	-	-	1	6	-	-
70 kt	-	-	-	-	-	-
80 kt	-	-	-	-	-	-
90 kt	1	7	-	-	1	8
100 kt	1	8	5	37	10	74
Total	**3**	**19**	**6**	**43**	**11**	**82**

Table B.2: Comparison of key supply chain components in solutions for S5-S100 when forcing and not forcing offshore transportation mode

Scen.	**Force transp. mode**	**Total length of pipelines**	**# Pipelines**	**# Ships**	**# Round trips**	**# Docks in each port**	**Buffer storage capacity in Kollsnes**	**Buffer storage capacity in Wilhelmshaven**
S5	-	458.3 km	2	2	5	1	91.2 kt	113.1 kt
S5	Pipelines	1264.3 km	3	-	-	-	-	-
S20	-	1265.2 km	4	-	-	-	-	-
S20	Ships	459.2 km	3	3	19	1	119.5 kt	111.3 kt
S50	-	2993.2 km	13	-	-	-	-	-
S50	Ships	1381.2 km	11	6	43	1	100.3 kt	115.7 kt
S100	-	4270.6 km	39	-	-	-	-	-
S100	Ships	2351.2 km	36	11	82	2	164.7 kt	158.5 kt

As presented by Table B.1, three ships with capacities 50, 90, and 100 kt are hired in the S20 ships only solution. These ships perform a total of 19 round trips. From Table B.2, we see that both Kollsnes and Wilhelmshaven need only one dock, as no ships are operating in the ports simulatenously. The buffer storage capacities are 119.5 and 111.3 kt in Kollsnes and Wilhelmshaven, respectively. The inventory levels throughout the planning horizon for the two ports are illustrated in Figure B.1. The transportation cost breakdown in B.2 shows that sailing and liquefaction account for the greatest shares of the transportation cost.

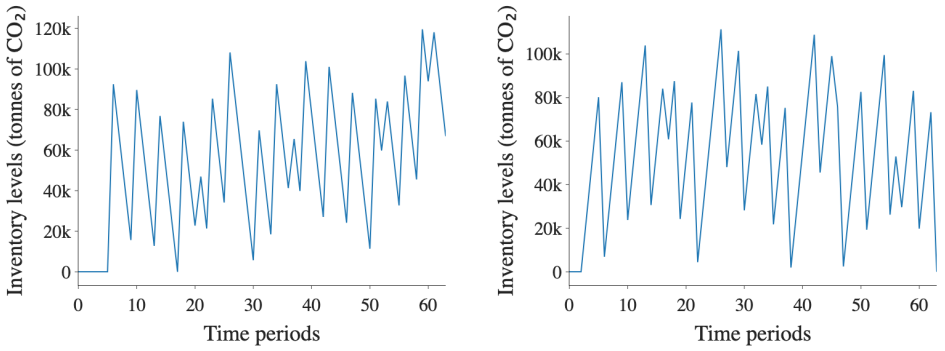

(a) Kollsnes **(b)** Wilhelmshaven

Figure B.1: Development of inventory levels for buffer storages in **(a)** Kollsnes and **(b)** Wilhelmshaven during a planning horizon of 30 days, i.e., 60 time periods, for scenario S20.

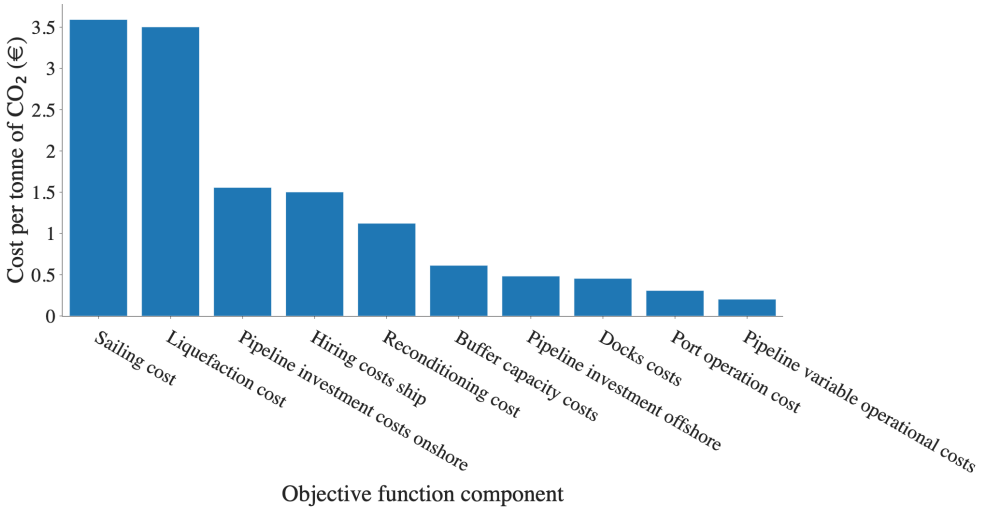

Figure B.2: The cost composition for the supply chain without capture and storage costs in scenario S20.

When forcing ships only for S50, the solution includes five 100 kt ships and one 60 kt ship. Combined, they perform 43 round trips, whereof the 100 kt ships perform 37 trips. Only one dock is needed in both Kollsnes and Wilhelmshaven, and the buffer storage capacities are 100.3 and 115.7 kt, respectively. The inventory levels throughout the planning horizon for the two ports are illustrated in Figure B.3. The transportation cost breakdown in B.4 shows that sailing and liquefaction account for the greatest shares of the transportation cost.

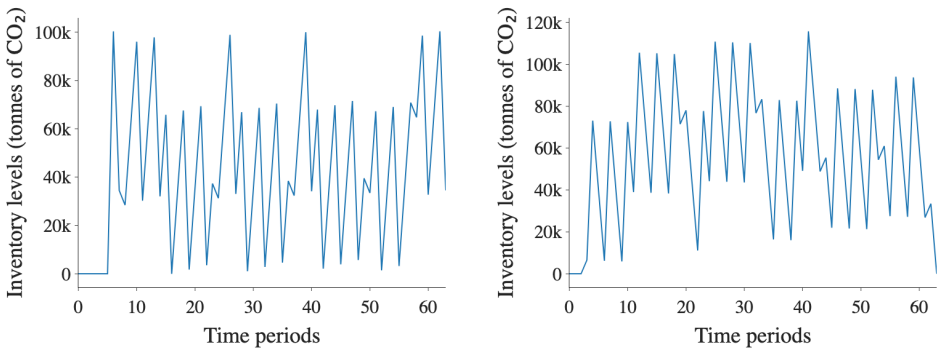

(a) Kollsnes **(b)** Wilhelmshaven

Figure B.3: Development of inventory levels for buffer storages in **(a)** Kollsnes and **(b)** Wilhelmshaven during a planning horizon of 30 days, i.e., 60 time periods, for scenario S50. The inventory levels are given in tonnes of CO_2.

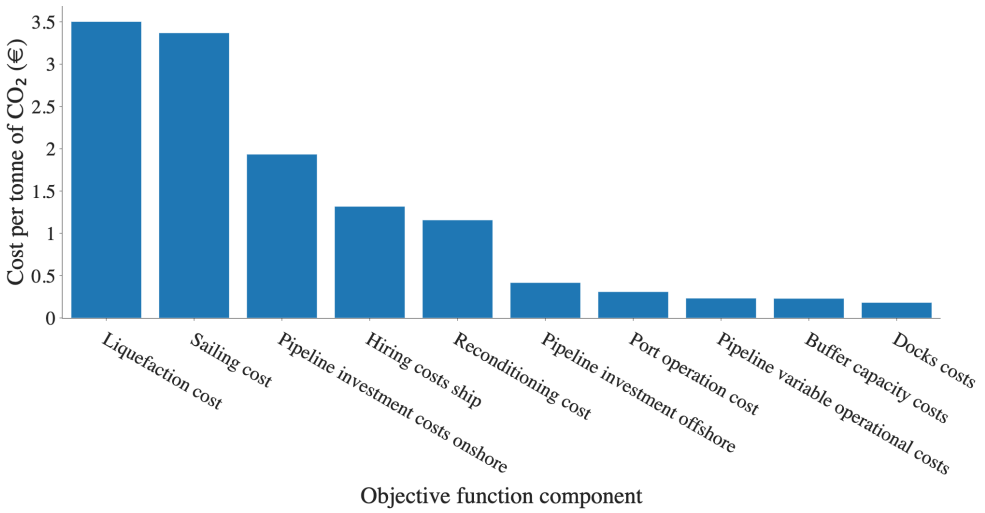

Figure B.4: The cost composition for the supply chain without capture and storage costs in scenario S50.

In the ships only solution for S100, 11 ships are needed, of which 10 are 100 kt ships. The last ship has a capacity of 90 kt. In contrast to S20 and S50, no ships smaller than

90 kt are chosen. The ship of 90 kt performs 8 round trips, while the larger ships perform 74 round trips combined. Furthermore, both Kollsnes and Wilhelmshaven need to invest in two docks to be able to serve the frequent ship visits. The frequent visits of large ships cause the sizes of the buffer storages to increase as well. Now, Kollsnes has a buffer storage capacity of 164.7 kt, while Wilhelmshaven has a buffer storage capacity of 158.5 kt. The inventory levels throughout the planning horizon for the two ports are illustrated in Figure B.5. The transportation cost breakdown in C.3 shows that sailing and liquefaction account for the greatest shares of the transportation cost.

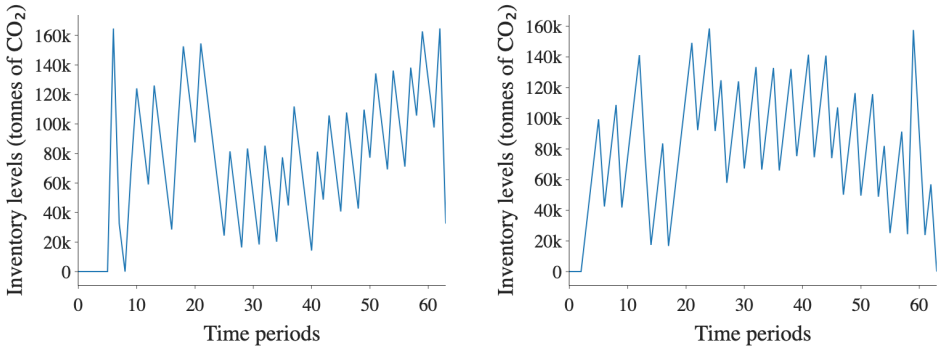

(a) Kollsnes **(b)** Wilhelmshaven

Figure B.5: Development of inventory levels for buffer storages in **(a)** Kollsnes and **(b)** Wilhelmshaven during a planning horizon of 30 days, i.e., 60 time periods, for scenario S100. The inventory levels are given in tonnes of CO_2.

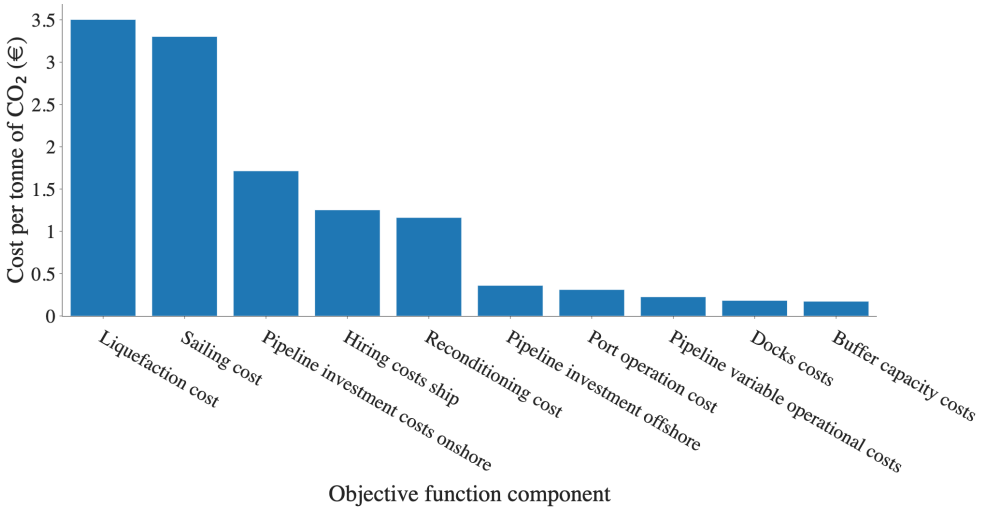

Figure B.6: The cost composition for the supply chain without capture and storage costs in scenario S100.

If ship transport is chosen despite its increased cost, ship sizes seem to be a limitation for large amounts of transported CO_2. In S100, almost all of the CO_2 is transported with ships with a capacity of 100 kt. The reason is that the cost of hiring larger ships is dominated by the net costs of hiring smaller ships. As an example, we could look at ships with a capacity of 100 kt compared to 50 kt. If two ships of size 50 kt are hired in favor of one ship of 100 kt, the hiring cost increases from 0.92 million euro to 1.28 million euro. Despite that the cost per round trip is reduced by 0.07 million euro, the total sailing cost increases by 0.90 million euro as the number of round trips needs to be doubled from an average of 7.4 to 14.8 per ship. Moreover, the increased number of ships in traffic may result in a larger number of docks needed in the ports. Each dock increases the transportation cost by 0.38 million euro. Thus, all cost components that are changed will be in favor of 100 kt ships. The same choices are seen for S50, and to some degree in S20. Thus, smaller ships only seem to be profitable when the amounts of CO_2 assigned to them are so small that they do not utilize the full capacity of larger ships.

Appendix C

Switching distance identification graphs

Here we present the graphs of the switching distance identification analysis referred to in Section 7.5

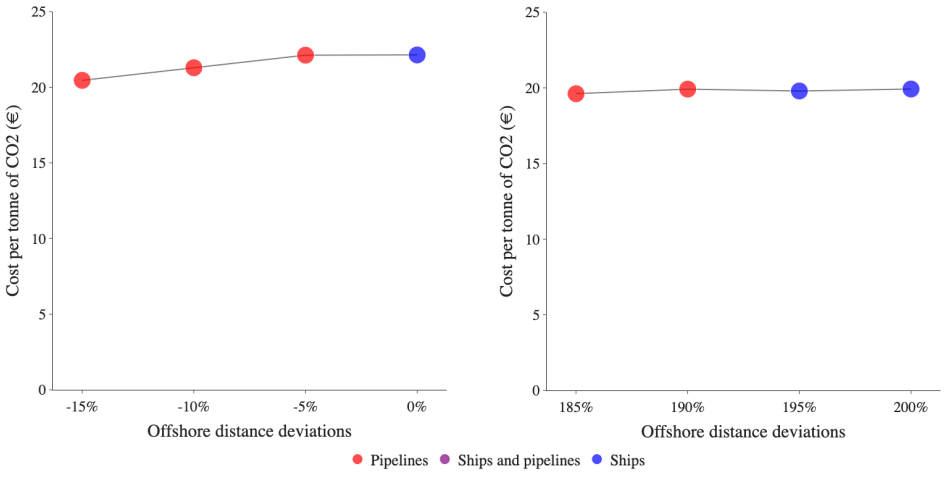

(a) S5 **(b)** S20

Figure C.1: Switching distance identification graphs for **(a)** S5 and **(b)** S20.

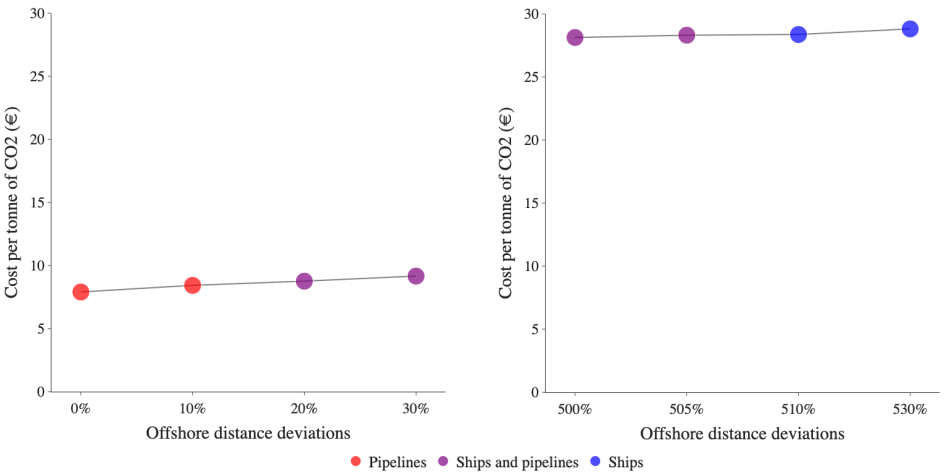

(a) Pipelines to combination **(b)** Combination to ships

Figure C.2: Switching distance identification graphs for scenario S50 for **(a)** pipelines to combination and **(b)** combination to ships.

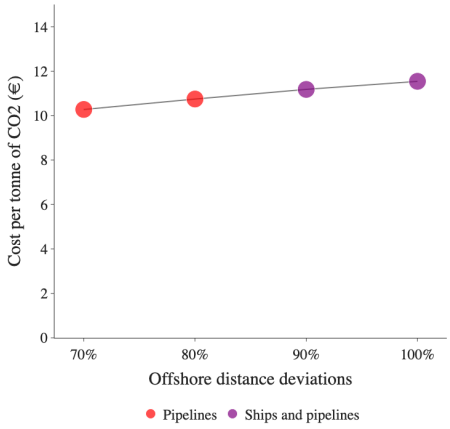

Figure C.3: Switching distance identification graph for scenario S100.

Appendix D

Emission sources

Table D.1: Table of German CO_2 emission sources and their emissons (The Federal Environment Agency 2018).

Emission source	**CO_2 emissions (Mtpa)**
LEAG Lausitz Energie Kraftwerke AG Kraftwerk Lippendorf	11.7
Salzgitter Flachstahl GmbH	7.94
BASF SE	6.94
Hüttenwerke Krupp Mannesmann GmbH	4.98
thyssenkrupp Steel Europe AG	4.82
ROGESA Roheisengesellschaft Saar mbH	4.68
thyssenkrupp Steel Europe AG	4.51
PCK Raffinerie GmbH Schwedt	3.81
thyssenkrupp Steel Europe AG	3.56
Ruhr Oel GmbH	2.86
INEOS Manufacturing Deutschland GmbH	2.77
Hüttenwerke Krupp Mannesmann GmbH	2.77
SKW Stickstoffwerke Piesteritz GmbH	2.67
Evonik Degussa GmbH	2.39
Basell Polyolefine GmbH	2.18
Vattenfall Wärme Berlin AG HKW Reuter-West	2.15
Shell Deutschland Oil GmbH	2.14
TOTAL Raffinerie Mitteldeutschland GmbH (Raffinerie/POX)	2.14
VEO Vulkan-Energiewirtschaft - Oderbrücke GmbH	2.14
Pruna Betreiber GmbH vertreten durch die KBS GmbH	2.06
SWM Heizkraftwerk Nord	2.04
MIRO-Mineralölraffinerie Oberrhein GmbH & Co.KG	2.02
RWE Power AG Veredlungsstandort Knapsacker Hügel	1.98
Rheinkalk GmbH	1.94
ArcelorMittal Eisenhüttenstadt GmbH	1.8
Zellstoff Stendal GmbH	1.8

RWE Power AG-Fabrik Frechen	1.41
CEMEX Zement GmbH	1.4
Shell Deutschland Oil GmbH	1.31
thyssenkrupp Steel Europe AG	1.3
Dow Olefinverbund GmbH Werk Böhlen	1.28
BP Europa SE	1.18
Gaskraftwerk Emsland	1.18
Vattenfall Wärme Hamburg GmbH	1.17
Vattenfall Wärme Hamburg	1.17
Stadtwerke Düsseldorf AG	1.11
BAYERNOIL Betriebsteil Neustadt	1.1
OMV Werk Burghausen	1.09
Holcim (Deutschland) GmbH	1.06
Heizkraftwerk Nord II	1.02
Dyckerhoff GmbH	1.02
ZKS - Zentralkokerei Saar GmbH	0.972
Vattenfall Wärme Berlin AG HKW Mitte	0.936
AGR mbH	0.934
Raffinerie Heide GmbH	0.93
RKB Raffinerie-Kraftwerks Betriebs GmbH	0.926
thyssenkrupp Steel Europe AG	0.926
SWM Heizkraftwerk Süd	0.908
OPTERRA Zement GmbH	0.904
GKW -Gichtgaskraftwerk Dillingen GmbH & Co. KG	0.876
Zementwerk Rohrdorf	0.856
EMPG - EAA Großenkneten	0.854
YARA Brunsbüttel GmbH	0.852
Rheinkalk GmbH	0.838
HeidelbergCement AG	0.828
SCHWENK Zement KG	0.802
Ruhr Oel GmbH	0.8
Solvay Chemicals GmbH	0.797
HeidelbergCement AG	0.792
MIBRAG Deuben	0.777
Wacker Chemie AG, Werk Burghausen	0.754
SCHWENK Zement KG	0.754
HeidelbergCement AG, Zementwerk Burglengenfeld	0.751
Gunvor Raffinerie Ingolstadt GmbH	0.736
SCHWENK Zement KG, Werk Karlstadt	0.729
DREWAG Gasturbinen-Heizkraftwerk Nossener Brücke	0.725
Spenner GmbH & Co. KG	0.718
Märker Zement GmbH	0.679
GMVA Gemeinschafts-Müllverbrennungsanlage Niederrhein GmbH	0.678
Dyckerhoff GmbH	0.675
HeidelbergCement AG	0.672
MIRO-Mineralölraffinerie Oberrhein GmbH & Co.KG	0.669
AG der Dillinger Hüttenwerke	0.661

Holcim (Deutschland) GmbH	0.654
Müllkraftwerk Schwandorf	0.645
MVV Umwelt Asset GmbH - MHKW Mannheim	0.63
Thermal Conversion Compound Industriepark Höchst GmbH	0.623
HeidelbergCement AG	0.618
Holborn Europa Raffinerie GmbH	0.604
Dow Deutschland Anlagenges. mbH	0.602
Vattenfall Wärme Berlin AG HKW Klingenberg	0.598
DK Recycling und Roheisen GmbH	0.589
Holcim WestZement GmbH	0.587
ArcelorMittal Bremen GmbH / BREMA Walzwerk GmbH	0.574
Opterra Wössingen GmbH	0.551
Holcim (Süddeutschland) GmbH	0.549
Portlandzementwerk -Wittekind-	0.548
Basell Polyolefine GmbH	0.539
HeidelbergCement AG Zementwerk Leimen	0.538
HeidelbergCement AG	0.531
swb Entsorgung GmbH & Co. KG / MHKW Bremen	0.523
Sappi Stockstadt GmbH	0.503
thyssenkrupp Steel Europe AG	0.502
Müllverwertung Borsigstraße GmbH, (MVB)	0.499
Heizkraftwerk Stuttgart-Münster (mit MVA)	0.494
BSR / MHKW	0.489
Stora Enso Maxau GmbH	0.478
Stadtwerke Düsseldorf AG	0.471
Enertec Hameln GmbH	0.468
LEIPA Georg Leinfelder Werk Schwedt Süd	0.464
EEW Energy from Waste Helmstedt GmbH	0.459
ROMONTA Amsdorf	0.452
FELS-WERKE Kalkwerk Kaltes Tal	0.446
CropEnergies Bioethanol GmbH	0.438
SOLVAY Chemicals GmbH	0.437
Pfleiderer Baruth GmbH	0.437
BAYERNOIL Betriebsteil Vohburg	0.436
Heizkraftwerk Sandreuth	0.429
MHKW/HKW Nordweststadt	0.429
Kraftwerke Mainz-Wiesbaden AG	0.428
UPM GmbH, Werk Schongau	0.425
Pfleiderer Neumarkt GmbH Spanplattenwerk 2 und 3	0.424
Linde Gas Produktionsgesellschaft mbH & Co. KG	0.42
Vattenfall Wärme Berlin AG HKW Moabit	0.42
AWG Abfallwirtschaftsgesellschaft mbH Wuppertal	0.42
Aluminium Oxid Stade GmbH	0.399
MVV Umwelt Asset GmbH	0.397
CIECH Energy Deutschland GmbH	0.393
BASF Schwarzheide GmbH	0.392
thomas zement GmbH & Co. KG	0.391
Müllheizkraftwerk Rothensee GmbH	0.386

EVI Abfallverwertung B.V. & Co. KG	0.386
MVA Bielefeld-Herford GmbH	0.378
Egger Holzwerkstoffe Brilon	0.374
RWE Power AG-Fabrik Fortuna Nord	0.371
MVA Weisweiler GmbH & Co. KG	0.371
Venator Germany GmbH	0.367
B+T Energie GmbH	0.366
Henkel AG & Co. KGaA	0.362
Portland-Zementwerke	0.348
Progroup Power 1 GmbH	0.348
Solnhofer Portland-Zementwerke GmbH & Co. KG	0.339
Trianel Gaskraftwerk Hamm GmbH & Co. KG	0.332
Sonae Arauco Beeskow GmbH	0.332
InfraLeuna GmbH WT 1	0.33
Fels-Werke GmbH	0.324
EGK Entsorgungsgesellschaft Krefeld GmbH & Co. KG	0.323
MVR Müllverwertung Rugenberger Damm GmbH & Co. KG	0.32
Hydro Aluminium Rolled Products GmbH	0.318
Orion Engineered Carbons GmbH	0.317
Statkraft Markets GmbH	0.317
Entsorgungsgesellschaft Mainz mbH	0.317
Schaefer Kalk GmbH & Co. KG	0.312
EEW Energy from Waste Saarbrücken GmbH	0.31
EEW Energy from Waste Stapelfeld GmbH	0.31
Evonik Röhm GmbH	0.306
Kraftwerk Obernburg GmbH	0.297
Kalkwerk Saal	0.296
FELS-WERKE Kalkwerk Rübeland	0.294
Phoenix Zementwerke	0.293
swb Entsorgung GmbH & Co. KG / MKK Bremen	0.292
Schaefer Kalk GmbH & Co. KG, Werk Steeden	0.289
Heidelberg Cement AG	0.288
Sappi Alfeld GmbH	0.287
SUEZ Energie und Verwertung GmbH	0.286
B+S Papenburg Energie GmbH	0.284
Südzucker AG Mannheim / Ochsenfurt, Werk Zeitz	0.283
ETN Wintershall	0.282
Stadtwerke Erfurt / HKW Ost	0.281
EEW Energy from Waste	0.28
IKW Rüdersdorf GmbH	0.28
Papier- u. Kartonfabrik Varel	0.278
TRIMET Aluminium SE	0.275
ArcelorMittal Hochfeld GmbH	0.273
AVG Abfallentsorgungs- und Verwertungsgesellschaft Köln mbH	0.271
Heizkraftwerk Jena Süd	0.262
Smurfit Kappa Zülpich Papier GmbH	0.259
Martinswerk GmbH	0.256

Daimler AG Mercedes-Benz Werk Sindelfingen	0.256
Statkraft Markets GmbH	0.256
Müllheizkraftwerk Burgkirchen	0.255
Industriekraftwerk Plattling	0.254
Opel Automobile GmbH	0.252
AVA Velsen	0.252
Currenta GmbH & Co. OHG	0.251
K+S KALI GmbH, Werk Zielitz	0.25
EEW Energy from Waste Großräschen GmbH	0.25
GKS-Gemeinschaftskraftwerk Schweinfurt GmbH	0.249
Dyckerhoff GmbH	0.249
Nordland Papier GmbH	0.247
Pilkington Deutschland AG	0.245
Kalkwerke H. Oetelshofen GmbH & Co. KG	0.243
MHB Hamm Betriebsführungsgesell	0.243
MIBRAG Wählitz	0.242
AVA Abfallverwertung Augsburg GmbH	0.24
Vattenfall Wärme Berlin AG GuD-HKW Lichterfelde	0.237
Moritz J. Weig GmbH & Co. KG	0.235
TRIMET Aluminium SE, Niederlassung Hamburg	0.232
Zweckverband Müllverwertungsanlage Ingolstadt	0.228
Müllverbrennungsanlage	0.228
Linde Gas Produktionsgesellschaft mbH & Co. KG	0.224
F ritz Winter Eisengießerei GmbH & Co. KG	0.221
Klingele Papierwerke GmbH & Co. KG	0.218
Vattenfall Wärme Berlin AG HKW Reuter	0.217
ZKW Otterbein Zementwerk	0.217
Kreis Weseler Abfallgesellschaft mbH & Co. KG	0.217
Stadtwerke Münster GmbH	0.216
ADM Hamburg Aktiengesellschaft	0.215
Biomassekraftwerk Lünen GmbH	0.214
Sasol Germany GmbH	0.212
Pilkington Deutschland AG	0.212
Dyckerhoff GmbH Werk Amöneburg	0.209
Energie- und Wasserversorgung Bonn/Rhein-Sieg GmbH	0.203
VW Kraftwerk GmbH, HKW Baunatal	0.202
thyssenkrupp Steel Europe AG	0.202
InfraServ GmbH & Co. Gendorf KG	0.201
Heizkraftwerk an der Friedensbrücke	0.201
Pfleiderer Gütersloh GmbH (Werk 2)	0.201
Fels-Werke GmbH	0.2
Stora Enso Sachsen GmbH	0.199
Müllheizkraftwerk Würzburg	0.199
Rottwerk Pocking	0.197
DS Smith Paper Deutschland GmbH	0.195
R.D.M. Arnsberg GmbH	0.194
ENTEGA AG (HSE)	0.194
GASCADE Gastransport GmbH	0.193
GASCADE Gastransport GmbH	0.193

LANXESS Deutschland GmbH	0.192
Stadtwerke Rostock AG	0.192
Papierfabrik A. Jass GmbH & Co.KG	0.192
Kronos Titan GmbH	0.191
Schoellershammer GmbH & Co. KG	0.191
IHKW Industrieheizkraftwerk Andernach GmbH c/o ThyssenKrupp Rasselstein GmbH	0.19
Wärmeverbundkraftwerk Freiburg GmbH	0.189
EEW Energy from waste Saarbrücken GmbH	0.189
Mark-E Aktiengesellschaft	0.182
Stadtwerke Leipzig GmbH, HKW Leipzig	0.182
GML Gemeinschafts Müllheizkraftwerk Ludwigshafen GmbH	0.182
EBE Holzheizkraftwerk GmbH	0.182
Pfeifer & Langen GmbH & Co. KG	0.181
Oxea Produktion GmbH & Co. KG	0.18
Georgsmarienhütte GmbH	0.18
Rheinkalk GmbH Kalkwerk Istein	0.18
FELS-WERKE Kalkwerk Hornberg	0.179
GSB Entsorgungsbetrieb Baar-Ebenhausen	0.179
Thermische Abfallbehandlung Lauta GmbH & Co. oHG	0.177
Heizkraftwerk Erlangen	0.176
EVH GmbH, Dieselstr.	0.175
Covestro Deutschland AG	0.173
VERA Klärschlammverbrennung	0.172
Lech-Stahlwerke GmbH	0.17
B.E.S. Brandenburger Elektrostahlwerke GmbH	0.17
EEW Energy from Waste Saarbrücken GmbH TREA Breisgau	0.17
1Heiz Energie GmbH Binnenhafen Eberswalde	0.168
Biomassekraftwerk Bischofferode/Holungen	0.168
Stadtwerke Frankfurt (Oder) GmbH	0.168
Märker Kalk GmbH	0.168
Aurubis AG	0.167
GuD-Anlage Bitterfeld	0.166
Peiner Träger GmbH	0.166
Walhalla Kalk GmbH & Co. KG	0.166
Dow Olefinverbund GmbH, Werk Schkopau	0.164
Erdgasverdichterstation MEGAL Waidhaus	0.164
Palm Power GmbH & Co. KG	0.164
Knapsack Power GmbH & Co. KG	0.162
Sasol-Huntsman GmbH & Co. KG	0.16
GuD HKW	0.16
Aluminium Norf GmbH	0.159
AVEA Entsorgungsbetriebe GmbH & Co. KG	0.159
Vattenfall Wärme Berlin AG HKW Lichterfelde	0.158
EEW MHKW Göppingen	0.157
Mainova, HKW Niederrad	0.156
TRIMET Aluminium SE	0.156

Saint-Gobain Glass Deutschland GmbH	0.156
Rütgers Germany GmbH	0.155
Nynas GmbH & Co. KG	0.154
VYNOVA Wilhelmshaven GmbH	0.153
Portlandzementwerk " Wotan"„ H. Schneider KG	0.153
Calcis Lienen GmbH & Co.KG	0.152
EEW Energy from Waste Premnitz GmbH	0.152
Heizkraftwerk Halle-Trotha	0.151
Evonik Degussa GmbH Werk Wesseling	0.149
Märker Kalk GmbH	0.149
Südzucker Werk Ochsenfurt	0.148
Calcis Warstein GmbH & Co. KG	0.148
Papierfabrik August Koehler SE	0.148
Kelheim Fibres GmbH	0.146
Kraftwerk Dessau GmbH	0.146
Stadtwerke Leipzig GmbH	0.144
Südzucker AG Werk Offstein	0.143
K+S KALI GmbH, Werk Werra, Standort Unterbreizbach	0.142
Sachsenmilch Leppersdorf GmbH	0.141
Smurfit Kappa Hoya Papier und	0.139
AHKW Neunkirchen	0.139
Pfeifer Holz GmbH - Werk Unterbernbach	0.137
Papierfabrik Palm GmbH & Co.KG	0.136
KRONOS TITAN GmbH	0.135
Nordzucker AG	0.135
Solvay & CPC Barium Strontium GmbH & Co KG	0.133
Vattenfall Wärme Berlin AG HKW Marzahn	0.133
RBB RMHKW Böblingen	0.133
Stadtwerke Bielefeld GmbH	0.132
Remondis Production GmbH	0.131
CIECH Soda Deutschland GmbH & Co. KG	0.13
Müllverbrennung Kiel GmbH & Co. KG - Müllheizkraftwerk Kiel	0.129
Südzucker Werk Plattling	0.128
Müllheizkraftwerk Bamberg	0.128
TWS Thüringer Wärme Service GmbH	0.126
INNOVATHERM -Ges.zur innovativen Nu	0.126
Uniper Kraftwerke GmbH, Kraftwerk Franken	0.125
EUROGLAS GmbH	0.125
Biomasse Heizkraftwerk Siegerland GmbH & Co. KG	0.125
SWK Stadtwerke Kaiserslautern Versorgungs-AG	0.124
Müllheizkraftwerk Kempten	0.124
AHKW Geiselbullach	0.123
MHKW Coburg	0.123
Grace GmbH	0.122
Gas- und Dampfturbinenanlage	0.122
GUARDIAN Flachglas GmbH	0.122
Verallia Deutschland AG	0.122
BMHKW Malchin	0.122

Schoeller Technocell GmbH & Co. KG	0.12
Zanders Paper GmbH	0.119
INEOS Solvents Germany GmbH	0.118
Heizkraftwerk Altenstadt GmbH & Co. KG	0.117
DREWAG AMD EVC 2 EnergyCenter Wilschdorf	0.116
Saint-Gobain Glass Deutschland GmbH	0.113
HIM GmbH	0.113
HBB Heizkraftwerk Bauernfeind Betreibergesellschaft mbH	0.112
FVS Fernwärme-Verbund Saar GmbH	0.111
InfraServ (Kalle-Albert)	0.111
EVC Dresden-Wilschdorf /Reichenberg	0.111
FS Karton GmbH	0.111
DSM Nutritional Products GmbH	0.11
Pfeifer & Langen GmbH & Co. KG, Werk Könnern	0.11
Verallia Deutschland AG	0.11
Nordzucker AG, Werk Klein Wanzleben	0.109
Schott AG - Standort Mitterteich	0.109
Ardagh Glass GmbH	0.109
Saint Gobain Glass Flachglas Torgau GmbH	0.109
AVG Abfall-Verwertungs-Gesellschaft mbH	0.109
AMK Abfallentsorgungsgesellschaft	0.106
Stahlwerk Thüringen GmbH	0.105
thyssenkrupp Hohenlimburg GmbH	0.105
Heizkraftwerk Energieversorgung Schwerin-Süd	0.102
RWE Generation SE, Region Kundenkraftwerke HKW Dortmund	0.101
MKW Weißenhorn	0.1
Total	**201.05**

A. Bennæs, M. Skogset, T. Svorkdal

Supply Chain Optimization for Carbon Capture and Storage: A German–Norwegian Case Study

NTNU
Norwegian University of
Science and Technology